

Individualisation of Transcranial Electric Stimulation to Improve Motor Function After Stroke

Current challenges and future perspective

Joris van der Cruisen

**Individualisation of Transcranial Electric Stimulation
to Improve Motor Function After Stroke: Current
challenges and future perspective**

Joris van der Crujsen

This work is part of the research programme NeuroCIMT-itDCS with project number 14902 which is financed by the Dutch Research Council (NWO).



Financial support for printing of this thesis was kindly provided by TMSi and MedCaT BV



Layout and printing by Optima Grafische Communicatie (www.ogc.nl)

ISBN: 978-94-6361-906-6

© Joris van der Crujisen, 2023

All rights reserved. No part of this thesis may be reproduced, stored in a retrieval system, or transmitted in any form by any means, without the prior written permission of the author or, when appropriate, of the publisher of the respective journals

Individualisation of Transcranial Electric Stimulation to Improve Motor
Function After Stroke: Current challenges and future perspective

Individualisatie van transcraniële elektrische stimulatie om motorisch herstel na een beroerte
te verbeteren: Huidige uitdagingen en toekomstperspectief

Proefschrift

ter verkrijging van de graad van doctor aan de
Erasmus Universiteit Rotterdam
op gezag van de
rector magnificus

Prof.dr. A.L. Bredenoord

en volgens besluit van het College voor Promoties.
De openbare verdediging zal plaatsvinden op

dinsdag 21 november 2023 om 15:30 uur

door

Joris van der Cruijssen
geboren te Nijmegen

Promotiecommissie:

Promotoren: Prof.dr. R.W. Selles
Prof.dr. M.A. Frens

Overige leden: Dr. J.N. van der Geest
Dr.ing. L. Marchal Crespo
Prof.dr. R.M. Dijkhuizen

Copromotor: Dr. T.F. Oostendorp

Contents

Chapter 1	General Introduction	7
Chapter 2	Theta but not beta power is positively associated with better explicit motor task learning	19
Chapter 3	Transcranial direct current stimulation targeting the entire motor network does not increase corticospinal excitability	43
Chapter 4	ASH: an Automatic pipeline to generate realistic and individualised chronic Stroke volume conduction Head models	63
Chapter 5	A method to experimentally estimate the conductivity of chronic stroke lesions: a tool to individualize transcranial electric stimulation	79
Chapter 6	Addressing the inconsistent electric fields of tDCS by using patient-tailored configurations in chronic stroke: implications for treatment	95
Chapter 7	General Discussion	121
	Summary	139
	Samenvatting	145
	Dankwoord	151
	About the author	157

Chapter 1

General Introduction

Stroke is one of the leading causes of long-term impairment and disability, affecting over 10 million people worldwide each year.¹ Stroke is a cerebrovascular event characterised by loss of function due to prolonged brain oxygen deprivation, either by vascular rupture or occlusion.¹ About 80% of all stroke patients suffer from motor impairments in the first 6 months following stroke.² In the chronic phase after stroke, from 6 months onwards, only a small percentage of stroke patients reach full motor recovery,³ limiting the quality of life of patients.^{4,5} Therefore, maximising motor recovery is an essential aim of stroke rehabilitation.

Motor recovery after stroke

Motor recovery occurs mainly during the first weeks to months post-stroke⁶⁻⁸ a phase in which the brain is in a state of high neuroplasticity.⁹ Neuroplasticity refers to the ability of the brain to modify existing neural connections, which makes it possible to restore motor function. Previous neuroimaging studies in stroke patients showed that clinically measured upper extremity motor function is associated with distinct patterns of functional organisation. For instance, neural restoration in the *perilesional* brain region correlates with good recovery of motor function.^{10,11} Alternatively, motor function reorganisation within the ipsilesional or towards the contralesional hemisphere has been associated in some studies with poor motor recovery^{10,12} but in other studies with good motor recovery.^{13,14}

Three theoretical frameworks are used in the literature to describe the relationships between motor function and neurophysiological activity patterns: the *interhemispheric competition* model, the *vicariation model* and, more recently, the *bimodal balance-recovery* model.¹⁵ These frameworks propose specific roles of the ipsilesional and contralesional hemispheres in the recovery process. The interhemispheric competition model hypothesises reduced transcallosal inhibition of the affected to the unaffected hemisphere, resulting in decreased excitability in the former and increased excitability in the latter.^{16,17} Consequently, according to this model, the contralesional hemisphere hinders the function of the ipsilesional hemisphere in patients with larger damage to the ipsilesional motor system and, thus, a larger imbalance in interhemispheric inhibition, resulting in lower motor recovery. This framework suggests that reducing the imbalance in interhemispheric inhibition could lead to better motor recovery in stroke patients and is supported by neuroimaging studies that show lower motor performance in patients with a larger imbalance in interhemispheric inhibition.¹⁸

In contrast, the vicariation model hypothesises that unaffected motor areas, for instance, ipsilesional secondary motor regions or contralesional motor regions, become more involved in controlling the paretic body side. This framework is based on neuroimaging studies of stroke patients that show contralesional activity during paretic hand movement in severely

affected patients and well-recovered patients.¹⁴ For these patients, the vicariation model suggests increased involvement of the contralesional motor cortex is beneficial for motor recovery.

The bimodal balance recovery model¹⁵ combines the interhemispheric competition and vicariation models and hypothesises that recovery depends on both the structural reserve and the degree of imbalance in interhemispheric inhibition. Consequently, the bimodal balance recovery model argues that increased excitability in the contralesional hemisphere may be beneficial if the ipsilesional motor system is highly impaired with little structural reserve. Therefore, the bimodal balance recovery model is more flexible in relating motor recovery to neurophysiological patterns of activity but requires functional neuroimaging to determine if increased contralesional excitability should be enhanced or inhibited to improve the recovery process.¹⁹

Non-invasive brain stimulation

The theoretical frameworks of motor recovery have inspired non-invasive brain stimulation methods to locally modulate neuroplasticity of the ipsilesional and contralesional hemisphere in order to improve motor recovery after stroke. Non-invasive brain stimulation can be categorised into transcranial magnetic stimulation (TMS) and transcranial electric stimulation (tES). Transcranial electric stimulation can be further divided into transcranial direct current stimulation (tDCS), transcranial alternating current stimulation (tACS) and transcranial random noise stimulation (tRNS). This thesis focuses on TMS as a tool to assess (changes in) corticospinal excitability and the application of tDCS to modulate brain activity and plasticity; however, the concepts described may also apply to tACS and tRNS.

TMS excites the neurons in the brain by generating a varying magnetic field on the scalp that results, through electromagnetic induction, in an electric field in the underlying cortex that is strongest directly below the TMS coil. The strength of the electric field in the cortex primarily depends on the stimulator output magnitude and the distance of the TMS coil to the cortex.^{20,21} If the magnetic pulse is large enough, the electric field it generates will activate neurons in the brain. Consequently, such a suprathreshold electric field over the motor cortex generates an action potential that translates into a muscle twitch. A recording of such a twitch by electromyography (EMG)²² is called a Motor Evoked Potential (MEP). The amplitude of MEPs is believed to be related to a balance in excitatory and inhibitory neurotransmitters.²³ As such, MEPs are considered a biomarker for corticospinal excitability. MEPs represent the most basic, reliable, and frequently used measure to quantify the effects of tDCS targeting the motor system.^{24,25}

TDCS modulates the brain by driving an electric direct current – typically between 0.1 and 4 mA – through the head via two or more stimulation electrodes placed on the scalp.²⁶ The current passes from a positive electrode (anode) through the scalp, skull and brain towards a negative electrode (cathode) and thus generates an electric field in the brain. In tDCS applications, this electric field is subthreshold, i.e., it is too small to activate neurons. The electric field is believed to enhance local neuroplasticity by locally modulating the balance between excitatory (e.g. glutamate) and inhibitory neurotransmitters (e.g. γ -aminobutyric acid) in a polarity-dependent way.^{27,28} The spatial distribution of the electric field and, therefore, the location and size of the stimulated brain area depend on controllable parameters such as the size and locations of the stimulation electrodes,^{29,30} and uncontrollable parameters such as the anatomy (i.e. scalp/skull/CSF layer thickness^{31–33}) and conductive properties of the different tissues comprising the head.^{33,34}

In healthy subjects, tDCS aimed to improve upper extremity motor function is typically performed with an anode centred above the hand area of the contralateral primary motor cortex (M1) and a cathode at the opposite supra orbita in healthy subjects.²⁵ In standardised electrode positions,³⁵ these locations correspond approximately to the C3/C4 and Fp2/Fp1 electrodes, respectively. This stimulation configuration is referred to as *conventional anodal* tDCS. In healthy subjects, conventional anodal tDCS has been used to modulate corticospinal excitability^{24,25,36} and improve performance on motor learning tasks.^{37–39} During conventional cathodal tDCS, the polarity of the electrodes is inverted to achieve effects opposite to those in anodal tDCS.^{36,38}

In stroke patients, the different theoretical frameworks for motor recovery are reflected in different electrode configurations that have been proposed. These configurations aim to 1) enhance the ipsilesional M1 without considering the contralesional M1 [anodal tDCS],^{40–42} while others aim to 2) enhance the ipsilesional M1 while actively suppressing the contralesional M1 [bihemispheric/dual tDCS],^{40,41} 3) suppress the contralesional M1 without considering the ipsilesional M1 [cathodal tDCS]^{40,41,43} or 4) enhance contralesional M1 without considering ipsilesional M1 [anodal contralesional tDCS].^{44,45} Electrode placement is typically equal to the same C3 and C4 positions used for healthy individuals. These tDCS configurations have been applied in stroke patients in order to attempt to modulate corticospinal excitability and motor learning/recovery. More so than for healthy subjects, meta-analyses have not been able to draw firm conclusions about the effectiveness of tDCS and describe conflicting findings for anodal tDCS, cathodal tDCS, bihemispheric tDCS, and anodal contralesional tDCS.

The variable tDCS effect sizes in human studies have been related to many factors of intrasubject and intersubject variability, such as the time of the day of the experiment, the pre-tDCS

level of function, the amount of sleep in the night before the experiment, age, sex, genetics.^{46,47} Furthermore, differences in head anatomy-related factors such as skull conductivity³⁴ and the thickness of the cerebrospinal fluid layer³³ affect the distribution of the electric field generated by tDCS. For stroke patients specifically, additional intersubject variability results from the lesion characteristics (lesion volume, location, and conductivity), which may further influence the electric field distribution in the brain, and motor function organisation, which may influence the brain region tDCS should target.

Scope of this thesis

The additional interindividual variability in stroke patients and the more inconsistent response to tDCS indicate that the current one-fits-all approach of tDCS may be ineffective for clinical implementation and has resulted in scepticism about the potential of tDCS as a supportive rehabilitation method.^{48,49} Currently, most clinical tDCS studies do not consider individual brain anatomy and motor function. As a result, whether the tDCS configurations in clinical studies stimulate the correct brain areas with the proper polarity and strength cannot be verified. More specifically, to what extent conventional tDCS configurations in stroke patients reach comparable electric fields to those described in healthy subjects is unknown. Simulation models of tDCS can be used to verify whether the intended brain areas are correctly stimulated,^{50,51} but this is currently time-consuming, and requires functional and structural neuroimaging in individual patients, which is usually unavailable. Consequently, the added value of individualising tDCS electrode positions remains to be elucidated.

Another challenge to interpreting the effectiveness of different study protocols is the outcome measures used. In motor learning tasks, tDCS effects are assessed on various behavioural outcome measures such as reaction times,⁵²⁻⁵⁴ speed/accuracy trade-offs,^{37,55} and force production,^{52,56} complicating the comparison between studies and thus the development of optimal tDCS strategies. For tDCS research on cortical excitability, motor-evoked potentials (MEPs) are commonly used as an outcome measure. However, MEPs are highly variable,^{57,58} and repetitive TMS pulses modulate corticospinal excitability, making it hard to determine tDCS effects without proper control conditions. Instead of assessing the tDCS effects on the *behavioural level*, monitoring changes in the fundamental *neurophysiological process* underlying corticospinal excitability and motor learning, for instance, with electroencephalography (EEG), could lead to more reliable measures to assess tDCS effects.

There are several challenges and opportunities with the current application of tDCS in stroke patients. Ideally, tDCS during motor rehabilitation would be tailored to patients' individually assessed motor function, with electrode locations to stimulate individualised function-related

brain areas optimally while, at the same time, monitoring the effects with reliable, objective outcome measures. Several steps should be taken in order to reach this point on the horizon.

This thesis describes the development of methods to facilitate the individualisation of tDCS configurations in stroke patients and contribute to objective neurophysiological targets to monitor the response to tDCS. To do so, we determined EEG correlates of the learning component – and not the motor activation component – of explicit motor learning in healthy subjects in **Chapter 2**. In **Chapter 3**, an attempt to replicate a report of enhanced corticospinal excitability in healthy subjects after simultaneous anodal stimulation of the left and right primary motor cortex (motor network tDCS) is described.⁵⁷ The enhanced response after motor network tDCS conflicts with the interhemispheric inhibition model and, therefore, could give new directions into the working mechanism and the effective application of tDCS. However, the effect has only been described once and requires replication.

In the following chapters, we report on simulations in MRI-based head models of stroke patients in order to propose methods to address stroke lesions as a source of intersubject variability. In **Chapter 4** a method to create volume conductor head models of stroke patients is described. With these models, the electric fields generated by tDCS configurations with one or more anodes/cathodes can be simulated and optimised to maximally stimulate a brain region of interest.

In **Chapter 5**, a method to experimentally determine the conductivity of stroke lesions and the necessary boundary conditions to do so is described. This method allows for a patient-specific estimate of the lesion conductivity, resulting in more accurate volume conductor models and, thus, a more reliable simulation of the electric fields generated by tDCS.

In **Chapter 6**, the necessity for individualising tDCS electrode locations in stroke patients is described. This study uses structural and functional neuroimaging to compare the electric fields generated by conventional anodal tDCS in healthy individuals and stroke patients to address intersubject variability in head anatomy and motor function. Furthermore, the study investigates if changing the electrode positions, depending on individual brain anatomy and function, can lead to more consistent electric fields between healthy individuals and stroke patients.

Finally, in the concluding **Chapter 7** the main findings of all preceding chapters are summarized and interpreted. This chapter focuses on methodological considerations of the current work and directions for future research regarding motor recovery after stroke and the role of tDCS and EEG therein.

References

1. Feigin, V. L. *et al.* Global, regional, and national burden of stroke and its risk factors, 1990–2019: a systematic analysis for the Global Burden of Disease Study 2019. *Lancet Neurol* **20**, 1–26 (2021).
2. Lawrence, E. S. *et al.* Estimates of the Prevalence of Acute Stroke Impairments and Disability in a Multiethnic Population. *Stroke* **32**, 1279–1284 (2001).
3. Kwakkel, G., Kollen, B. J., van der Grond, J. v. & Prevo, A. J. H. Probability of regaining dexterity in the flaccid upper limb: Impact of severity of paresis and time since onset in acute stroke. *Stroke* **34**, 2181–2186 (2003).
4. Franceschini, M., la Porta, F., Agosti, M. & Massucci, M. Is health-related-quality of life of stroke patients influenced by neurological impairments at one year after stroke? *Eur J Phys Rehabil Med* **46**, (2010).
5. Lieshout, E. C. C. van, van de Port, I. G., Dijkhuizen, R. M. & Visser-Meily, J. M. A. Does upper limb strength play a prominent role in health-related quality of life in stroke patients discharged from inpatient rehabilitation? <https://doi.org/10.1080/10749357.2020.1738662> **27**, 525–533 (2020).
6. Duncan, P. W., Goldstein, L. B., Matchar, D., Divine, G. W. & Feussner, J. Measurement of motor recovery after stroke. Outcome assessment and sample size requirements. *Stroke* **23**, 1084–1089 (1992).
7. Broeks, J. G. *et al.* The long-term outcome of arm function after stroke: results of a follow-up study. <https://doi.org/10.1080/096382899297459> **21**, 357–364 (2009).
8. van der Vliet, R. *et al.* Predicting Upper Limb Motor Impairment Recovery after Stroke: A Mixture Model. *Ann Neurol* **87**, (2020).
9. Wieloch, T. & Nikolich, K. Mechanisms of neural plasticity following brain injury. *Curr Opin Neurobiol* **16**, 258–264 (2006).
10. Loubinoux, I. *et al.* Correlation between cerebral reorganization and motor recovery after subcortical infarcts. *Neuroimage* **20**, 2166–2180 (2003).
11. Calautti, C. & Baron, J. C. Functional neuroimaging studies of motor recovery after stroke in adults: A review. *Stroke* **34**, 1553–1566 (2003).
12. Saes, M. *et al.* How does upper extremity Fugl-Meyer motor score relate to resting-state EEG in chronic stroke? A power spectral density analysis. *Clinical Neurophysiology* **130**, (2019).
13. Buetefisch, C. M. Role of the contralesional hemisphere in post-stroke recovery of upper extremity motor function. *Front Neurol* **6**, 1–10 (2015).
14. Cramer, S. C. *et al.* A Functional MRI Study of Subjects Recovered From Hemiparetic Stroke. *Stroke* **28**, 2518–2527 (1997).
15. di Pino, G. *et al.* Modulation of brain plasticity in stroke: A novel model for neurorehabilitation. *Nat Rev Neurol* **10**, 597–608 (2014).
16. Ferbert, A. *et al.* Interhemispheric inhibition of the human motor cortex. *J Physiol* **453**, 525–546 (1992).
17. Boddington, L. J. & Reynolds, J. N. J. Targeting interhemispheric inhibition with neuromodulation to enhance stroke rehabilitation. *Brain Stimul* **10**, 214–222 (2017).
18. Murase, N., Duque, J., Mazzocchio, R. & Cohen, L. G. Influence of interhemispheric interactions on motor function in chronic stroke. *Ann Neurol* **55**, 400–9 (2004).
19. Bertolucci, F., Chisari, C. & Fregni, F. The potential dual role of transcallosal inhibition in post-stroke motor recovery. *Restor Neurol Neurosci* **36**, 83–97 (2018).
20. Herbsman, T. *et al.* Motor threshold in transcranial magnetic stimulation: the impact of white matter fiber orientation and skull-to-cortex distance. *Hum Brain Mapp* **30**, 2044–2055 (2009).

21. Stokes, M. G. *et al.* Distance-adjusted motor threshold for transcranial magnetic stimulation. *Clin Neurophysiol* **118**, 1617–1625 (2007).
22. Barker, A. T., Jalinous, R. & Freeston, I. L. Non-Invasive Magnetic Stimulation of Human Motor Cortex. *The Lancet* vol. 325 1106–1107 Preprint at [https://doi.org/10.1016/S0140-6736\(85\)92413-4](https://doi.org/10.1016/S0140-6736(85)92413-4) (1985).
23. Ziemann, U. *et al.* TMS and drugs revisited 2014. *Clinical Neurophysiology* **126**, 1847–1868 (2015).
24. Dissanayaka, T., Zoghi, M., Farrell, M., Egan, G. F. & Jaberzadeh, S. Does transcranial electrical stimulation enhance corticospinal excitability of the motor cortex in healthy individuals? A systematic review and meta-analysis. *Eur J Neurosci* **46**, 1968–1990 (2017).
25. Horvath, J. C., Forte, J. D. & Carter, O. Evidence that transcranial direct current stimulation (tDCS) generates little-to-no reliable neurophysiologic effect beyond MEP amplitude modulation in healthy human subjects: A systematic review. *Neuropsychologia* **66**, 213–236 (2015).
26. Bikson, M. *et al.* Response to letter to the editor: Safety of transcranial direct current stimulation: Evidence based update 2016. *Brain Stimul* **10**, 986–987 (2017).
27. Stagg, C. J. *et al.* Polarity-sensitive modulation of cortical neurotransmitters by transcranial stimulation. *Journal of Neuroscience* **29**, 5202–5206 (2009).
28. Yamada, Y. & Sumiyoshi, T. Neurobiological Mechanisms of Transcranial Direct Current Stimulation for Psychiatric Disorders; Neurophysiological, Chemical, and Anatomical Considerations. *Front Hum Neurosci* **15**, 21 (2021).
29. Mikkonen, M., Laakso, I., Tanaka, S. & Hirata, A. Cost of focality in TDCS: Interindividual variability in electric fields. *Brain Stimul* **13**, 117–124 (2020).
30. Dmochowski, J. P., Datta, A., Bikson, M., Su, Y. & Parra, L. C. Optimized multi-electrode stimulation increases focality and intensity at target. *J Neural Eng* **8**, 046011 (2011).
31. Truong, D. Q., Magerowski, G., Blackburn, G. L., Bikson, M. & Alonso-Alonso, M. Computational modeling of transcranial direct current stimulation (tDCS) in obesity: Impact of head fat and dose guidelines. *Neuroimage Clin* **2**, 759–766 (2013).
32. Opitz, A., Paulus, W., Will, S., Antunes, A. & Thielscher, A. Determinants of the electric field during transcranial direct current stimulation. *Neuroimage* **109**, 140–150 (2015).
33. Laakso, I., Tanaka, S., Koyama, S., De Santis, V. & Hirata, A. Inter-subject variability in electric fields of motor cortical tDCS. *Brain Stimul* **8**, 906–913 (2015).
34. McCann, H. & Beltrachini, L. Does participant's age impact on tDCS induced fields? Insights from computational simulations. *Biomed Phys Eng Express* **7**, (2021).
35. Oostenveld, R. & Praamstra, P. The five percent electrode system for high-resolution EEG and ERP measurements. *Clinical Neurophysiology* **112**, 713–719 (2001).
36. Nitsche, M. A. & Paulus, W. Excitability changes induced in the human motor cortex by weak transcranial direct current stimulation. *Journal of Physiology* **527**, 633–639 (2000).
37. Reis, J. *et al.* Noninvasive cortical stimulation enhances motor skill acquisition over multiple days through an effect on consolidation. *Proceedings of the National Academy of Sciences* **106**, 1590–1595–1590–1595 (2009).
38. Stagg, C. J. *et al.* Polarity and timing-dependent effects of transcranial direct current stimulation in explicit motor learning. *Neuropsychologia* **49**, 800–804 (2011).
39. Vines, B. W., Nair, D. G. & Schlaug, G. Contralateral and ipsilateral motor effects after transcranial direct current stimulation. *Neuroreport* **17**, 671–674 (2006).
40. Elsner, B., Kwakkel, G., Kugler, J. & Mehrholz, J. Transcranial direct current stimulation (tDCS) for improving capacity in activities and arm function after stroke: a network meta-analysis of randomised controlled trials. *J Neuroeng Rehabil* **14**, (2017).

41. Bornheim, S. *et al.* Evaluating the effects of tDCS in stroke patients using functional outcomes: a systematic review. *Disabil Rehabil* **44**, 13–23 (2022).
42. Butler, A. J. *et al.* A meta-analysis of the efficacy of anodal transcranial direct current stimulation for upper limb motor recovery in stroke survivors. *J Hand Ther* **26**, 162–171 (2013).
43. Chen, J. L. *et al.* Does Cathodal vs. Sham Transcranial Direct Current Stimulation Over Contralesional Motor Cortex Enhance Upper Limb Motor Recovery Post-stroke? A Systematic Review and Meta-analysis. *Front Neurol* **12**, 400 (2021).
44. Klomjai, W. *et al.* Anodal tDCS of contralesional hemisphere modulates ipsilateral control of spinal motor networks targeting the paretic arm post-stroke. *Clinical Neurophysiology* **136**, 1–12 (2022).
45. Lee, S. H., Kim, W. S., Park, J., Kim, J. & Paik, N. J. Effects of anodal transcranial direct current stimulation over the contralesional hemisphere on motor recovery in subacute stroke patients with severe upper extremity hemiparesis: Study protocol for a randomized controlled trial. *Medicine* **99**, (2020).
46. Li, L. M., Uehara, K. & Hanakawa, T. The contribution of interindividual factors to variability of response in transcranial direct current stimulation studies. *Front Cell Neurosci* **9**, 181 (2015).
47. Ridding, M. C. & Ziemann, U. Determinants of the induction of cortical plasticity by non-invasive brain stimulation in healthy subjects. *Journal of Physiology* **588**, 2291–2304 (2010).
48. Hordacre, B., McCambridge, A. B., Ridding, M. C. & Bradnam, L. v. Can Transcranial Direct Current Stimulation Enhance Poststroke Motor Recovery? *Neurology* **97**, 170–180 (2021).
49. Vöröslakos, M. *et al.* Direct effects of transcranial electric stimulation on brain circuits in rats and humans. *Nat Commun* **9**, 1–17 (2018).
50. Huang, Y., Datta, A., Bikson, M. & Parra, L. C. Realistic volumetric-approach to simulate transcranial electric stimulation-ROAST-a fully automated open-source pipeline. *J Neural Eng* **16**, (2019).
51. Thielscher, A., Antunes, A. & Saturnino, G. B. Field modeling for transcranial magnetic stimulation: A useful tool to understand the physiological effects of TMS? in *Proceedings of the Annual International Conference of the IEEE Engineering in Medicine and Biology Society, EMBS* vols 2015–Novem 222–225 (2015).
52. Hummel, F. C. *et al.* Effects of brain polarization on reaction times and pinch force in chronic stroke. *BMC Neurosci* **7**, 1–10 (2006).
53. Horvath, J. C., Carter, O. & Forte, J. D. No significant effect of transcranial direct current stimulation (tDCS) found on simple motor reaction time comparing 15 different stimulation protocols. *Neuropsychologia* **91**, 544–552 (2016).
54. Kang, E. K. & Paik, N. J. Effect of a tDCS electrode montage on implicit motor sequence learning in healthy subjects. *Exp Transl Stroke Med* **3**, 1–6 (2011).
55. Lefebvre, S. *et al.* Dual-tDCS Enhances Online Motor Skill Learning and Long-Term Retention in Chronic Stroke Patients. *Front Hum Neurosci* **0**, 343 (2013).
56. Kang, N., Summers, J. J. & Cauraugh, J. H. Non-Invasive Brain Stimulation Improves Paretic Limb Force Production: A Systematic Review and Meta-Analysis. *Brain Stimul* **9**, 662–670 (2016).
57. López-Alonso, V., Cheeran, B., Río-Rodríguez, D. & Fernández-Del-Olmo, M. Inter-individual variability in response to non-invasive brain stimulation paradigms. *Brain Stimul* **7**, 372–380 (2014).
58. López-Alonso, V., Fernández-del-Olmo, M., Costantini, A., Gonzalez-Henriquez, J. J. & Cheeran, B. Intra-individual variability in the response to anodal transcranial direct current stimulation. *Clinical Neurophysiology* **126**, 2342–2347 (2015).

Chapter 2

Theta but not beta power is positively associated with better explicit motor task learning

Joris van der Cruijssen, Mana Manoochehri, Zeb D. Jonker, Eleni-Rosalina Andrinopoulou, Maarten A. Frens, Gerard M. Ribbers, Alfred C. Schouten, Ruud W. Selles

NeuroImage 240, 10 2021. doi: [10.1016/j.neuroimage.2021.118373](https://doi.org/10.1016/j.neuroimage.2021.118373)

Abstract

Neurophysiologic correlates of motor learning that can be monitored during neurorehabilitation interventions can facilitate the development of more effective learning methods. Previous studies have focused on the role of the beta band (14–30 Hz) because of its clear response during motor activity. However, it is difficult to discriminate between beta activity related to learning a movement and performing the movement.

In this study, we analysed differences in the electroencephalography (EEG) power spectra of complex and simple explicit sequential motor tasks in healthy young subjects. The complex motor task (CMT) allowed EEG measurement related to motor learning. In contrast, the simple motor task (SMT) made it possible to control for EEG activity associated with performing the movement without significant motor learning.

Source reconstruction of the EEG revealed task-related activity from 5 clusters covering both primary motor cortices (M1) and 3 clusters localised to different parts of the cingulate cortex (CC). We found no association between M1 beta power and learning, but the CMT produced stronger bilateral beta suppression compared to the SMT. However, there was a positive association between contralateral M1 theta (5–8 Hz) and alpha (8–12 Hz) power and motor learning, and theta and alpha power in the posterior mid-CC and posterior CC were positively associated with greater motor learning.

These findings suggest that the theta and alpha bands are more related to motor learning than the beta band, which might merely relate to the level of perceived difficulty during learning.

Introduction

Motor learning – defined as acquiring new skills, improving existing skills, or regaining/reinforcing skills through practice – is critical for developing motor function at all stages of life.¹ However, the neurophysiology of motor learning is complex and not fully understood. Differences in brain structure and function² and genetic factors³ contribute to the variability in motor learning capacity among healthy individuals. To better understand this variability, investigators have analysed neurophysiologic correlates of motor learning by electroencephalography (EEG)/magnetoencephalography (MEG). This has allowed real-time monitoring of motor learning during rehabilitation,^{4,5} the development of brain-computer interfaces⁶, and the improvement of non-invasive brain stimulation techniques.⁷

Complex sequential learning tasks involve working memory, attention, and cognitive control and are easy to combine with neuroimaging. Previous imaging studies have revealed the involvement of various brain regions in complex motor learning, including the dorsolateral prefrontal cortex,⁸ anterior cingulate cortex (ACC),^{8,9} basal ganglia¹⁰ supplementary motor area, and primary motor cortex (M1).¹¹ M1 beta-band activity (14–30 Hz) is known to modulate with motor execution¹² and has been related to motor learning in studies with healthy subjects^{13–15} and patients suffering from neurological disorders.^{16,17} Studies with Parkinson's disease patients indicate reduced motor learning capacity results from the affected basal ganglia-thalamo-cortical network, reflected by enhanced beta power compared to healthy individuals.^{17,18} In addition to the beta band, motor learning has also been suggested to be related to theta (5–8 Hz), alpha (8–12 Hz), and gamma (60–90 Hz) frequency band modulation.^{17,19–21} However, none of these studies controlled for brain activity associated with performing the movement; therefore, it is unclear whether the activity is specifically associated with motor learning.

To address this point, this study aimed to investigate EEG-based neurophysiologic correlates of motor learning that solely reflect learning the movement by controlling for performing the movement. To this end, we used a complex motor learning task²² that induces motor learning²³ and a simplified motor task that requires very similar movement but induces little or no learning. During both tasks, participants applied a pinch force to a force transducer to move a cursor according to a fixed complex or simple sequence displayed on a computer screen. We administered both motor learning tasks in a within-subjects design to identify neurophysiologic correlates specific to online motor learning and not to motor movement. We do so by calculating the difference in learning between the complex motor learning task and the simple motor learning task and comparing these with differences in EEG power in the theta, alpha, and beta frequency bands. Although motor control also involves the gamma

band,²⁴ this is typically through phase-amplitude coupling (PAC) with slower oscillations,^{25–27} which is beyond the current analysis scope.

Methods

Participants

Twenty healthy volunteers participated in this experiment (age: 18–30 years, 13 females). Due to the explorative nature of the study, no a priori sample size estimation was performed. All participants provided written, informed consent before the experiment. Participants were self-reported as right-handed and free of any neuromuscular disorders. The study was approved by the medical ethics review board of the Erasmus University Medical Center (NL64529.078.18) and conducted in accordance with the Declaration of Helsinki (2013).

Experimental design

Participants performed 2 sequential visual isometric pinch tasks in a counterbalanced order: a complex motor task (CMT) that has been shown to induce learning over many repetitions and a simple motor task (SMT) which required little to no learning over repetitions. The CMT was adapted from previous research demonstrating that participants showed an approximately linear improvement within and over multiple sessions without reaching a plateau.^{22,23} The SMT was based on the CMT, but the task was made easier so that participants would reach an early learning plateau.

In both tasks (Figure 2.1 panel A and B), participants had to move a cursor from the “home” position to a target on the screen by pinching a force transducer between the right thumb and index finger. Between targets, the participant had to move the cursor back to the home position by releasing the force on the transducer. In the CMT, a trial consisted of moving the cursor to 1 of 5 targets sequentially, whereas in the SMT, the participant had to reach the same target 5 times. The relationship between pinch force and cursor position varied according to the maximum pinch force that was applied. In the CMT, the relationship was logarithmic: for low displacement, a small force increase produced a large displacement, and the displacement decreased with increasing pinch force. Because of the nonlinear nature of the force–cursor position relationship, motor learning was required to perform the task well (see Figure 2.1 panel D). In contrast, in the SMT the relationship between force and cursor position was linear and there was only a single, wide target; as such, it required little to no learning to perform the task well. We controlled for performing the movement in the CMT by ensuring that the average force required to reach five targets in a single trial was similar for both tasks.

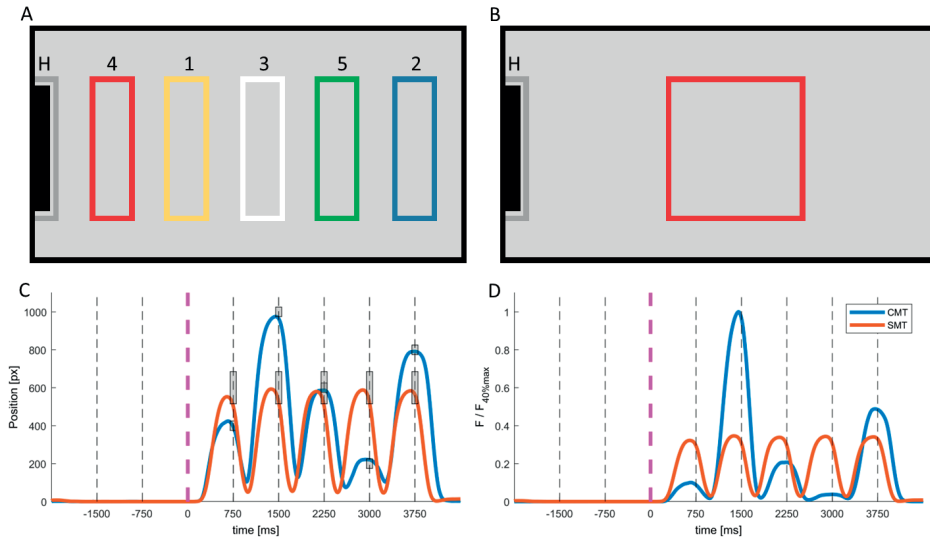


Figure 2.1. Overview of the experimental tasks. Panel A shows the complex motor task, in which participants had to move the black cursor from the ‘home’ position, indicated with ‘H’, in sequence to targets 1 to 5. Panel B: the simple motor learning task, in which participants had to move the black cursor inside the red target five consecutive times. Panel C and D show the average cursor position over time (C) and average force over time (D), respectively, of a single subject during the complex (blue) and simple (red) motor learning task. Dashed lines indicate a beep of the metronome. The magenta dashed line indicates the metronome beep corresponding to the start of the trial, at which the EEG amplifier received a synchronisation trigger. Black dashed lines succeeding the synchronisation trigger indicate metronome beeps at which targets had to be reached. The grey shaded areas indicate the margins in time (x-axis) and position (y-axis) for which the cursor position successfully reached the target.

A metronome (80 beats/min) provided cues for the start of the trial and the pace at which participants had to reach the target(s). The metronome was used to constrain the single-trial duration and to align trials to facilitate the EEG analysis. A countdown of 3 high-pitched beeps indicated the start of the trial. A synchronisation trigger was sent to the EEG amplifier upon the third high-pitched beep to indicate the start of each trial, set as $t=0$. After trial onset, as indicated by the metronome, participants had 750 ms to reach each target. A target was successfully reached if the maximum cursor position within a 50-ms time window around the metronome beep was within a 50-pixel window around the target’s centre (see Figure 2.1 panel C). This dichotomous measure was used as a single measure suitable to quantify performance in both the CMT and SMT. Numeric measures such as accuracy, precision, or error rate were not considered suitable, as they require a fixed reference point that cannot be defined for the SMT. Participants were instructed to reach correctly as many targets as possible in both tasks.

The CMT and SMT started with three practice blocks to familiarise the participant with the task, followed by 20 blocks of 10 trials. Consecutive blocks were separated by 30-s breaks and consecutive trials by 2 s. After each block, the percentage of successfully reached targets was presented to the participant. Furthermore, the percentage successfully reached targets per target for the latest block was provided.

For both tasks, learning was defined as the slope of the best fitting linear line through all the individual performance points per block. Previous studies employing the CMT describe subjects improve approximately linearly over time,^{22,23} making the slope a suitable quantity to describe learning. As such, positive slopes indicated learning, whereas negative slopes indicated a reduction in performance over time. The difference in slopes between the CMT and SMT was the final measure used for motor learning in the subsequent analysis to correct for (unexpected) learning in the SMT.

EEG recordings

EEG was performed throughout the experiment using 62 Ag–AgCl electrodes aligned according to the international 10–5 system²⁸ in an EEG gel head cap (TMSi, Enschede, The Netherlands). Two additional electrodes were placed at the right temple and slightly above the nasion to record horizontal and vertical eye movements, respectively. The ground electrode was positioned at the right mastoid. A bipolar montage was used to record muscle activity of the right first dorsal interosseous muscle. The impedance of all electrodes was maintained below 5 kOhm. All electrophysiologic data were collected at 2048 Hz, referenced to the common average, using a biosignal amplifier (Refa 128; TMSi) that received a synchronisation signal at the start of each CMT or SMT trial.

EEG analysis

EEG preprocessing

All data were processed using EEGLAB v14²⁹ in MATLAB (Mathworks, Natick, MA, USA). Each task's data were downsampled to 1024 Hz and then bandpass-filtered between 1 and 60 Hz (order: 3380) using EEGLAB's built-in finite impulse response filter. A notch filter was applied at 50 Hz (48–52 Hz, order: 1690) to remove apparent line noise identified in the power spectra of the data. The data of both tasks were concatenated to apply all the following steps on both the CMT and SMT data. Most importantly, this ensured that the source localisations were equal for both tasks to allow between-task comparisons of the EEG. Bad channels were detected by visual inspection and rejected, and the remaining channels were re-referenced to the common average. On average, 1.4 ± 1.54 (mean \pm standard deviation) electrodes were rejected.

Source-level analysis

For source-level analysis, the following steps were carried out on a copy of the continuous preprocessed data. The data were downsampled to 256 Hz to reduce the computation time of subsequent steps, and data points outside the window of -2 to 5 s around the synchronisation trigger ($t=0$) were removed. To keep as much data as possible during artefact rejection, we first split the remaining data into 0.5-s epochs. Then, a built-in automated rejection protocol was applied to remove bad epochs with data points above the epoch mean ± 6 times the standard deviation of the full 0.5-s epoch.

Adaptive mixture independent component analysis (ICA)³⁰ was performed on the clean 0.5-s data epochs of individual subjects to reconstruct the source-level activity of the recorded data. Due to our experimental design, EEG signals comprise a mixture of task-related sources of motor, visual, and auditory activity but also unrelated activity from artefacts such as eye movement and muscle activity. ICA is a reliable tool for separating different sources of cortical activity from each other and artifacts.³¹ ICA information (weight and sphering matrix) was copied back to the continuous preprocessed dataset. From this dataset, epochs of -2 to 5 s around the synchronisation trigger ($t=0$) were generated to obtain full-trial component activations. The full trials were cleaned by applying an automated rejection algorithm to the component activations to remove trials containing data points larger than the trial mean ± 6 standard deviations. Then, we verified by visual inspection that no noisy trials were included in the following steps. On average, 189.8 ± 5.5 and 190.3 ± 6.2 trials were included in the analysis for the CMT and SMT, respectively (mean \pm sd). Horizontal electrooculogram (EOG) components were visually identified on the time course of the signal that was most highly correlated with cursor position during the task. Vertical EOG components showed blinking only up to -1.5 s before the start of the trial and at the end of each trial. Both horizontal and vertical EOG components were discarded from the analysis.

Source localisation was performed on the independent components by fitting equivalent dipoles (DIPFIT 2.3 plugin for EEGLAB) to the cleaned component activations, simulated on a 3-compartment boundary element model derived from the MNI canonical template brain. The model consisted of compartments for scalp, skull, and brain with corresponding conductivities of 0.33 S/m, 0.0041 S/m and 0.33 S/m, respectively. A template brain with fixed conductivities results in approximate locations of the dipolar sources that generate the reconstructed source-level activity. Only components that could be fitted as a dipole in the brain with a residual variance $< 10\%$ ³¹ and with $1/f$ power spectra were considered for further analysis. All remaining components of all subjects were clustered by k-means clustering of the dipole location³² by minimising the distance between individual dipole locations and k means. The number of generated clusters was equal to the number of included components divided by the number of subjects. We set a minimum of 10 participants per cluster to be

retained for further analysis. The coordinates of the cluster means were used to approximate the brain region represented by the cluster based on the nearest grey matter point in Talairach coordinates.^{33,34}

Time–frequency representations of full trials of independent components included in the selected clusters were calculated based on Morlet wavelet convolutions at 100 logarithmically distributed frequency steps between 3 and 60 Hz and a linearly increasing number of cycles from 3 to 16. Time–frequency decompositions were calculated per subject per for both the CMT and SMT trials. Single trials were normalised by dividing by the mean full single-trial power spectrum before averaging over trials to reduce sensitivity to noise.³⁵ Multiple components of the same subject within a cluster were first averaged before averaging over all subjects.

Average power per motor task was calculated during trial execution ($t=[0, 3750]$ ms) within theta (5–8 Hz), alpha (8–12 Hz), and beta (14–30 Hz) frequency bands. We defined EEG power enhancement as event-related synchronisation (ERS) and power suppression as event-related desynchronisation (ERD). The EEG power ratio between CMT and SMT for every cluster was calculated and subtracted by 1 for the subsequent statistical analysis to correct for any unexpected learning in the SMT. As such, a power ratio of 0 indicates that EEG power was equal during both tasks. Positive values indicate that EEG power for a specific frequency band/cluster combination was higher during CMT compared to SMT.

Statistical analysis

We analysed the learning rate differences in the behavioural data using a linear mixed-effect model with main effects for *task* and *block* and an interaction term $task \times block$. Furthermore, the linear mixed-effects model included nested random intercepts and random (linear) slopes per subject per condition to describe between-subject variability in starting performance and learning rate. Using this model, we investigated the differences between the CMT and SMT in mean starting performance (main effect *task*) and learning rate (main effect *block* and interaction term $task \times block$).

To identify whether EEG correlates on motor learning, we fitted a generalised estimating equation (GEE) model. In the GEE model, EEG band power was the dependent variable. The GEE approach was used since the regression parameters are sensitive to random-effect assumptions. Given our objective is to investigate the population average of EEG power with covariate groups, we assume a GEE with robust sandwich estimators.³⁶ We included main effects for the independent variables *cluster*, *frequency band*, and *learning* in the model. Due to the sample size, we limited interactions to only the two-way interaction terms $cluster \times learning$ and $cluster \times frequency$. We computed the GEE's marginal effects to explore the relationship between learning and EEG band power per cluster. The marginal effects estimate

both an intercept and a slope to predict how EEG band power per cluster relates to motor learning. Given the nature of our measure for learning (the difference in learning slopes between CMT and SMT) and EEG power (the ratio $CMT/SMT-1$), significant positive slopes indicate that EEG power from a particular frequency band/cluster is positively associated with motor learning. Furthermore, significant intercepts indicate that the mean power in a frequency band – cluster combination was different between the CMT and SMT. All statistical analysis were performed in R 4.0.3 (R Core Team, 2019) and the packages *geepack*³⁷ and *nlme*.³⁸

Results

Motor learning

The main effects of the linear mixed effects model revealed that mean starting performance in the SMT ($\beta_0=78.5\%$, $SE=2.414$, $p<0.001$) was significantly higher than during the CMT ($\beta_0=-53.4\%$, $SE=3.41$, $p<0.001$). Furthermore, mean performance significantly increased over blocks in the SMT (main effect for *block*: $\beta_1=0.406$, $SE=0.128$, $p=0.002$), but more during the CMT (interaction term *block* \times *task* $\beta_1=0.529$, $SE=0.181$, $p=0.003$). The random effects (Figure 2.2) showed that 16/20 subjects (80%) had a steeper slope during the CMT compared to the SMT, indicating a greater degree of learning in the former task.

EEG

Source-level activity

EEG channel activations were localised and clustered into 5 distinct areas (Table 2.1 and Figure 2.3). The cluster centres were approximated to the contralateral IM1 and ipsilateral (i)M1 and CC (anterior mid-CC [aMCC], posterior [p]MCC,³⁹ and posterior CC [PCC]).

Visual inspection of the mean time-frequency decompositions of the bilateral M1 clusters shows during both tasks alpha and beta ERS during task preparation ($t=[-2, 0]$) and beta and alpha ERD during task execution ($t=[0, 3.75]$). For the aMCC cluster, theta ERD was observed during preparation, followed by theta ERS after trial onset. Theta ERS was time-locked to the auditory cue at 750-ms intervals after trial onset during the execution phase. In the SMT, these theta bursts were absent. In the pMCC cluster, theta ERS bursts were time-locked with the metronome to 750-ms intervals after trial onset in the mean time-frequency decompositions for both tasks. The PCC cluster exhibited an alpha ERD and theta ERS burst-like pattern time-locked to the metronome, and trial execution was also accompanied by beta ERD in both motor learning tasks. Interestingly, the alpha ERD bursts preceded the metronome beeps, whereas theta ERS bursts succeeded the metronome, suggesting that the activity was related to distinct parts of the motor task.

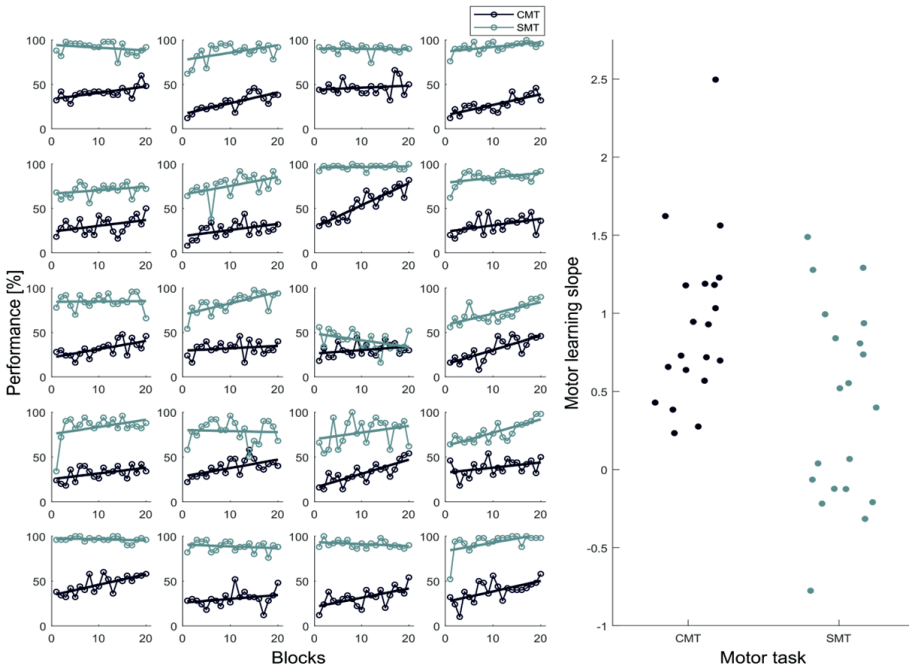


Figure 2.2. Left panel: performance (y-axis) per block (x-axis) of individual subjects. Performance in the CMT and SMT is shown in black and grey, respectively. The random intercept and slope for each condition indicate the starting performance and the degree of motor learning, respectively. Right panel: motor learning slopes (y-axis) sorted by task (x-axis).

Table 2.1. Source localisation results

Cluster	Number of subjects (components)	Coordinates of mean dipole location cluster centres, mm			
		X	Y	Z	Nearest Brodmann area
cM1	14 (19)	-43	-12	41	BA4
iM1	15 (21)	40	-9	39	BA6
aMCC	15 (18)	-3	28	23	BA32
pMCC	14 (17)	3	6	46	BA32
PCC	17 (23)	8	-32	39	BA31

Abbreviations: aMCC, anterior mid-cingulate cortex; cM1, contralateral primary motor cortex; iM1, ipsilateral primary motor cortex; pMCC, posterior mid-cingulate cortex; PCC: posterior cingulate cortex.

EEG-task performance

Analysis of the GEE model showed no main effect of learning ($\beta_1 = -0.008$, $SE = 0.009$, $p = 0.392$), but significant interaction effects between learning and the theta ($\beta_1 = 0.023$, $SE = 0.007$, $p < 0.001$) and alpha frequency band ($\beta_1 = 0.025$, $SE = 0.007$, $p < 0.001$). Additionally, there was a significant interaction between the PCC cluster and learning ($\beta_1 = 0.036$, $SE = 0.017$, $p = 0.036$).

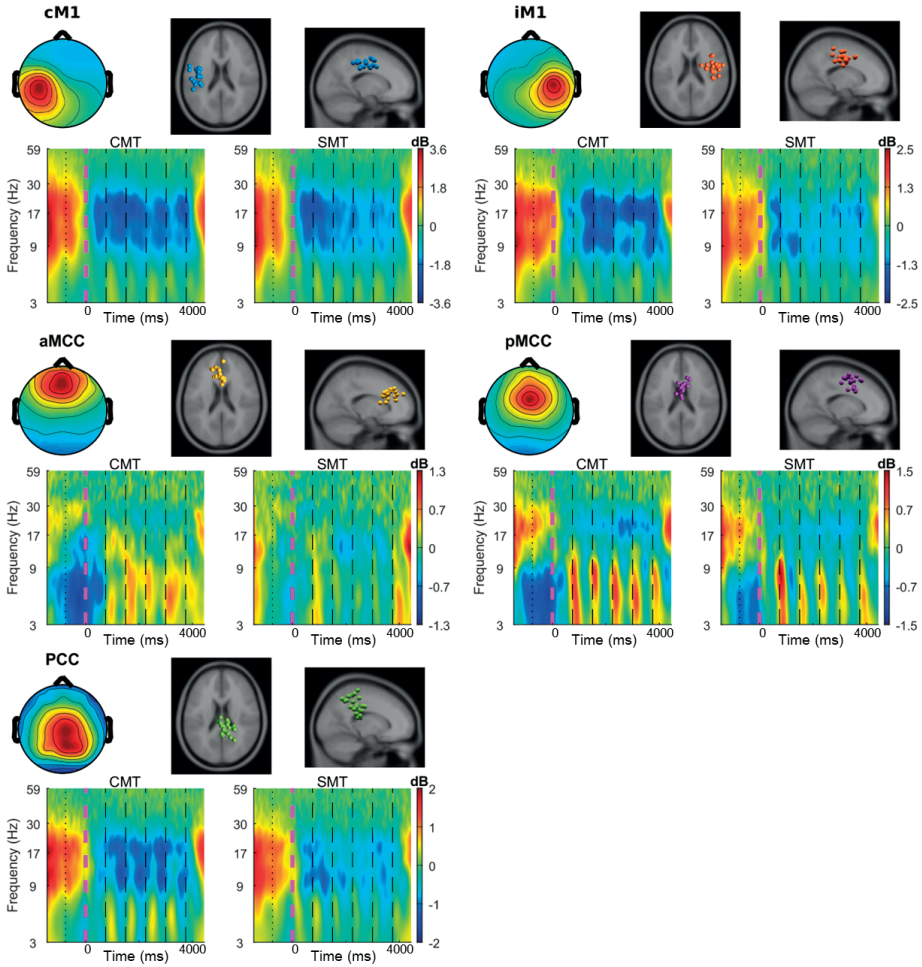


Figure 2.3. Cluster-wise visualisation of the time–frequency representation. For each cluster reported in Table 2.1, the upper row shows the scalp maps and positions of individual dipoles fitted in the standardised MNI152 brain. The lower row shows the time–frequency representations for CMT, SMT. The dashed magenta line indicates the start of the trial. Succeeding dashed black lines correspond to metronome beeps at which participants had to reach the targets in the task.

In addition to the main effects and interaction terms, we computed the GEE’s model marginal effects to explore the relationship between learning and frequency band per cluster (see Figure 2.4). The marginal effects indicated that in the cM1, learning was positively associated with both theta ($\beta_1=0.047$, $CI=[0.010, 0.085]$) and alpha power ($\beta_1=0.049$, $CI=[0.002, 0.097]$) but not with beta power ($\beta_1=0.024$, $CI=[-0.020, 0.068]$). Power in iM1 was not associated with higher learning rates for any of the analysed frequency bands. However, mean differences in EEG power were found in cM1 for the beta ($\beta_0=-0.061$, $CI=[-0.102, -0.020]$) band. In iM1, a mean difference was found for both the alpha ($\beta_0=-0.038$, $CI=[-0.068,$

-0.008]) and beta ($\beta_0=-0.056$, $CI=[-0.085, -0.026]$), indicating a difference between the motor learning tasks not translating into higher learning rates.

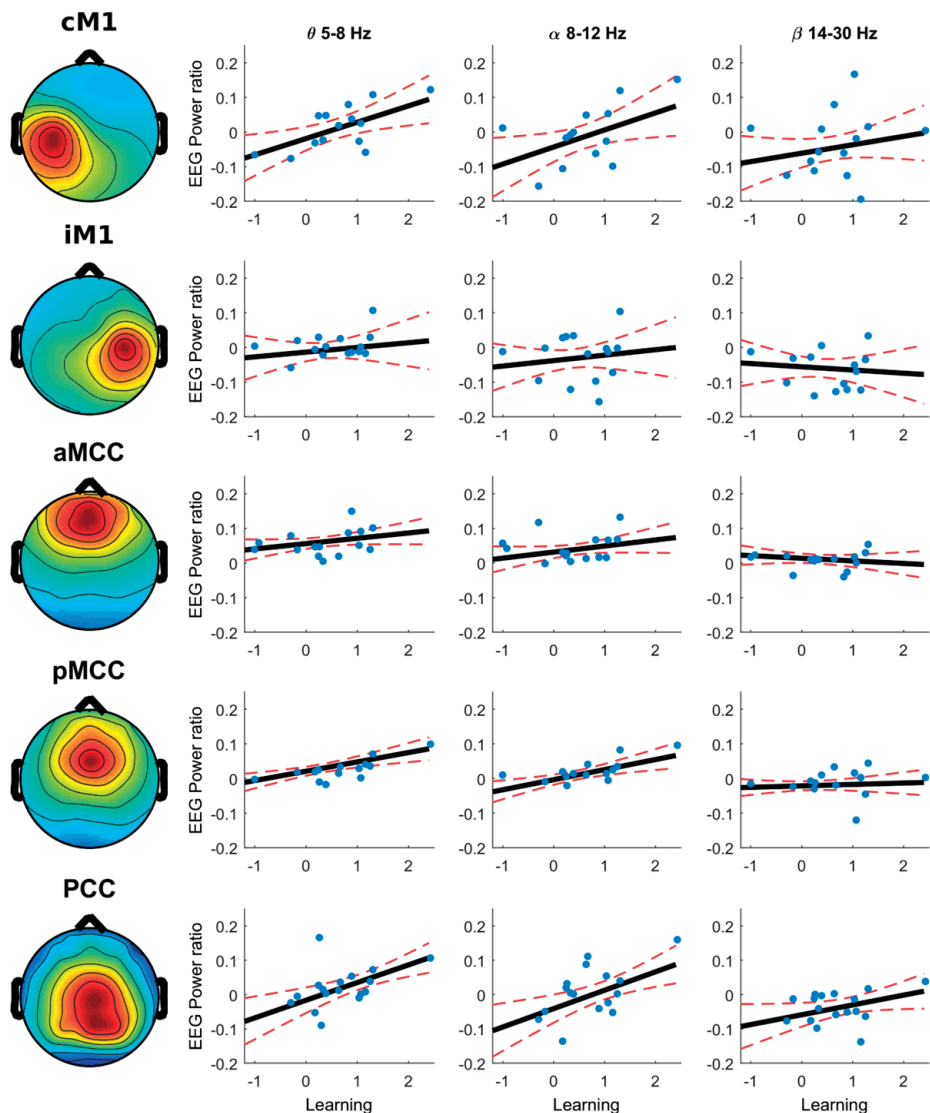


Figure 2.4. Cluster-wise visualisation of the marginal effects between the degree of motor learning and the EEG band power ratio during task execution ($t=[0, 3.75]$ minus 1. Column 1 shows scalp maps of corresponding clusters; columns 2–4 show theta, alpha, and beta band power ratios minus 1 (y axis) vs differences in learning slopes between CMT and SMT (x axis). Black lines show the marginal effects of the presented data; blue circles represent the individual data points, and the red lines the 95% confidence intervals of the estimated relationship.

For the cingulate cortex clusters, aMCC power was not associated with better learning. However, theta ($\beta_1=0.027$, $CI=[0.011, 0.043]$) and alpha ($\beta_1=0.029$, $CI=[0.010, 0.048]$) power in the pMCC and theta ($\beta_1=0.051$, $CI=[0.021, 0.082]$) and alpha ($\beta_1=0.054$, $CI=[0.017, 0.090]$) power in the PCC were both positively associated with motor learning. Full details of the analysis of the marginal effects can be found in Supplementary Table 2.1.

Discussion

Our study design was verified by participants learning more in the CMT than the SMT, although most participants also improved significantly in the SMT. In our evaluations of between-subject differences in learning and differences in EEG power, a higher degree of motor learning was positively associated with higher theta and alpha power in cM1, the pMCC and PCC. Bilateral M1 beta power was higher during the CMT than the SMT, but not associated with higher motor learning.

M1

Controlling for EEG activity related to performing a movement, we found a positive relationship between motor learning and M1 theta and alpha power, but not beta power. The positive association between motor learning and cM1 theta power observed in our study has been previously reported.¹⁷ Moreover, increasing theta power through neurofeedback was shown to improve learning in an explicit motor sequence task.⁴⁰ Both studies suggested that the relationship between motor learning and theta power was related to memory consolidation. However, in the present study, theta power relates to increased ongoing motor learning in a complex motor learning task. The nature of the CMT we applied requires changes in the motor plan, involving multiple brain regions from the motor network.⁴¹ Therefore, the relationship between motor learning and theta band activity fits with a previous report that relates the theta band to motor plan updates and communication between multiple brain regions.^{42,43} More specifically, theta band's role in communication between distant cortical regions has been shown by phase-amplitude coupling (PAC) with the gamma frequency band,²⁵ with higher theta power resulting in higher PAC. Additionally, M1-targeted gamma transcranial alternating current stimulation phase-locked to the theta band resulted in enhanced motor learning in an explicit motor learning task in healthy subjects.⁴⁴ In PD patients, M1 tACS enhanced cortical plasticity, reducing the effects of the impaired basal ganglia-thalamo-cortical network.⁴⁵ Given these reports, we believe that the positive association between learning and theta power in our study could reflect increased cortical plasticity by higher coupling with the gamma band and thus promoting motor learning.

In addition to theta power, cM1 alpha power was positively associated with motor learning. Motor cortical alpha oscillations show similar modulation as beta oscillations during voluntary movement, i.e., ERD during movement anticipation and execution and ERS in the absence of motor output.¹² Previous research with simultaneous EEG/fMRI during a motor task localised alpha-band activity to the post-central cortex, ie. Related to processing sensory information. In line with previous research,^{15,21} the positive relationship in the alpha band power and learning could reflect lower demand for sensory processing with skill acquisition.

In contrast with previous reports, we did not observe a relationship between M1 beta power and learning; the time-frequency decompositions during both motor tasks showed ERS during rest, ERD during motor execution, and a burst of ERS after the movement ended. It has been suggested that beta ERS represents a state of maintenance of the current motor plan, while beta ERD may be an adaptive state that enables learning.⁴⁶ Furthermore, beta activity is also suggested to be involved in working memory and information processing.⁴⁷ Following Engel and Fries (2010), enhanced beta suppression would be expected to coincide with better learning. This idea is supported by clinical studies with Parkinson's disease (PD) patients, who exhibit less M1 beta suppression and have reduced motor learning capacity.^{14,17} Similarly, stroke patients were found to have intact but lower learning capacity compared to healthy controls, accompanied by generally higher beta power.¹⁶ However, both PD and stroke patients often suffer from motor impairment in general, irrespective of learning capacity. Therefore, comparing patients with healthy controls cannot rule out that the identified beta power differences reflect limited motor control instead of limited motor learning.

Within healthy subjects, stronger beta power suppression was also associated with reduced reaction time¹⁵ and faster force production.⁴⁸ As cM1 beta power suppression results from motor output,¹² the relationship between beta suppression and reaction time¹⁵ and force production^{48,49} could merely relate to changes in motor output. In the motor task we employed, learning requires optimising a motor plan but not increasing force output or reaction time. By constraining the timing of both motor learning tasks with the metronome and controlling for motor force output with the SMT, the current study finds no relationship between motor learning and beta power.

An additional explanation for the lack of a relation between cM1 beta power and learning may be the time point at which we considered beta power since we considered beta power only during trial execution and not during the post-movement beta rebound. After voluntary movement, beta power typically shows a burst of ERS. This post-movement beta power has been associated with adjustments in motor plans^{16,50,51} but was currently not analysed.

There was less bilateral M1 beta ERD during execution of the SMT compared to the CMT, but individual differences in beta ERD did not correlate with differences in learning. Reduced iM1 beta ERD has previously been linked to lower perceived task difficulty in younger subjects than elderly⁵² and motor performance in healthy subjects compared to elderly.¹³ During unimanual motor tasks in right-handed subjects, the ipsilateral (right) hemisphere functions as a feedback processing system, whereas the contralateral (left) hemisphere acts as a feedforward predictive system.^{53,54} Thus, the amount of iM1 beta ERD may be related to perceived difficulty through increased reliance on supportive mechanisms during the CMT compared to the SMT. In line with this possibility, a combination of interindividual differences in motor learning capacity and perceived difficulty may explain why motor learning was unrelated to iM1 beta power in our study. Nonetheless, we would expect a reduction in ipsilateral beta ERD within subjects over a longer learning period in the CMT, although this was not investigated.

CC regions

Three additional clusters were localised to subregions of the CC, which is frequently associated with feedback processing.⁵⁵ The role of the MCC or dorsal ACC is typically analysed by measuring the scalp activity of the Fz or FCz electrode.⁵⁶ Through ICA combined with dipole fitting, we unexpectedly detected motor learning-related source-level activity in 2 additional, different CC subregions with different time-frequency patterns. These CC subregions have been previously investigated, but primarily using neuroimaging methods such as positron emission tomography (PET) and fMRI^{9,57,58} and less on an electrophysiologic level by EEG⁵⁹ or MEG.

The most apparent between-task differences in time-frequency decompositions were found in the aMCC—namely, theta and alpha ERS throughout the execution phase during the CMT but absent during the SMT. During the CMT, this ERD was observed in the high-frequency beta range (21–30 Hz), whereas low-frequency beta ERD (14–20 Hz) was more apparent during the SMT. The aMCC's activity was approximated to originate from the anterior cingulate motor area,⁵⁸ which is activated before M1 in motor control⁵⁷; moreover, the activity is thought to be related to attentional processes⁹. No relationship was found between any of the frequency bands in this cluster and motor learning. Therefore, the between-task EEG differences in the aMCC are likely related solely to the different demands that the CMT and SMT place on attention, working memory, and motor control to achieve good performance.

The pMCC is often associated with performance monitoring and feedback processing, which appeared in time-frequency decompositions through theta ERS bursts⁵⁶ that time-locked to the 750-ms interval of the metronome that indicated when the cursor had to reach the target

location. As such, the observed association between theta power and motor learning may reflect the importance of feedback on performance and errors while learning a complex motor task. Furthermore, the alpha band – which is often associated with attentional demands and memory⁶⁰ – was positively associated with motor learning. As a mechanism underlying feedback processing, higher pMCC theta power has been linked to increased connectivity to other brain regions such as M1.⁶¹ As such, higher theta power may drive motor learning through more efficient processing of visual feedback on performance and interact with M1 to enable adjustment of motor control. The positive association between alpha power and learning was unexpected, as it did not support the theory that alpha power suppression is proportional to increases in attentional demand, which would be expected in the CMT as compared to the SMT.⁶² However, it has also been suggested that attention and memory are modulated by different sub-bands of the alpha band.⁶⁰ Thus, it is possible that greater alpha power suppression during the SMT reflects an increased reliance on memory retrieval to maintain high performance. In contrast, less suppression during learning in the CMT corresponds to motor plan adjustments.

Finally, the third identified cluster in the CC was localised to the PCC, which is part of the default mode network and plays an important role in cognition, attention and memory.⁶³ In the PCC, alpha ERD bursts preceded the metronome ticks theta ERS bursts succeeded the metronome, suggesting distinct functions for the theta and alpha band related to retrieving/encoding task-related memory⁶⁴ or attentional processes.⁶⁵ Cona et al. (2020) suggest that increased theta ERS reflects internally directed attention and alpha ERD external attention. Consequently, participants who learn better might require less external information during the task, such as auditory cues or visual feedback. However, additional analyses are needed to understand how theta and alpha power are related to each other and learning.

Limitations

Our results were acquired by analysing EEG data recorded during a complex and simple explicit motor learning task. Therefore, it is unclear whether our results generalise to other motor learning task types such as adaptation learning or implicit learning. Furthermore, EEG records only cortical activity, although motor learning also involves subcortical structures such as the basal ganglia.⁴¹ We acquired our results by applying ICA-based source reconstruction, through which we identified task-related cortical activity localised to M1 and 3 clusters in the CC. A limitation of ICA is that none of the constructed clusters included all participants in the study, which reduced the statistical power of an already small sample size. Furthermore, the identified brain regions were determined by dipole fitting of independent components in a three-shell head model based on the MNI template brain model with default conductivity values for scalp, skull, CSF, and brain. However, intersubject variability in anatomy and particularly skull conductivity⁶⁶ influence dipole fitting accuracy.⁶⁷ For the M1 clusters, the source reconstruction

provided time–frequency decompositions typically observed during motor tasks, verifying the dipole localisation. However, this was not possible for the CC clusters due to the limited availability of electrophysiologic time–frequency activations in these regions. Only error-related theta modulation around the metronome ticks was available as a reference to verify the pMCC cluster’s location. Given these limitations, our study results should be taken as exploratory. Nonetheless, they provide a basis for more hypothesis-driven research to elucidate the EEG correlates of motor learning.

Conclusion

This study shows that – controlling for performing a movement – contralateral M1 theta and alpha but not beta power are positively associated with motor learning, as are theta and alpha power in the pMCC and PCC. In the beta band, M1 suppression was stronger during the CMT than during the SMT, but this was not associated with a higher degree of motor learning. Our findings support theta and alpha oscillations’ involvement in learning a complex, explicit motor task, possibly by enhancing communication between distant cortical regions, error monitoring and attentional processes. Furthermore, they suggest that M1 beta power merely relates to interindividual differences in the capability of performing but not learning a motor task. We propose that further analysis of theta cross–frequency interactions between M1, CC regions and the basal ganglia may provide additional insight into the electrophysiologic basis of complex motor learning.

References

1. Magill, R. & Anderson, D. Motor learning and control : concepts and applications / Richard A. Magill. (McGraw-Hill Education, 2017).
2. Tomassini, V. et al. Structural and functional bases for individual differences in motor learning. *Hum Brain Mapp* **32**, 494–508 (2011).
3. McHughen, S. A. et al. BDNF val66met polymorphism influences motor system function in the human brain. *Cerebral Cortex* **20**, 1254–1262 (2010).
4. Amo, C. et al. Induced gamma band activity from EEG as a possible index of training-related brain plasticity in motor tasks. *PLoS One* **12**, e0186008–e0186008 (2017).
5. Mane, R. et al. Prognostic and monitory EEG-biomarkers for BCI upper-limb stroke rehabilitation. *IEEE Transactions on Neural Systems and Rehabilitation Engineering* **27**, 1654–1664 (2019).
6. Saha, S. & Baumert, M. Intra- and Inter-subject Variability in EEG-Based Sensorimotor Brain Computer Interface: A Review. *Front Comput Neurosci* **13**, 87 (2020).
7. Thut, G. et al. Guiding transcranial brain stimulation by EEG/MEG to interact with ongoing brain activity and associated functions: A position paper. *Clinical Neurophysiology* **128**, 843–857 (2017).
8. Ghilardi, M. F. et al. Patterns of regional brain activation associated with different forms of motor learning. *Brain Res* **871**, 127–145 (2000).
9. Jueptner, M. et al. Anatomy of motor learning. I. Frontal cortex and attention to action. *J Neurophysiol* **77**, 1313–1324 (1997).
10. Brittain, J. S. & Brown, P. Oscillations and the basal ganglia: Motor control and beyond. *NeuroImage* vol. 85 637–647 Preprint at <https://doi.org/10.1016/j.neuroimage.2013.05.084> (2014).
11. Ashe, J., Lungu, O.V., Basford, A. T. & Lu, X. Cortical control of motor sequences. *Curr Opin Neurobiol* **16**, 213–221 (2006).
12. Pfurtscheller, G., Stancák, A. & Neuper, C. Post-movement beta synchronisation. A correlate of an idling motor area? *Electroencephalogr Clin Neurophysiol* **98**, 281–293 (1996).
13. Espenhahn, S. et al. Cortical beta oscillations are associated with motor performance following visuo-motor learning. *Neuroimage* **195**, 340–353 (2019).
14. Meziane, H. B. et al. Movement preparation and bilateral modulation of beta activity in aging and asking's disease. *PLoS One* **10**, e0114817–e0114817 (2015).
15. Pollok, B., Latz, D., Krause, V., Butz, M. & Schnitzler, A. Changes of motor-cortical oscillations associated with motor learning. *Neuroscience* **275**, 47–53 (2014).
16. Espenhahn, S. et al. Sensorimotor cortex beta oscillations reflect motor skill learning ability after stroke. *Brain Commun* **2**, (2020).
17. Meissner, S. N., Krause, V., Südmeyer, M., Hartmann, C. J. & Pollok, B. The significance of brain oscillations in motor sequence learning: Insights from Parkinson's disease. *Neuroimage Clin* **20**, 448–457 (2018).
18. Weiss, D. et al. Subthalamic stimulation modulates cortical motor network activity and synchronisation in Parkinson's disease. *Brain* **138**, 679–693 (2015).
19. Boonstra, T. W., Daffertshofer, A., Breakspear, M. & Beek, P. J. Multivariate time-frequency analysis of electromagnetic brain activity during bimanual motor learning. *Neuroimage* **36**, 370–377 (2007).
20. Sugata, H. et al. Modulation of Motor Learning Capacity by Transcranial Alternating Current Stimulation. *Neuroscience* **391**, 131–139 (2018).
21. Zhuang, P. et al. Event-related desynchronisation (ERD) in the alpha frequency during development of implicit and explicit learning. *Electroencephalogr Clin Neurophysiol* **102**, 374–381 (1997).

22. Reis, J. et al. Non-invasive cortical stimulation enhances motor skill acquisition over multiple days through an effect on consolidation. *Proc Natl Acad Sci U S A* **106**, 1590–1595 (2009).
23. Coxon, J. P., Peat, N. M. & Byblow, W. D. Primary motor cortex disinhibition during motor skill learning. *J Neurophysiol* **112**, 156–164 (2014).
24. Nowak, M., Zich, C. & Stagg, C. J. Motor Cortical Gamma Oscillations: What Have We Learnt and Where Are We Headed? *Curr Behav Neurosci Rep* **5**, 136–142 (2018).
25. Canolty, R. T. et al. High gamma power is phase-locked to theta oscillations in human neocortex. *Science* (1979) **313**, 1626–1628 (2006).
26. Chacko, R.V. et al. Distinct phase-amplitude couplings distinguish cognitive processes in human attention. *Neuroimage* **175**, 111–121 (2018).
27. Osipova, D., Hermes, D. & Jensen, O. Gamma Power Is Phase-Locked to Posterior Alpha Activity. *PLoS One* **3**, e3990 (2008).
28. Oostenveld, R. & Praamstra, P. The five percent electrode system for high-resolution EEG and ERP measurements. *Clinical Neurophysiology* **112**, 713–719 (2001).
29. Delorme, A. & Makeig, S. EEGLAB: An open source toolbox for analysis of single-trial EEG dynamics including independent component analysis. *J Neurosci Methods* **134**, 9–21 (2004).
30. Palmer, J. A., Makeig, S., Kreutz-Delgado, K. & Rao, B. D. Newton method for the ica mixture model. In *ICASSP, IEEE International Conference on Acoustics, Speech and Signal Processing – Proceedings 1805–1808* (IEEE, 2008). Doi:10.1109/ICASSP.2008.4517982.
31. Delorme, A., Palmer, J., Onton, J., Oostenveld, R. & Makeig, S. Independent EEG sources are dipolar. *PLoS One* **7**, e30135–e30135 (2012).
32. Arthur, D. & Vassilvitskii, S. K-means++: The advantages of careful seeding. In *Proceedings of the Annual ACM-SIAM Symposium on Discrete Algorithms vols 07-09-Janu 1027–1035* (2007).
33. Lancaster, J. L. et al. Automated asking of the human brain: A preliminary report on the development and evaluation of a forward-transform method. *Hum Brain Mapp* **5**, 238–242 (1997).
34. Lancaster, J. L. et al. Automated Talairach Atlas labels for functional brain mapping. *Hum Brain Mapp* **10**, 120–131 (2000).
35. Grandchamp, R. & Delorme, A. Single-trial normalisation for event-related spectral decomposition reduces sensitivity to noisy trials. *Front Psychol* **2**, 236 (2011).
36. Hubbard, A. E. et al. To GEE or not to GEE: Comparing population average and mixed models for estimating the associations between neighborhood risk factors and health. *Epidemiology* vol. 21 467–474 Preprint at <https://doi.org/10.1097/EDE.0b013e3181caeb90> (2010).
37. Halekoh, U., Hojsgaard, S. & Yan, J. The R package geepack for generalised estimating equations. *J Stat Softw* (2006) doi:10.18637/jss.v015.i02.
38. Pinheiro, J., Bates, D., DebRoy, S., Sarkar, D. & R Core Team. *Nlme: Linear and Nonlinear Mixed Effects Models*. <https://cran.r-project.org/package=nlme> (2020).
39. Vogt, B. A. Midcingulate cortex: Structure, connections, homologies, functions and diseases. *J Chem Neuroanat* **74**, 28–46 (2016).
40. Rozengurt, R., Barnea, A., Uchida, S. & Levy, D. A. Theta EEG neurofeedback benefits early consolidation of motor sequence learning. *Psychophysiology* **53**, 965–973 (2016).
41. Doyon, J. et al. Contributions of the basal ganglia and functionally related brain structures to motor learning. *Behavioural Brain Research* vol. 199 61–75 Preprint at <https://doi.org/10.1016/j.bbr.2008.11.012> (2009).
42. Caplan, J. B. et al. Human θ oscillations related to sensorimotor integration and spatial learning. *Journal of Neuroscience* **23**, 4726–4736 (2003).

43. Pellegrino, G., Tomasevic, L., Herz, D. M., Larsen, K. M. & Siebner, H. R. Theta Activity in the Left Dorsal Premotor Cortex During Action Re-Evaluation and Motor Reprogramming. *Front Hum Neurosci* **12**, 364 (2018).
44. Akkad, H. et al. Increasing motor skill acquisition by driving theta-gamma coupling. *bioRxiv* (2019) doi:10.1101/2019.12.20.883926.
45. Guerra, A. et al. Enhancing Gamma Oscillations Restores Primary Motor Cortex Plasticity in Parkinson's Disease. *Journal of Neuroscience* **40**, 4788–4796 (2020).
46. Engel, A. K. & Fries, P. Beta-band oscillations—signalling the status quo? *Curr Opin Neurobiol* **20**, 156–165–156–165 (2010).
47. Spitzer, B. & Haegens, S. Beyond the status quo: A role for beta oscillations in endogenous content (RE)activation. *eNeuro* vol. 4 Preprint at <https://doi.org/10.1523/ENEURO.0170-17.2017> (2017).
48. Joundi, R. A., Jenkinson, N., Brittain, J. S., Aziz, T. Z. & Brown, P. Driving oscillatory activity in the human cortex enhances motor performance. *Current Biology* **22**, 403–407 (2012).
49. Pogosyan, A., Gaynor, L. D., Eusebio, A. & Brown, P. Boosting Cortical Activity at Beta-Band Frequencies Slows Movement in Humans. *Current Biology* **19**, 1637–1641 (2009).
50. Tan, H., Wade, C. & Brown, P. Post-movement beta activity in sensorimotor cortex indexes confidence in the estimations from internal models. *Journal of Neuroscience* **36**, 1516–1528 (2016).
51. Schmidt, R. et al. Beta oscillations in working memory, executive control of movement and thought, and sensorimotor function. In *Journal of Neuroscience* vol. 39 8231–8238 (Society for Neuroscience, 2019).
52. Rossiter, H. E., Davis, E. M., Clark, E. v., Boudrias, M. H. & Ward, N. S. Beta oscillations reflect changes in motor cortex inhibition in healthy ageing. *Neuroimage* **91**, 360–365 (2014).
53. Davare, M., Duque, J., Vandermeeren, Y., Thonnard, J. L. & Olivier, E. Role of the ipsilateral primary motor cortex in controlling the timing of hand muscle recruitment. *Cerebral Cortex* **17**, 353–362 (2007).
54. Mutha, P. K., Haaland, K. Y. & Sainburg, R. L. Rethinking Motor Lateralization: Specialised but Complementary Mechanisms for Motor Control of Each Arm. *PloS One* **8**, e58582–e58582 (2013).
55. Shenhav, A., Botvinick, M. M. & Cohen, J. D. The expected value of control: An integrative theory of anterior cingulate cortex function. *Neuron* **79**, 217–240 (2013).
56. Cohen, M. X., Wilmes, K. & van de Vijver, I. Cortical electrophysiological network dynamics of feedback learning. *Trends Cogn Sci* **15**, 558–566 (2011).
57. Ball, T. et al. The role of higher-order motor areas in voluntary movement as revealed by high-resolution EEG and fMRI. *Neuroimage* **10**, 682–694 (1999).
58. Picard, N. & Strick, P. L. Motor areas of the medial wall: A review of their location and functional activation. *Cerebral Cortex* **6**, 342–353 (1996).
59. Herrojo Ruiz, M., Maess, B., Altenmüller, E., Curio, G. & Nikulin, V. V. Cingulate and cerebellar beta oscillations are engaged in the acquisition of auditory-motor sequences. *Hum Brain Mapp* **38**, 5161–5179 (2017).
60. Klimesch, W. EEG-alpha rhythms and memory processes. *International Journal of Psychophysiology* **26**, 319–340 (1997).
61. Cohen, M. X. Error-related medial frontal theta activity predicts cingulate-related structural connectivity. *Neuroimage* **55**, 1373–1383 (2011).
62. Klimesch, W. EEG alpha and theta oscillations reflect cognitive and memory performance: A review and analysis. *Brain Res Rev* **29**, 169–195 (1999).
63. Leech, R. & Sharp, D. J. The role of the posterior cingulate cortex in cognition and disease. *Brain* **137**, 12–32 (2014).

64. Kim, D., Jeong, W., Kim, J. S. & Chung, C. K. Single-Trial EEG Connectivity of Default Mode Network Before and During Encoding Predicts Subsequent Memory Outcome. *Front Syst Neurosci* **14**, 86 (2020).
65. Cona, G. et al. Theta and alpha oscillations as signatures of internal and external attention to delayed intentions: A magnetoencephalography (MEG) study. *Neuroimage* **205**, 116295 (2020).
66. McCann, H., Pisano, G. & Beltrachini, L. Variation in Reported Human Head Tissue Electrical Conductivity Values. *Brain Topogr* **32**, 825–858 (2019).
67. Vorwerk, J., Aydin, Ü., Wolters, C. H. & Butson, C. R. Influence of Head Tissue Conductivity Uncertainties on EEG Dipole Reconstruction. *Front Neurosci* **13**, 531 (2019).

Supplementary material

Supplementary Table 2.1. Results of the GEE model between EEG band power per cluster and frequency band, and learning.

Cluster	Intercept	CI95%	Slope	CI95%
cM1				
Theta	-0.019	-0.053, 0.015	0.047	0.010, 0.085
Alpha	-0.043	-0.086, 0.000	0.049	0.002, 0.097
Beta	-0.061	-0.102, -0.020	0.024	-0.020, 0.068
iM1				
Theta	-0.013	-0.040, 0.013	0.014	-0.027, 0.054
Alpha	-0.038	-0.068, -0.008	0.016	-0.028, 0.059
Beta	-0.056	-0.085, -0.026	-0.009	-0.051, 0.033
aMCC				
Theta	0.056	0.041, 0.071	0.015	-0.004, 0.035
Alpha	0.032	0.014, 0.049	0.018	-0.005, 0.040
Beta	0.014	0.000, 0.027	-0.008	-0.026, 0.011
pMCC				
Theta	0.021	0.008, 0.034	0.027	0.011, 0.043
Alpha	-0.004	-0.018, 0.011	0.029	0.010, 0.048
Beta	-0.021	-0.034, -0.008	0.004	-0.013, 0.021
PCC				
Theta	-0.017	-0.054, 0.021	0.051	0.021, 0.082
Alpha	-0.041	-0.082, 0.000	0.054	0.017, 0.090
Beta	-0.059	-0.093, -0.024	0.029	-0.004, 0.061

Abbreviations: aMCC, anterior mid-cingulate cortex; CI95%, 95% confidence interval of estimated coefficients; cM1, contralateral primary motor cortex; iM1, ipsilateral primary motor cortex; pMCC, posterior mid-cingulate cortex; PCC: posterior cingulate cortex.

Chapter 3

Transcranial direct current stimulation targeting the entire motor network does not increase corticospinal excitability

Joris van der Crujsen, Zeb D. Jonker, Eleni-Rosalina Andrinopoulou, Jessica E. Wijngaarden, Ditte A. Tangkau, Joke H.M. Tulen, Maarten A. Frens, Gerard M. Ribbers, Ruud W. Selles

Front. Hum. Neurosci. 16:842954. Doi: 10.3389/fnhum.2022.842954

Abstract

Transcranial direct current stimulation (tDCS) over the contralateral primary motor cortex of the target muscle (conventional tDCS) has been described to enhance corticospinal excitability, as measured with transcranial magnetic stimulation. Recently, tDCS targeting the brain regions functionally connected to the contralateral primary motor cortex (motor network tDCS) was reported to enhance corticospinal excitability more than conventional tDCS.

We compared the effects of motor network tDCS, 2 mA conventional tDCS, and sham tDCS on corticospinal excitability in 21 healthy participants in a randomized, single-blind within-subject study design. We applied tDCS for 12 minutes and measured corticospinal excitability with TMS before tDCS and at 0, 15, 30, 45, and 60 minutes after tDCS.

Statistical analysis showed that neither motor network tDCS nor conventional tDCS significantly increased corticospinal excitability relative to sham stimulation. Furthermore, the results did not provide evidence for superiority of motor network tDCS over conventional tDCS.

Motor network tDCS seems equally susceptible to the sources of intersubject and intrasubject variability previously observed in response to conventional tDCS.

Introduction

Research involving transcranial direct current stimulation (tDCS) has been growing exponentially since Nitsche & Paulus (2000) described its enhancing effects on the excitability of the motor system¹. Nitsche & Paulus (2000) applied transcranial magnetic stimulation (TMS) to assess changes in corticospinal excitability (CSE), reflected by motor evoked potentials (MEPs). They reported that motor evoked potentials significantly increased after 10 minutes of tDCS to the contralateral primary motor cortex (cM1). In tDCS motor studies, it has frequently been suggested that tDCS could lead to better motor learning²⁻⁵ and could benefit motor rehabilitation, for example after stroke.^{6,7} On the other hand, however, other studies have failed to demonstrate a consistent effect of tDCS on corticospinal excitability⁸⁻¹¹ and motor learning.^{12,13}

A significant part of the tDCS effectiveness research focuses on finding optimal stimulation parameters to improve the reliability and magnitude of tDCS effects. These stimulation parameters include stimulation duration,^{1,14} focality,¹⁵ and location. For instance, stimulation of the premotor cortex, instead of the M1, has been found to result in a more robust increase in M1 excitability.^{16,17} These findings indicate that stimulating other motor-related brain regions than the M1 can also modulate corticospinal excitability.

Recently, applying tDCS to regions functionally connected to the M1 was found to increase corticospinal excitability more than stimulation of M1 alone.¹⁸ The rationale behind motor network tDCS was that the contralateral M1 does not act in isolation but communicates with functionally connected brain regions; consequently, brain regions connected to contralateral M1 influence the effect of stimulation on the contralateral M1. Therefore, Fischer et al.¹⁸ hypothesized that multifocal stimulation of the entire motor system would result in a larger change in corticospinal excitability. Although the stimulation field strength directly on the contralateral M1 was lower during motor network tDCS than for conventional tDCS,¹⁸ the increase in corticospinal excitability was larger during motor network than conventional stimulation. Therefore, motor network tDCS may provide new leads to more effective tDCS interventions and a better understanding of the physiological basis of corticospinal excitability.

The promising results of motor network tDCS on corticospinal excitability have been described by only a single study. Since reproducibility in tDCS has been challenged due to low sample sizes¹⁹ and intersubject and intrasubject variability,^{8,11,20-23} replicating these findings is necessary to assess the reliability of motor network tDCS. Therefore, the primary goal of our study was to verify in a within-subject design if tDCS applied to the entire motor network leads to higher increases in corticospinal excitability than conventional tDCS

targeting only the contralateral M1. The secondary goal of the study was to assess whether motor network tDCS and conventional tDCS increased corticospinal excitability compared to sham stimulation.

Methods

Participants

Twenty-one healthy subjects participated in this study (age: 18 to 30 years; 13 female). All participants gave written informed consent before the experiment. Participants were self-reported right-handed and free of known neuromuscular disorders. The study was approved by the medical ethics review board of the Erasmus University Medical Center (NL64529.078.18). All experimental procedures were conducted in accordance with the Declaration of Helsinki (2013).

Experimental design

TDCS conditions

Participants received non-invasive brain stimulation in three different tDCS configurations in a randomized, counterbalanced order in three experimental sessions separated by at least 48 hours.²⁴ Randomization of the applied stimulation configuration was performed a priori for the entire study. The participants were fully blinded, and the investigators were partially blinded to the applied tDCS condition due to the different electrode locations in which stimulation electrodes were inserted for each stimulation configuration. To blind participants, stimulation electrodes were inserted in all nine electrode locations used in this experiment, regardless of whether the electrodes were used in a specific electrode configuration. Since the StarStim8 only allows connecting eight electrodes, the investigators could not be blinded to the difference between motor network and conventional tDCS. However, investigators were blinded to the difference between motor network and sham tDCS.

All tDCS was applied using a StarStim8 stimulator (NeuroElectrics, Spain) and a 128-channel EEG cap (TMSi, the Netherlands) which was aligned according to the international 10/5 system.²⁵ We used platinum stimulation electrodes that could be manually inserted into any electrode location of the EEG cap. The surface contact area of the stimulation electrodes with the scalp was 0.79 cm². We injected Sigma Gel (Parker Laboratories, New Jersey, USA) and used NIC 2.1 software (NeuroElectrics, Spain) to reduce the skin-electrode impedance below 2 k Ω when stimulation was applied.

Motor network tDCS

Motor network tDCS (Figure 3.1A) was performed as described by Fischer et al.¹⁸ to stimulate the entire motor network with 8 electrodes in total. Positive stimulation electrodes were placed over the primary motor cortices at C1, C2, C3, C4, T8 with input currents of 0.872 mA, 0.888 mA, 1.135 mA, 0.922 mA, and 0.183 mA, respectively. Negative stimulation electrodes were inserted at Fz, P3, and P4 with currents of -1.843 mA, -1.121 mA, and -1.035 mA, respectively. An additional electrode was inserted at the Fp2 channel (only actively used during conventional tDCS) to blind participants to the difference between motor network and conventional tDCS.

Conventional tDCS

Conventional tDCS (Figure 3.1B) was based on Nitsche & Paulus¹ with a single positive electrode placed over the contralateral primary motor cortex and a negative electrode on the ipsilateral supra orbita. Contrary to the original report by Nitsche & Paulus, we placed the anode at C3 instead of directly above the motor hand area. C3 has been used as a standardized alternative in studies in which stimulation was applied through an EEG head cap, leading to similar changes in corticospinal excitability.^{18,26,27} Using standardized locations, we inserted a positive stimulation electrode at C3 and a negative stimulation electrode at Fp2. A 2-mA current was generated in between these electrodes to stimulate the contralateral primary motor cortex. Compared to motor network tDCS, the injection currents used for conventional tDCS lead to the highest current density (25.46 A/m²) at the scalp. This current density has been described as safe, with minimal sensation and no skin damage.²⁸ To blind the participants, stimulation electrodes were also inserted at the electrode locations used for motor network tDCS.

Motor network sham

Sham tDCS (Figure 3.1A) has been widely used as a control condition in tDCS/TMS research and mimics the sensation of active tDCS.²⁹ Sham protocols only inject current at the beginning and the end of stimulation, resembling what participants experience in active stimulation conditions. We used the same electrode locations as the motor network condition in our sham stimulation.

Stimulation protocol

The total stimulation duration was 12 minutes for all stimulation conditions. Both non-sham stimulation conditions consisted of three phases: 1) ramp up, in which the stimulation intensity linearly builds up from 0% to 100% in 60 seconds, 2) 10 minutes of constant stimulation at 100%, and 3) 60 seconds ramp down in which current linearly reduced from 100% to 0%. The sham condition was designed to give the same sensation as during active stimulation.²⁹ It, therefore, consisted of a similar ramp-up phase of 60 seconds, directly followed by a ramp down phase of 60 seconds, which was repeated 10 minutes after the start of the stimulation session, resulting in a total duration of 12 minutes. In the sham condition, injection currents were built up to the same levels as motor network stimulation.

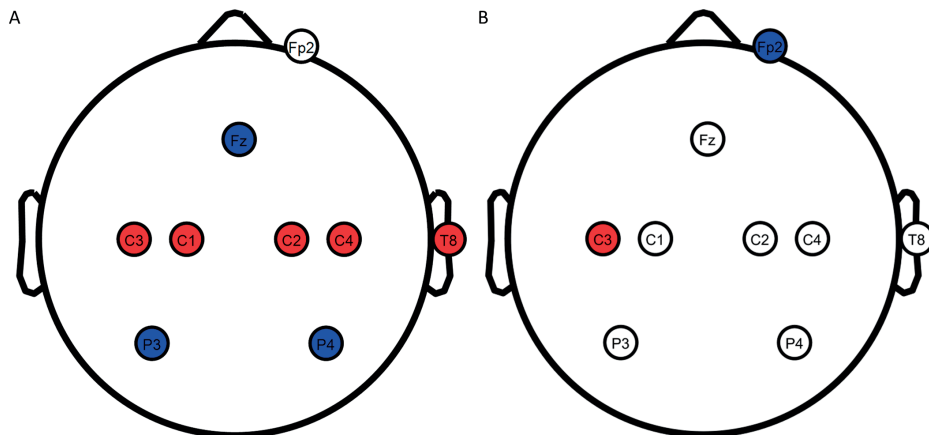


Figure 3.1. TDCS electrode configurations overview. (A) motor network and sham tDCS configurations. (B) conventional tDCS configuration. Red: anodes; blue: cathodes; white: electrodes not actively used for the stimulation configuration. Stimulation electrodes were inserted at all locations in all conditions to blind the participants from the applied configuration.

Corticospinal excitability measurements

We assessed corticospinal excitability³⁰ before we applied tDCS and at 0, 15, 30, 45, and 60 minutes after tDCS finished. Corticospinal excitability was assessed by measuring MEPs from the first dorsal interosseous (FDI) resulting from monophasic TMS pulses (MagPro X100 stimulator with an MC-B70 figure-eight coil, MagVenture, Denmark) applied to the motor hand area guided by a neuronavigational system (Polaris Spectra motion tracking system, NDI, Canada and Visor2 software, ANT Neuro, the Netherlands) to ensure MEP stability³¹. We calculated MEPs from EMG activity, recorded at 5000 Hz with Ag/AgCl electrodes in a belly-tendon montage connected to a custom biosignal amplifier (TMSi, the Netherlands).

From the EMG data, MEPs were online calculated as the largest peak-to-peak amplitude within 50 ms after a TMS pulse. The motor hand area was identified as the scalp location corresponding to the highest recorded MEPs. We stimulated at 50% of the maximum stimulator output on the motor cortex region (around C3 electrode) as an initial starting location to find the motor hand area. Throughout this process, we held the TMS coil tangent to the scalp, with the coil handle in the posterolateral direction rotated 45 degrees from the midline. We increased the stimulation intensity in 5% increments until a scalp location was found for which the MEP exceeded 50 μ V. At this location, about 10 to 20 pulses were required to determine the RMT, i.e., the stimulation intensity resulting in an MEP greater than 50 μ V with a probability of 50%.³²

At this motor hand area, corticospinal excitability was assessed before tDCS (baseline) and 0, 15, 30, 45, and 60 minutes after tDCS using a fixed series of 65 TMS pulses on each time point. In these series, the inter-stimulus interval varied randomly between 2 and 5 seconds at a stimulation intensity of 120% of the RMT. Coil position and orientation relative to the scalp were monitored in real-time using the neuronavigational system to ensure a constant position throughout the measurement. EMG activity preceding the TMS pulses was also visually monitored. If persistent EMG activity was detected, we paused the TMS pulses and instructed participants to relax their muscles while providing real-time visual feedback on their EMG activity. The coil position during all TMS pulses and all EMG data were stored for offline analysis.

Power estimation

We estimated the statistical power to find a significant tDCS effect based on the MEP data published by Fischer et al.¹⁸ We considered the baseline-normalized data and identified the mean and standard errors of the mean (SEM) at time points directly after tDCS, and at 15, 30 and 60 minutes after the intervention. Due to the unbalanced distribution of these time points, the grand average of corticospinal excitability is biased towards early time points, where post-tDCS corticospinal excitability is generally lower. Therefore, we added a measurement point at 45 minutes after tDCS by linearly interpolating the MEP means and SEMs at 30 and 60 minutes to compensate for this bias. We calculated the statistical power to find a significant effect between motor network tDCS and conventional tDCS, between motor network tDCS and sham tDCS, and conventional tDCS and sham tDCS.

The power analysis was performed by simulation, assuming corticospinal excitability was normally distributed around each time point. For motor network tDCS and conventional tDCS, we considered the data of the left hemisphere, and for sham tDCS, we used the data recorded from the right M1 during conventional tDCS targeting the left M1. We converted all SEMs to standard deviations by multiplying with the square root of the sample size (15) of Fischer et al. (2017)¹⁸. Using the means and standard deviations, we calculated the MEP ratios (\pm sd) averaged over all time points (motor network tDCS: 1.324 ± 0.284 ; conventional tDCS: 1.151 ± 0.144 ; sham tDCS: 1.008 ± 0.151), removing the time information to enhance statistical power. We simulated 10,000 data sets for sample sizes ranging from 10 to 50 subjects. We applied a linear mixed effect model (see Section 0) with a fixed intercept and fixed term for stimulation condition to each dataset to investigate if post-tDCS/pre-tDCS MEP ratio differed between tDCS configurations. For each sample size, we extracted the number of p-values below 0.05 as a measure for statistical power. The simulations showed that a sample size of 21 subjects had a power of 70% to find that motor network tDCS significantly ($p < .05$) increases the post/pre-tDCS MEP ratio compared to conventional stimulation. Additional computations showed that the inclusion of 21 subjects in a within-

subjects design provided a power of 99% to find that motor network tDCS increases the MEP ratio compared to sham tDCS, and a power of 86% to find that conventional tDCS increases the MEP ratio compared to sham tDCS.

Analysis

We calculated MEPs from the raw, continuous EMG data using Eeglab³³ for experimental sessions. We first high-pass filtered the data (3 Hz, order: 1650) and then calculated MEPs as the peak-to-peak amplitude of the EMG signal within 50 ms after each TMS pulse. The mean and standard deviation (sd) of the coil position for all MEPs were calculated per session. Any TMS pulses applied while the coil position exceeded the mean coil position + 3 sd were discarded from the analysis. Furthermore, TMS pulses in which the pre-TMS EMG amplitude in the 100 ms before the pulse exceeded the mean EMG amplitude + 3 sd of all pulses within an experimental session were removed. The remaining pulses were considered the cleaned MEP data.

As a first step in the statistical analysis, we investigated if baseline corticospinal excitability differed between experimental sessions by applying a linear mixed-effects model. We defined two mixed-effects models with random intercepts per subject. For the full model, we included an intercept and the variable *stimulation condition* in the fixed-effects part. In both models, visual inspection indicated that baseline corticospinal excitability required a log-transform to ensure the residuals were normally distributed and homoscedastic. The likelihood ratio test was applied between both models to determine if baseline corticospinal excitability systematically varied between stimulation conditions. By doing so, we could identify potential systematic differences in baseline excitability that could intervene with any condition effects.

Since the variability in tDCS response has previously been attributed to intersubject variability, we screened for the presence of consistent responders in our sample. We looked for consistent responders in our data and defined those as subjects in which both network and conventional stimulation resulted in MEP ratios greater than one and were higher than the MEP ratio recorded during sham tDCS. We calculated the individual response to each stimulation condition as the ratio between the grand average of post-tDCS MEPs and baseline corticospinal excitability. As such, ratios above 1 correspond to enhanced cortical excitability, considered positive responses.

Next, we assessed the group effects of the different tDCS configurations on MEP ratios by applying a linear mixed-effects model with a random intercept per subject and a fixed effect term for *stimulation condition*. We evaluated two versions of the linear mixed-effects model. In the first model, visual inspection indicated log-transform was required for the outcome to ensure the residuals were both normally distributed and homoscedastic. In the second

model, we performed a sensitivity analysis in which we removed outliers from the data, after which the residuals were normally distributed and homoscedastic, and the data was modelled accordingly. In this second mixed-effect model, we subtracted 1 from all MEP ratios, such that the intercept of the model corresponding to the average MEP ratio of sham stimulation could be interpreted. Finally, we investigated if the MEP ratio depended on baseline excitability by calculating the correlation coefficient between baseline excitability and the MEP ratio. After visually evaluating the distribution of MEP ratio and baseline corticospinal excitability, we calculated Pearson's correlation coefficient for each stimulation condition. All statistical analyses were performed in MATLAB (Mathworks, Natick, MA, USA).

Results

TMS data

Subject-specific resting motor threshold and baseline corticospinal excitability per condition are described in Supplementary Table 3.1. One participant (319) was unable to undergo the conventional stimulation protocol due to technical issues with the tDCS device. Within subjects, the mean (\pm sd) difference between the highest and lowest resting motor threshold (RMT) in all experimental sessions was $5\% \pm 3$, indicating that RMTs were relatively constant over multiple sessions. On average, we discarded 6.2 ± 3.8 trials per subject from the analysis because the coil position deviated too much from the mean coil position or because too strong EMG activity preceded the TMS pulse. Comparison of the full and null linear mixed-effects models indicated the differences in baseline corticospinal excitability between sham stimulation ($2203 \pm 1562 \mu\text{V}$), conventional tDCS ($1753 \pm 1349 \mu\text{V}$), and motor network tDCS ($2043 \pm 1252 \mu\text{V}$) were non-significant ($\lambda_{LR}(2) = 1.45, p = .485$).

Corticospinal excitability – subject level

Inspection of the MEP ratios for the different tDCS conditions (Figure 3.2) indicated that during conventional tDCS, three subjects were outliers compared to the rest of the subjects. These subjects had MEP ratios higher than 2, compared to the condition median of 1.01. The baseline excitability of these subjects was lower than the condition average ($1860 \pm 1297 \mu\text{V}$) with $482.6 \mu\text{V}$, $489.6 \mu\text{V}$ and $514.1 \mu\text{V}$. In our data, MEP ratios above 1 were found 11 times during sham, 12 times during conventional, and 11 times during network stimulation, but corticospinal excitability was not consistently modulated within subjects as hypothesized. More specifically, only one subject could be considered a consistent tDCS responder, i.e. showing an increase in corticospinal excitability for network and conventional tDCS greater than registered during sham stimulation. All other subjects had at least once MEP ratios below 1 for conventional or network tDCS or a stronger response from sham stimulation compared to conventional or network tDCS.

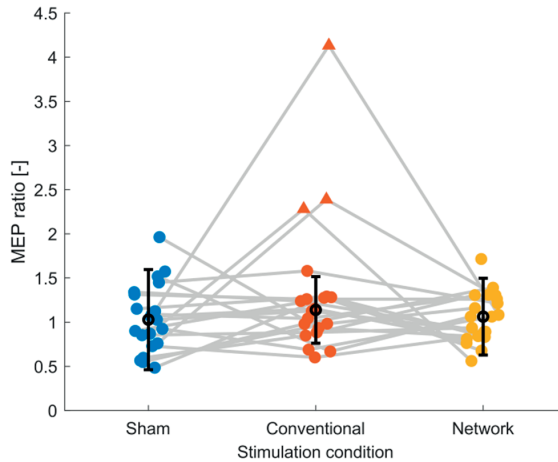


Figure 3.2. Scatter plot of the post-tDCS/pre-tDCS MEP ratio for sham, conventional and network tDCS. Each data point corresponds to a single subject. Three subjects, shown as triangles, were considered outliers (outside the median (black marker) ± 1.5 times the interquartile range (error bars), explaining the high standard deviations and the relatively high group response observed after conventional tDCS. Data of the same subject are connected with grey lines. Note: jitter was applied to the plot to enhance the readability.

Corticospinal excitability – group level

The group-level statistical analysis on the post-tDCS/pre-tDCS MEP ratios revealed no effect for conventional stimulation ($b = 0.198$, $t(59) = 1.755$, $p = .084$) or network stimulation ($b = 0.035$, $t(59) = 0.317$, $p = .753$), indicating that averaged over all subjects tDCS did not enhance corticospinal excitability relative to sham stimulation. The average time courses of corticospinal excitability are shown in Supplementary Figure 3.1. Due to the three outliers identified in Figure 3.2 in the conventional tDCS response, we performed a sensitivity analysis to determine the effect of outliers on the statistical analysis. When we excluded the three outlier subjects from all three conditions and applied the linear mixed-effects model, the conventional condition effect (MEP ratio (mean \pm sd): $1.05 \pm 0.26 \mu\text{V}$) diminished ($b = -0.005$, $t(50) = -0.052$, $p = .959$) and the network effect (MEP ratio (mean \pm sd): $1.05 \pm 0.26 \mu\text{V}$) remained equally low ($b = -0.007$, $t(50) = -0.071$, $p = .944$). In addition, the model's intercept ($b = 0.061$, $t(50) = 0.822$, $p = .415$), i.e. the response to sham tDCS (MEP ratio (mean \pm sd): $1.06 \pm 0.40 \mu\text{V}$), indicated that there was no mean change in corticospinal excitability for the control condition. Overall, these results indicate that MEP ratios were highly variable and on average for both conventional and motor network tDCS were equal to sham stimulation. Finally, we found that baseline excitability did not correlate with the MEP ratio of sham ($p = .27$), conventional ($p = .05$) or network tDCS ($p = .14$).

Discussion

The primary goal of this study was to investigate if tDCS targeting the motor network of healthy subjects leads to larger changes in corticospinal excitability compared to conventional stimulation. Compared to sham stimulation, our sample of 21 healthy participants showed no significant increase in corticospinal excitability after motor network tDCS or conventional tDCS. Consequently, the results did not provide evidence for the superiority of motor network tDCS over conventional tDCS.

Our study is, to our knowledge, the first that attempts to replicate the effect of motor network tDCS on corticospinal excitability. We conducted the experiment in a larger sample ($n = 21$) than the original study ($n = 15$).¹⁸ Furthermore, we added sham stimulation as a control condition to distinguish potential TMS effects from tDCS effects. Nonetheless, no effect of motor network tDCS relative to conventional or even sham stimulation was found in our study. The inability to replicate the effects of motor network tDCS on corticospinal excitability fits with previous studies that recently challenged the potential of conventional tDCS^{8,9,34,35} and hd-tDCS³⁶ to enhance corticospinal excitability.

Several factors may explain why we found no effect of motor network tDCS on corticospinal excitability. First, we did not control for intersubject and intrasubject variability in baseline corticospinal excitability. Previous studies that described positive effects of anodal tDCS controlled baseline corticospinal excitability by adjusting TMS intensity to elicit MEPs between 1 mV and 1.5 mV.^{37,38} However, this would increase the intersubject variability in stimulation intensity, increasing the likelihood of stimulation intensity being an extraneous variable. Importantly, we found baseline corticospinal excitability did not correlate with the change in corticospinal excitability after tDCS. Also, baseline corticospinal excitability did not significantly vary between sessions in our sample. Furthermore, several studies show that adjusting TMS intensity to control for baseline corticospinal excitability is not a prerequisite for finding positive tDCS effects.^{38–41} Therefore, we do not consider variability in baseline excitability to explain the absence of a tDCS effect in our study.

A second factor explaining why tDCS did not affect corticospinal excitability could be the applied TMS protocol. In our study, the number of TMS pulses was relatively high (65 per interval; 390 per session) and the inter-stimulus-interval relatively short (2 to 5 seconds), which can affect corticospinal excitability,^{42,43} and potentially intervene with a tDCS effect. However, a similar number of pulses has been used to demonstrate the enhancing effect of anodal tDCS on corticospinal excitability.⁹ Furthermore, we used a sham condition to distinguish tDCS from potential effects on corticospinal excitability introduced by the TMS protocol. Our statistical analysis revealed no effect of sham stimulation on corticospinal

excitability. Consequently, we argue that our TMS protocol did not interfere with potential tDCS effects.²¹ We also inspected the response per subject for the three stimulation conditions to investigate subgroups of tDCS *responders* in our sample. Previous research has shown that in the absence of group effects, subgroups of tDCS responders may exist.⁹ While MEP ratios above 1 were found in all conditions, there was no consistent corticospinal excitability enhancement for conventional and network tDCS in individual subjects. Only in one subject, conventional and network tDCS resulted in a stronger increase of cortical excitability compared to sham stimulation.

Finally, we applied TMS only on the contralateral motor cortex, which is different compared to Fischer et al. (2017), who applied TMS to both hemispheres. Thus, the effect of motor network tDCS described by Fischer et al. (2017) could originate from a combination of bilateral mixed TMS and tDCS and therefore be absent in our current study. An additional difference is the smaller electrode size we used for tDCS. Smaller electrodes lead to more focal electric fields in the brain.⁴⁴ Together with the standardized electrode locations we used, it could thus be that the peak electric fields were not located at the intended M1 target due to interindividual differences in brain anatomy relative to standardized EEG locations.⁴⁵ Nonetheless, modelling studies indicate that the small stimulation electrodes generate electric fields in M1 that exceed those of large electrodes (up to 35 cm²) in a broad cortical area,⁴⁴ supporting the use of small electrodes in standardized EEG locations.

There are some limitations in our study that need to be considered. First, the primary goal of this study is somewhat limited by the relatively low power for the comparison between motor network tDCS and conventional tDCS. Our a priori power calculation, based on the data published by Fischer et al., indicated that our within-subject design of 21 healthy participants provided 70% chance of finding an effect of motor network tDCS relative to conventional tDCS. Thus, we should be careful with concluding that motor network stimulation is non-superior compared to conventional stimulation. However, because we did not find effects of both motor network tDCS and conventional tDCS relative to sham tDCS, despite high a priori powers for these comparisons (99% and 86%, respectively), it is unlikely that one intervention worked better than the other.

An additional limitation follows from the conventional sham protocol, which is under debate because it was shown that sham stimulation could not reliably mask active stimulation from sham stimulation in within-subject design studies.^{46–48} Recently, new protocols have been suggested to better blind participants from active stimulation, for instance, by continuous stimulation in a montage that exceeds the skin's perception threshold but is not strong enough to pass the skull⁴⁹. However, we were unaware of this alternative type of sham stimulation at the start of the data collection of this study. Although these limitations with the

used sham protocol exist, it allowed us to distinguish potential effects on corticospinal excitability of the used TMS protocol from the potential effects of tDCS. However, questionnaires about the participants' awareness of the used tDCS configurations could have helped control awareness-related tDCS response effects.

Finally, our statistical analysis did not control for sources of intersubject variability, such as genetics,^{12,50,51} the electric field strength at stimulated brain areas,^{52,53} or intrasubject variability, such as circadian or hormonal cycles.²⁰ One source of intrasubject variability was caused by the difference in stimulation currents of motor network tDCS and conventional tDCS, which resulted in different current densities at the contralateral M1. Due to safety constraints,²⁸ it was not possible to match the current densities between the two conditions. Consequently, it remains an open question whether the original findings of motor network tDCS are due to stimulation of the entire motor network or if they reflect the previously described non-linear relationship between the tDCS response and electric field strength at the contralateral M1.⁵⁴

In conclusion, our study provides no evidence that motor network tDCS or conventional tDCS increases corticospinal excitability compared to sham tDCS. Consequently, the results did not provide evidence for superiority of motor network tDCS over conventional tDCS. While the rationale for tDCS targeting the entire motor network could be valid from the neurophysiological perspective, our results indicate that motor network tDCS might be equally susceptible to sources of intrasubject and intersubject variability as previously demonstrated for conventional tDCS. Including neurophysiologic measures such as EEG or magnetic resonance spectroscopy to control intrasubject and intersubject variability may facilitate the exploration of the potential of motor network tDCS and tDCS in general.

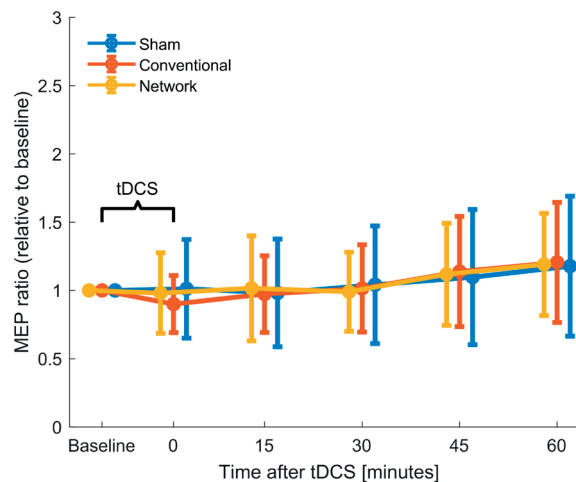
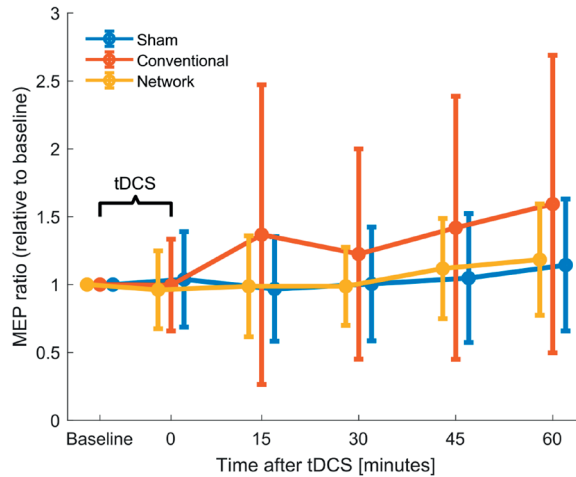
References

1. Nitsche, M. A. & Paulus, W. Excitability changes induced in the human motor cortex by weak transcranial direct current stimulation. *Journal of Physiology* **527**, 633–639 (2000).
2. Antal, A. *et al.* Facilitation of visuo-motor learning by transcranial direct current stimulation of the motor and extrastriate visual areas in humans. *European Journal of Neuroscience* **19**, 2888–2892 (2004).
3. Reis, J. *et al.* Noninvasive cortical stimulation enhances motor skill acquisition over multiple days through an effect on consolidation. *Proceedings of the National Academy of Sciences* **106**, 1590–1595–1590–1595 (2009).
4. Stagg, C. J. *et al.* Polarity and timing-dependent effects of transcranial direct current stimulation in explicit motor learning. *Neuropsychologia* **49**, 800–804 (2011).
5. Saucedo Marquez, C. M., Zhang, X., Swinnen, S. P., Meesen, R. & Wenderoth, N. Task-Specific Effect of Transcranial Direct Current Stimulation on Motor Learning. *Front Hum Neurosci* **7**, 333 (2013).
6. Santos Ferreira, I. *et al.* Searching for the optimal tDCS target for motor rehabilitation. *Journal of NeuroEngineering and Rehabilitation* vol. 16 90 Preprint at <https://doi.org/10.1186/s12984-019-0561-5> (2019).
7. Hummel, F. C. & Cohen, L. G. Non-invasive brain stimulation: a new strategy to improve neurorehabilitation after stroke? *Lancet Neurology* vol. 5 708–712 Preprint at [https://doi.org/10.1016/S1474-4422\(06\)70525-7](https://doi.org/10.1016/S1474-4422(06)70525-7) (2006).
8. Jonker, Z. D. *et al.* No effect of anodal tDCS on motor cortical excitability and no evidence for responders in a large double-blind placebo-controlled trial. *Brain Stimul* **14**, 100–109 (2021).
9. Wiethoff, S., Hamada, M. & Rothwell, J. C. Variability in response to transcranial direct current stimulation of the motor cortex. *Brain Stimul* **7**, 468–475 (2014).
10. Bastani, A. & Jaberzadeh, S. A-tDCS differential modulation of corticospinal excitability: The effects of electrode size. *Brain Stimul* **6**, 932–937 (2013).
11. Dyke, K., Kim, S., Jackson, G. M. & Jackson, S. R. Intra-Subject Consistency and Reliability of Response Following 2 mA Transcranial Direct Current Stimulation. *Brain Stimul* **9**, 819–825 (2016).
12. van der Vliet, R., Ribbers, G. M., Vandermeeren, Y., Frens, M. A. & Selles, R. W. BDNF Val66Met but not transcranial direct current stimulation affects motor learning after stroke. *Brain Stimul* **10**, 882–892 (2017).
13. Ammann, C., Spampinato, D. & Márquez-Ruiz, J. Modulating motor learning through transcranial direct-current stimulation: An integrative view. *Front Psychol* **7**, (2016).
14. Agbooda, D., Samani, M. M., Jamil, A., Kuo, M.-F. & Nitsche, M. A. Expanding the parameter space of anodal transcranial direct current stimulation of the primary motor cortex. *Scientific Reports* **2019 9:1** **9**, 1–11 (2019).
15. Dmochowski, J. P., Datta, A., Bikson, M., Su, Y. & Parra, L. C. Optimized multi-electrode stimulation increases focality and intensity at target. *J Neural Eng* **8**, 046011 (2011).
16. Lefebvre, S. *et al.* Differences in high-definition transcranial direct current stimulation over the motor hotspot versus the premotor cortex on motor network excitability. *Sci Rep* **9**, (2019).
17. Boros, K., Poreisz, C., Münchau, A., Paulus, W. & Nitsche, M. A. Premotor transcranial direct current stimulation (tDCS) affects primary motor excitability in humans. *European Journal of Neuroscience* **27**, 1292–1300 (2008).
18. Fischer, D. B. *et al.* Multifocal tDCS targeting the resting state motor network increases cortical excitability beyond traditional tDCS targeting unilateral motor cortex. *Neuroimage* **157**, 34–44 (2017).
19. Minarik, T. *et al.* The importance of sample size for reproducibility of tDCS effects. *Front Hum Neurosci* **10**, 1–5 (2016).

20. Horvath, J. C., Carter, O. & Forte, J. D. Transcranial direct current stimulation: Five important issues we aren't discussing (but probably should be). *Front Syst Neurosci* **8**, 1–8 (2014).
21. Horvath, J. C., Forte, J. D. & Carter, O. Evidence that transcranial direct current stimulation (tDCS) generates little-to-no reliable neurophysiologic effect beyond MEP amplitude modulation in healthy human subjects: A systematic review. *Neuropsychologia* **66**, 213–236 (2015).
22. López-Alonso, V., Fernández-del-Olmo, M., Costantini, A., Gonzalez-Henriquez, J. J. & Cheeran, B. Intra-individual variability in the response to anodal transcranial direct current stimulation. *Clinical Neurophysiology* **126**, 2342–2347 (2015).
23. López-Alonso, V., Cheeran, B., Río-Rodríguez, D. & Fernández-Del-Olmo, M. Inter-individual variability in response to non-invasive brain stimulation paradigms. *Brain Stimul* **7**, 372–380 (2014).
24. Alonzo, A., Brassil, J., Taylor, J. L., Martin, D. & Loo, C. K. Daily transcranial direct current stimulation (tDCS) leads to greater increases in cortical excitability than second daily transcranial direct current stimulation. *Brain Stimul* **5**, 208–213 (2012).
25. Oostenveld, R. & Praamstra, P. The five percent electrode system for high-resolution EEG and ERP measurements. *Clinical Neurophysiology* **112**, 713–719 (2001).
26. Murray, L. M. *et al.* Intensity Dependent Effects of Transcranial Direct Current Stimulation on Corticospinal Excitability in Chronic Spinal Cord Injury. *Arch Phys Med Rehabil* **96**, S114–S121 (2015).
27. Rawji, V. *et al.* tDCS changes in motor excitability are specific to orientation of current flow. *Brain Stimul* **11**, 289–298 (2018).
28. Bikson, M., Datta, A. & Elwassif, M. Establishing safety limits for transcranial direct current stimulation. *Clinical Neurophysiology* **120**, 1033–1034 (2009).
29. Woods, A. J. *et al.* A technical guide to tDCS, and related non-invasive brain stimulation tools. *Clinical Neurophysiology* vol. 127 1031–1048 Preprint at <https://doi.org/10.1016/j.clinph.2015.11.012> (2016).
30. Barker, A. T., Jalinous, R. & Freeston, I. L. Non-Invasive Magnetic Stimulation of Human Motor Cortex. *The Lancet* vol. 325 1106–1107 Preprint at [https://doi.org/10.1016/S0140-6736\(85\)92413-4](https://doi.org/10.1016/S0140-6736(85)92413-4) (1985).
31. Julkunen, P. *et al.* Comparison of navigated and non-navigated transcranial magnetic stimulation for motor cortex mapping, motor threshold and motor evoked potentials. *Neuroimage* **44**, 790–795 (2009).
32. Awiszus, F. & Borckardt, J. TMS motor threshold assessment Tool 2.0.
33. Delorme, A. & Makeig, S. EEGLAB: An open source toolbox for analysis of single-trial EEG dynamics including independent component analysis. *J Neurosci Methods* **134**, 9–21 (2004).
34. Horvath, J. C., Vogrin, S. J., Carter, O., Cook, M. J. & Forte, J. D. Effects of a common transcranial direct current stimulation (tDCS) protocol on motor evoked potentials found to be highly variable within individuals over 9 testing sessions. *Exp Brain Res* **234**, 2629–2642 (2016).
35. Tremblay, S. *et al.* Systematic assessment of duration and intensity of anodal transcranial direct current stimulation on primary motor cortex excitability. *European Journal of Neuroscience* **44**, 2184–2190 (2016).
36. Pellegrini, M., Zoghi, M. & Jaberzadeh, S. The effects of transcranial direct current stimulation on corticospinal and cortico-cortical excitability and response variability: Conventional versus high-definition montages. *Neurosci Res* **166**, (2020).
37. Kuo, H. I. *et al.* Comparing cortical plasticity induced by conventional and high-definition 4 × 1 ring tDCS: A neurophysiological study. *Brain Stimul* **6**, 644–648 (2013).
38. Nitsche, M. A. *et al.* GABAergic modulation of DC stimulation-induced motor cortex excitability shifts in humans. *European Journal of Neuroscience* **19**, 2720–2726 (2004).
39. Pellicciari, M. C., Brignani, D. & Miniussi, C. Excitability modulation of the motor system induced by transcranial direct current stimulation: A multimodal approach. *Neuroimage* **83**, 569–580 (2013).

40. Di Lazzaro, V. *et al.* The effects of prolonged cathodal direct current stimulation on the excitatory and inhibitory circuits of the ipsilateral and contralateral motor cortex. *J Neural Transm* **119**, 1499–1506 (2012).
41. Lang, N., Nitsche, M. A., Paulus, W., Rothwell, J. C. & Lemon, R. N. Effects of transcranial direct current stimulation over the human motor cortex on corticospinal and transcallosal excitability. *Exp Brain Res* **156**, 439–443 (2004).
42. Pellicciari, M. C., Miniussi, C., Ferrari, C., Koch, G. & Bortoletto, M. Ongoing cumulative effects of single TMS pulses on corticospinal excitability: An intra- and inter-block investigation. *Clinical Neurophysiology* **127**, 621–628 (2016).
43. Julkunen, P., Säisänen, L., Hukkanen, T., Danner, N. & Könönen, M. Does second-scale intertrial interval affect motor evoked potentials induced by single-pulse transcranial magnetic stimulation? *Brain Stimul* **5**, 526–532 (2012).
44. Mikkonen, M., Laakso, I., Tanaka, S. & Hirata, A. Cost of focality in TDCS: Interindividual variability in electric fields. *Brain Stimul* **13**, 117–124 (2020).
45. Scrivener, C. L. & Reader, A. T. Variability of EEG electrode positions and their underlying brain regions: visualizing gel artifacts from a simultaneous EEG-fMRI dataset. *Brain Behav* **12**, e2476 (2022).
46. Ambrus, G. G. *et al.* The fade-in – Short stimulation – Fade out approach to sham tDCS – Reliable at 1 mA for naïve and experienced subjects, but not investigators. *Brain Stimul* **5**, 499–504 (2012).
47. Fonteneau, C. *et al.* Sham tDCS: A hidden source of variability? Reflections for further blinded, controlled trials. *Brain Stimul* **12**, 668–673 (2019).
48. Greinacher, R., Buhöt, L., Möller, L. & Learmonth, G. The time course of ineffective sham-blinding during low-intensity (1 mA) transcranial direct current stimulation. *European Journal of Neuroscience* **50**, 3380–3388 (2019).
49. Neri, F. *et al.* A novel tDCS sham approach based on model-driven controlled shunting. *Brain Stimul* **13**, 507–516 (2020).
50. Teo, J. T. H. *et al.* Late cortical plasticity in motor and auditory cortex: role of met-allele in BDNF Val66Met polymorphism. *Int J Neuropsychopharmacol* **17**, 705–713 (2014).
51. Antal, A. *et al.* Brain-derived neurotrophic factor (BDNF) gene polymorphisms shape cortical plasticity in humans. *Brain Stimul* **3**, 230–237 (2010).
52. Laakso, I., Mikkonen, M., Koyama, S., Hirata, A. & Tanaka, S. Can electric fields explain inter-individual variability in transcranial direct current stimulation of the motor cortex? *Sci Rep* **9**, 1–10 (2019).
53. Laakso, I., Tanaka, S., Koyama, S., De Santis, V. & Hirata, A. Inter-subject variability in electric fields of motor cortical tDCS. *Brain Stimul* **8**, 906–913 (2015).
54. Batsikadze, G., Moliadze, V., Paulus, W., Kuo, M. F. & Nitsche, M. A. Partially non-linear stimulation intensity-dependent effects of direct current stimulation on motor cortex excitability in humans. *J Physiol* **591**, 1987 (2013).

Supplementary material



Supplementary Figure 3.1 Group-average change in corticospinal excitability, averaged over all subjects. The x-axis shows time in minutes, and the y-axis the baseline normalised MEPs in μV . The error bars reflected standard deviations over the subjects per time point. Left: time courses of corticospinal excitability before the removal of 3 outlier subjects. Right: time courses of corticospinal excitability after the removal of 3 outlier subjects.

Supplementary Table 3.1. Baseline corticospinal excitability and resting motor threshold (RMT) per participant.

Subject	Sham		Conventional		Motor Network	
	Baseline	RMT	Baseline	RMT	Baseline	RMT
301	2314.3	68	490.2	71	3680.3	71
302	660.4	51	489.6	48	3511.6	54
303	3089.4	63	1449.7	59	1076.7	56
304	1788.7	52	1651.4	51	2601.8	54
305	2248.9	53	3558.1	60	1436.1	52
306	3289.2	66	2360.2	60	1996.0	62
307	1450.1	68	6051.9	66	2282.1	65
308	497.7	68	921.0	75	605.6	76
309	908.1	71	1752.2	72	1096.8	70
310	2525.4	48	653.0	46	1210.7	52
311	1889.9	50	1991.8	51	2068.4	48
312	1261.5	54	1261.9	58	1232.6	62
313	3084.4	44	1185.1	44	2449.3	44
314	7500.7	40	3253.2	37	4026.1	40
315	2692.4	61	2635.9	59	2053.5	62
316	1000.3	59	1916.1	63	5514.4	56
317	1276.2	53	1461.8	55	1326.5	56
318	705.6	68	958.2	65	874.2	74
319	1458.0	63	NA	NA	1820.0	66
320	4325.6	59	2603.4	53	1286.0	62
321	2487.3	80	548.5	83	729.6	88

Baseline: corticospinal excitability (μV) averaged over all pre-tDCS MEPs; RMT: resting motor threshold in percentage of maximum stimulator output.

Chapter 4

ASH: an Automatic pipeline to generate realistic and individualised chronic Stroke volume conduction Head models

Maria Carla Piastra, Joris van der Crujisen, Vitória Piai, Floor E M Jeukens, Mana Manoochehri, Alfred C Schouten, Ruud W Selles, Thom Oostendorp

J. Neural Eng. 18 044001. Doi: 10.1088/1741-2552/abf00b

Abstract

Objective. Large structural brain changes, such as chronic stroke lesions, alter the current pathways throughout the patients' head and therefore have to be taken into account when performing transcranial direct current stimulation simulations.

Approach. We implement, test and distribute the first MATLAB pipeline that automatically generates realistic and individualised volume conduction head models of chronic stroke patients by combining the already existing software SimNIBS, for mesh generation and lesion identification with neighbourhood data analysis, for lesion identification. To highlight the impact of our pipeline, we investigated the sensitivity of the electric field distribution to the lesion location and lesion conductivity in 16 stroke patients' datasets.

Main results. Our pipeline automatically generates 1 mm-resolution tetrahedral meshes, including the lesion compartment in less than three hours. Moreover, for large lesions, we found a high sensitivity of the electric field distribution to the lesion conductivity value and location.

Significance. This work facilitates optimising electrode configurations with the goal of obtaining more focal brain stimulations of the target volumes in rehabilitation for chronic stroke patients.

Introduction

Stroke is the leading cause of long-term adult disability worldwide. According to the World Health Organization, one out of six people suffers from a stroke.¹ During a stroke, a deficit in oxygen supply due to either a haemorrhage or an infarction causes damage to a certain brain area, lesioning the tissue. In 80% of the cases, the motor cortex is involved.²

Transcranial direct current stimulation (tDCS) is one of the therapeutic interventions aiming at stimulating the reorganisation of the motor cortex to improve motor impairments and enhance recovery. TDCS is considered a viable tool due to its limited side effects, safety, availability, portability and relatively low costs.³ During tDCS, anodal and cathodal electrodes are placed on the scalp, and a low-intensity direct current, commonly between 0.5 and 2 mA, is delivered and conducted by head tissues. It has been reported that cortical regions exposed to higher electric field strength are more likely to modulate.⁴ Therefore, in motor stroke rehabilitation, for example, it is crucial to target the motor cortex precisely and with a sufficiently strong electric field.

So far, literature shows mixed findings regarding stroke patients' response to tDCS brain stimulation.^{3,5} Targeting the correct cortical area by identifying the optimal electrode configuration is indeed still a challenge in tDCS and in brain stimulation in general.⁶ Volume conduction effects, which are subject-dependent, determine the current pathways throughout the head and will be affected by large structural brain changes, such as stroke lesions, in terms of lesion location and conductivity, which is so far unknown or inconsistent throughout the literature.⁷⁻⁹

Simulations with volume conduction models that include the lesion compartment might, therefore, improve and guide tDCS stroke rehabilitation. Furthermore, fulfilling safety margins, i.e., the maximal electric field strength distribution, which is safe to induce in the head, can be secured via simulations. Here, we present a pipeline that enables performing safety and tolerability tests on the skin of the participant,¹⁰ as well as in the brain tissue.

There are several software tools dedicated to simulating brain stimulation.¹¹⁻¹³ In our study, we focused on SimNIBS.¹³ SimNIBS is a free and open-source software package for the simulation of non-invasive brain stimulation, which allows calculating the electric field induced by transcranial magnetic stimulation (TMS) and transcranial electric stimulation¹ in a realistic head model. SimNIBS uses the finite element method to simulate brain stimulation and therefore requires volumetric meshes. However, by default, stroke lesions are not auto-

1 <https://simnibs.github.io/simnibs/build/html/index.html>

matically included in the volumetric meshes created by modelling tools such as SimNIBS. Lesion compartments can be identified from MRI scans either by dedicated software tools like^{14,15} or manually by researchers. A disadvantage of manual identification is that it is highly time-consuming and rater dependent.

The aim of our study is to implement, test, and distribute an automatic MATLAB-based pipeline, ASH (an automatic pipeline to generate realistic and individualised chronic stroke volume conduction head models), that provides a realistic and individualised volumetric mesh of chronic stroke patients. ASH is SimNIBS compatible, makes use of lesion identification with neighbourhood data analysis (LINDA) to automatically identify the lesion, and can facilitate large-scale group analysis in stroke patients. In addition, to demonstrate the impact of our pipeline, we conducted tDCS simulations in SimNIBS on data from 16 stroke patients to show the sensitivity of the electric field distribution to the lesion location and lesion conductivity.

Methods

In this section, we describe: (1) the dataset used in the study; (2) the MATLAB pipeline that automatically generates volume conduction head models for chronic stroke patients; (3) the SimNIBS tDCS simulations.

The dataset

In this study, we analysed T1-weighted (T1w) MRI scans of 16 chronic stroke patients. The first MRI scan (subject 401) was obtained in a previous study¹⁶ and was acquired with a 3T scanner (GE Discovery MR750). The other 15 subjects were scanned at the Donders Centre for Cognitive Neuroimaging with a 3T MAGNETOM Prisma or a 3T MAGNETOM PrismaFit scanner. The anonymised MRI scans of the latter group are available online as a Donders Data Sharing Collection,¹⁷ together with the output data of this study and the MATLAB code. MRIs of the 15 subjects were acquired under the approval of the Ethics Committee ‘CMO regio Arnhem-Nijmegen’ (NL58437.091.17). Written informed consent was received from each chronic stroke patient.

The pipeline

The MATLAB-based automatic pipeline we introduce requires as input a T1w MRI of the subject and generates a realistic and individualised volumetric mesh which includes the lesion compartment of a chronic stroke patient. As already mentioned, the ASH pipeline uses the SimNIBS¹³ and LINDA¹⁵ software toolboxes. A sketch of the pipeline is visualised in Figure 4.1, and its application requires the four following steps:

- 1) MRI data selection: To create individualised models, SimNIBS requires a T1-weighted image. T2-weighted images are optional but highly recommended. LINDA requires a T1-weighted image only; therefore, we used anonymised, defaced, and realigned (to RAS orientation) T1w MRI scans.
- 2) Segmentation and meshing of the whole head: The T1w MRI is processed by SimNIBS, generating a tetrahedral volumetric mesh with six homogeneous and isotropic compartments: scalp, skull, eyes, cerebrospinal fluid (CSF), grey matter, and white matter. In particular, we utilise the SimNIBS function *headreco* with the option *cat* which leads to the use of SPM12¹⁸ with the extension library CAT12¹⁹ for the segmentation routine. Segmentations with CAT12 have a more accurate reconstruction of the cortical grey and white matter.
- 3) Segmentation of the lesion: Since the segmentation and meshing of the lesion compartment are not performed by SimNIBS, we use LINDA. LINDA is a neuroimaging toolkit for the automatic segmentation of chronic stroke lesions based on machine learning techniques.¹⁵ LINDA requires a T1w MRI as input and generates a volumetric mask of the lesion.
- 4) Generation of the final mesh: The volumetric mesh generated in step 2 is modified to incorporate the lesion compartment generated in step 3. To do so, the mesh elements whose centroids are within the lesion mask are relabelled as ‘lesion’. In addition, we make sure that the resulting lesion compartment does not contain elements of the scalp, skull, or eye compartments.

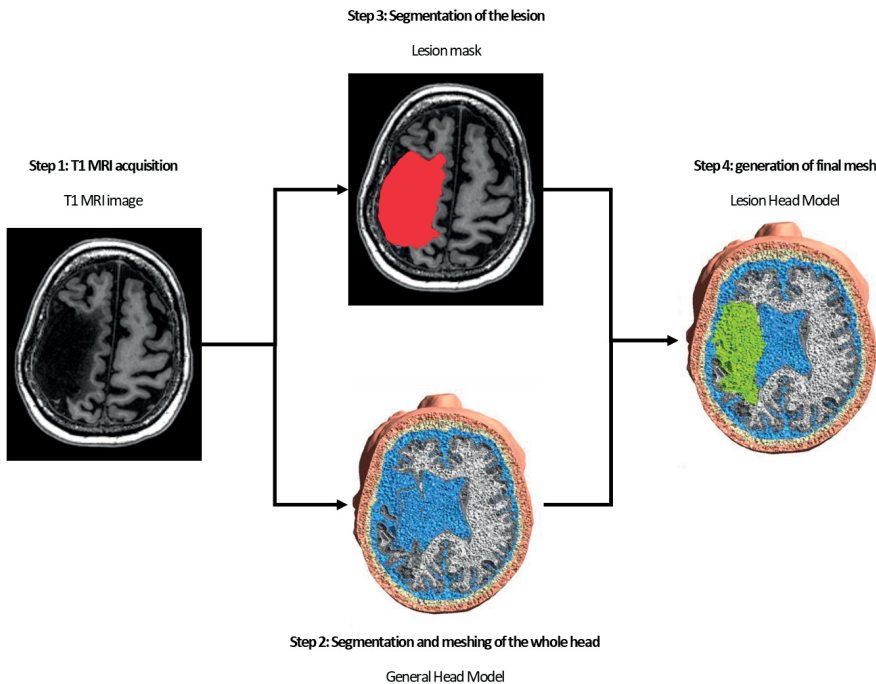


Figure 4.1. Sketch of the automatic pipeline. The white background indicates input/output, blue background steps.

The steps described above are implemented in MATLAB scripts which can be found online on the ASH GitHub page² and in the Donders repository.¹⁷

TDCS simulations

To investigate the influence of lesion conductivity and location on the induced electric field, we performed and compared several tDCS simulations in SimNIBS on the datasets of 16 stroke patients. For each stroke subject, we created two head models:

- a General Head Model without a lesion, based on the output of SimNIBS (step 2)
- a Lesion Head Model based on the output of our pipeline (step 4).

For both models, the conductivity values of healthy tissues were the default values used in SimNIBS (scalp = 0.465 S m^{-1} , skull = 0.01 S m^{-1} , eyes = 0.5 S m^{-1} , CSF = 1.654 S m^{-1} , grey matter = 0.275 S m^{-1} and white matter = 0.126 S m^{-1}). It is visible from Figure 4.1 (step 1) that the lesion is made of inhomogeneous tissue, and we can presume that it contains a combination of white matter, grey matter, and CSF (see MRI scans of Figures 1A and B in Minjoli et al. (2017)).²⁰ For this reason, in the Lesion Head Model, 16 different lesion conductivity values between 0.126 and 1.654 S m^{-1} (i.e., the conductivity of the white matter and CSF, respectively) were assigned.

Subsequently, we performed tDCS simulations in SimNIBS. Two tDCS electrode pairs at C3-Fp2 and at C4-Fp1 were selected for the ipsi- and contra-lesional primary motor cortex stimulation, respectively (see Figure 4.2), following, for example, Brunoni et al. (2012).²¹ We visually identified and marked the ‘target volumes’ for the tDCS stimulation as the centre of the left- and right-hand motor cortex (the so-called hand knob) from the T1w MRI or from the grey matter model of each chronic stroke patient. Next, the left and right tDCS target volumes were defined as all the grey matter elements within a 1 cm sphere around the centre of the left- and right-hand motor cortex. In Figure 4.2, both the target volumes (in purple) and the lesion (in green) are visualised for subject 401. We, therefore, computed and visualised the maximum values of the simulated electric field strength (E_{max}) both in the General Head Model and the Lesion Head Model, with varying lesion conductivity values (Figure 4.5). In addition, we calculated the relative difference in the percentage of the E_{max} between the General Head Model and the Lesion Head Model, with varying lesion conductivity values (Figure 4.5, percentages in black). As a further analysis, we studied the relation between the absolute relative difference in E_{max} and the volume (in cm^3) of the lesion (Figure 4.6). Finally, to verify the fulfilment of safety margins, we computed the maximum electric field strength in the whole grey matter volume among all subjects.

2 <https://github.com/mcpiastro/ASH>

Results

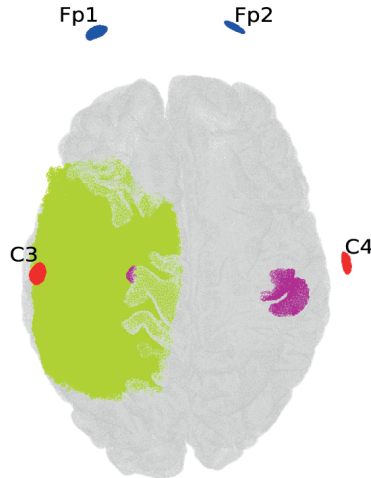


Figure 4.2. Visualisation of the volume conduction models used in the simulations for subject 401. In purple, the tDCS target volumes (i.e., grey matter elements within a 1 cm sphere around the centre of the left- and right-hand motor cortex) are depicted, and the lesion volume is visualised in green. The ipsi- and contra-lesional electrode configurations, C3-Fp2 and C4-Fp1, respectively, are shown (in red, the anodes C3 and C4, and in blue, the cathodes Fp1 and Fp2).

Pipeline results

Our pipeline generated meshes with approximately 3.5 million tetrahedral elements for each subject. The size of the lesion varied considerably throughout subjects, i.e., from a lesion of $\approx 183 \text{ cm}^3$ (subject 401) to one of $\approx 3 \text{ cm}^3$ (subjects 44 and 53). More precisely, the 16 lesion volumes, i.e. the sum of volumes of the tetrahedral elements labelled as ‘lesion’, range from 2.6 to 183 cm^3 , with a median of $\approx 38 \text{ cm}^3$ and interquartile range of $\approx 90 \text{ cm}^3$. Figure 4.3 shows a coronal, axial, and sagittal slice of the lesion mask generated by LINDA overlaying the MRI scan (output of step 3) for subject 401. The lesion mask, in red, has a volume of $\approx 183 \text{ cm}^3$.

Furthermore, in Figure 4.4, the clipped General Head Model and Lesion Head Model of subject 401 are visualised in the coronal, axial and sagittal plane, showing the stroke lesion mesh in the left hemisphere (in green).

All the calculations were done both on a workstation and on a personal laptop. The workstation is operated with version 16.04 of Ubuntu with 128 GB of RAM and an Intel Xeon W-2155 CPU. One full computation took less than 2 h. In 86 min, the General Head Model was generated by SimNIBS; in 19 min the lesion mask was created by LINDA; the generation of the Lesion Head Model took less than a second, and one tDCS simulation with SimNIBS

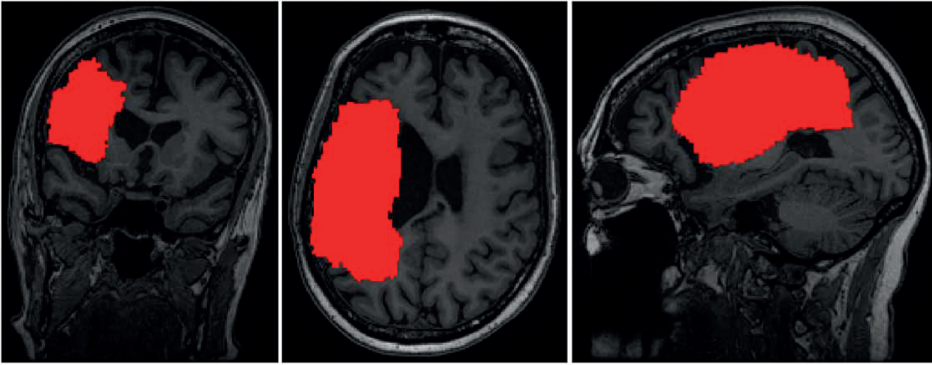


Figure 4.3. Coronal, axial and sagittal slices of the lesion mask (in red) identified by LINDA overlaid to MRI scan (in greyscale) of subject 401.

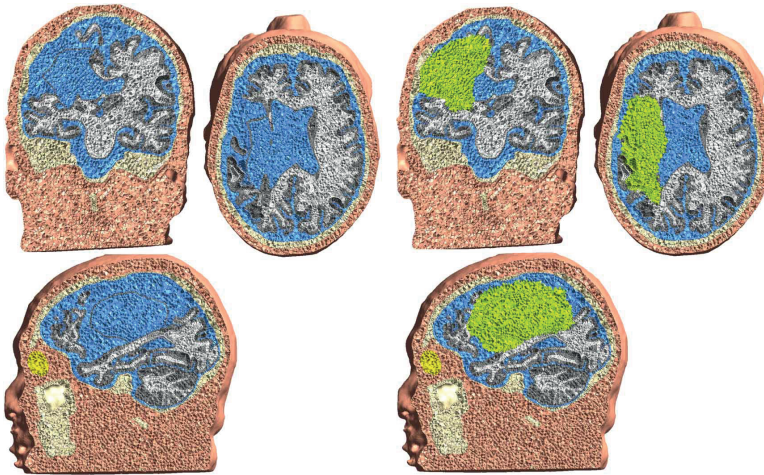


Figure 4.4. Clipped tetrahedral mesh of the General Head Model (on the left) and the Lesion Head Model (on the right) of subject 401 in the coronal, axial and sagittal plane. The lesion compartment is depicted in green.

took around 1 min. The personal laptop has version 20.04 of Ubuntu with 15 GB of RAM and an Intel Core i7-8650U CPU. One full computation took less than 3 h. In approximately 90 min, the General Head Model was generated by SimNIBS; in approximately 80 min, the lesion mask was created by LINDA; the generation of the Lesion Head Model took less than a minute, and one tDCS simulation with SimNIBS took around two minutes.

TDCS simulation results

We visualised E_{max} only for subjects 44 and 401, since they have the smallest and largest lesions (≈ 3 and 183 cm^3 , respectively). Figure 4.5 shows that the results for the ipsi- and contra-lesional stimulations differ considerably for both subjects. For the contralesional stimulation, variations

of the E_{max} are very limited, as well as the relative difference values, for both subjects. By contrast, for the ipsilesional stimulation, results differ considerably between the two subjects. For subject 44 there is almost no difference E_{max} when the General Head Model or the Lesion Head Model is used, independently from the lesion conductivity. However, for subject 401, the E_{max} decreases with increasing lesion conductivity value. The E_{max} ranges from 1.29 to 0.43 V m⁻¹ for the Lesion Head Model, and 1.16 V m⁻¹ for the General Head Model, corresponding to relative differences of 11% and -63%, respectively.

Figure 4.6 demonstrates a trend between lesion volumes and the maximum relative difference between E_{max} for the General Head Model and the Lesion Head Model. The larger the lesion volume is, the higher the relative difference. In particular, for lesions larger than approximately 10 cm³ the absolute maximum relative difference exceeds 5%. Finally, we found the maximum electric field strength in the whole grey matter volume among all subjects to be 6.56 V m⁻¹.

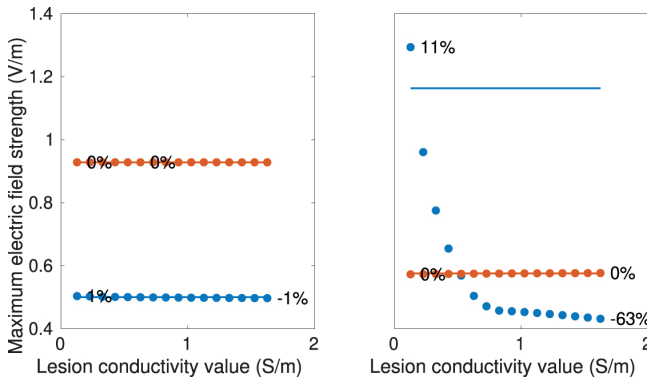


Figure 4.5. Maximum values of the electric field strength in the target volume for the ipsi-lesional (in blue) and contra-lesional (in orange) stimulations when the General Head Model (continuous line) and the Lesion Head Model (dotted line) are used to perform the simulations, for varying lesion conductivity values, for the subject with the smallest stroke lesion (subject 44; left) and with the largest stroke lesion (subject 401; right). The maximum and minimum percentage relative difference in percentage between the electric field strength computed with the different head models is displayed. For the ipsilesional stimulation, results differ considerably between the two subjects.

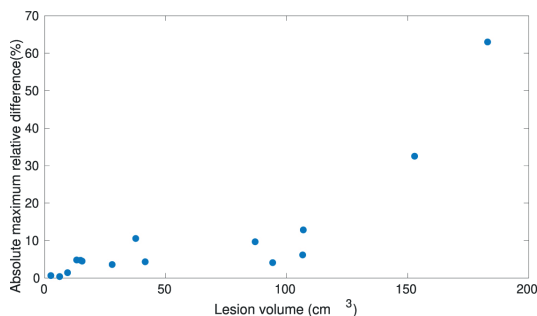


Figure 4.6. Relation between the volume of lesions and the absolute maximum relative difference between E_{max} . For the General Head Model and the Lesion Head Model in the ipsilesional target volume for each subject. The larger the volume of the lesion is, the higher the relative difference.

Discussion

In this study, we implemented, tested and distributed the first automatic MATLAB-based pipeline that provides a realistic and individualised volumetric mesh of chronic stroke patients. The pipeline is SimNIBS compatible and is available on the ASH GitHub page. The data and code are publicly available as a Donders Data Sharing Collection [27]. In addition, we demonstrated the relevance of our pipeline by conducting tDCS simulations in SimNIBS with data from 16 chronic stroke patients. We compared the electric field distribution resulting from a volume conduction head model where the lesion compartment is neglected and the one from a volume conduction head model where the lesion is included, with varying conductivity values, in each subject.

Several findings in our study underline that individualised analysis, including the presence of a large stroke lesion, is crucial in brain stimulation simulations. Firstly, we showed that, for lesions larger than 10 cm³, the absolute maximum relative difference exceeds 5%. Moreover, it can be seen that when the lesion is modelled as CSF, as done so far in most studies (e.g., in ^{14,20,22}), there might be a remarkable difference (up to 63 percentage points, see Figure 4.5) from the scenarios that use a different lesion conductivity value.

In contrast to our study, in the literature ^{14,20,22}, the lesion is usually delineated by hand and filled with CSF, thus leading to potentially inaccurate models. Lesion delineation by hand, currently considered the gold standard, is indeed often conducted by researchers who are not radiologists nor neurologists and might not have been trained. Therefore, it might change from rater to rater, and it requires up to several hours per lesion/patient. Consequently, large-scale group analyses are hampered. The pipeline we propose in this study is fully automatic, easy to use, fast, and integrated into already existing state-of-the-art software toolboxes such as SimNIBS and LINDA. In addition, there are scenarios where the lesion is not a CSF-filled

cavity nor a homogeneous tissue. See, for example, Figure 4.1 (step 1) and Figure 1(A) of Minjoli et al. (2017).²⁰ Shunting effects caused by the presence of additional CSF of the lesion volume in the head model, or ignoring the inhomogeneity of the lesion, might, therefore, alter the electric field distribution both in the whole grey matter volume and in the target volumes. An incorrect model of such a large structural brain change can thus lead to ineffective and uncontrolled tDCS rehabilitation treatments. Our work indicates such a huge variation and suggests, therefore, that more effort should be taken in order to estimate the lesion conductivity value. Our present and future work can actually facilitate such an estimation. We plan to build lesion head models for patients on which we apply current by tDCS and record the resulting scalp potentials by using EEG electrodes. The estimate for lesion conductivity will be the value that minimises the difference between recorded and model potentials.²³

Our simulations are fulfilling the safety margins since the maximal E_{max} in the grey matter throughout all 16 subjects resulting from our study is 6.56 V m^{-1} , i.e. one order of magnitude lower than the limit indicated in Antal et al. (2017).²⁴ In general, only rough indications are present in the literature, and many investigations are still ongoing. Nevertheless, Antal et al. (2017) indicated a range of $6.3\text{--}13 \text{ A m}^{-2}$, which corresponds to $19\text{--}39 \text{ V m}^{-1}$ in the grey matter, like the one in which brain injury could occur in animals.²⁴

The lesion compartment resulting from our pipeline is not necessarily connected since we do not modify the original mesh not containing the lesion. Isolated lesion mesh elements might lead to unwanted high potential values due to conductivity jumps, especially when the CSF conductivity is assigned to the lesion compartment. Nevertheless, we do not expect our results and conclusions to be affected by such cases since the target volumes are not necessarily overlapping with the lesion compartments. In order to obtain connected lesion compartments with smooth boundaries, one option is to include the lesion mask prior to the meshing procedure. This would require a more intense modification of the SimNIBS code by the user, which will hamper the usability. In addition, in our study, we did not want to change the geometrical properties of the models, i.e. the mesh, but only the number of compartments in the model, i.e. with and without the lesion.

Recent literature increasingly highlights the necessity of an individualised volume conduction head model in brain stimulation simulations.^{25,26} By testing our pipeline with data from 16 chronic stroke patients, we could show the high impact of the lesion conductivity on the simulation results, already for lesions 10 cm^3 large. Both in this line of work and in clinical practice, the ultimate goal is individual electrode configuration optimisation in order to control the electric field distribution in both the grey matter and target volumes and to guarantee the fulfilment of the current safety margins. Our work fits perfectly in this context

in that it provides a preliminary step needed to conduct large-scale group analysis in stroke rehabilitation.

Conclusion

A fully automated, easy-to-use, open-source, and fast MATLAB-based pipeline that provides a realistic and individualised volumetric mesh of chronic stroke lesions is implemented, tested and distributed. The pipeline embeds the already existing software toolboxes SimNIBS and LINDA and leads to more accurate and controlled tDCS (and TMS) simulations in SimNIBS for stroke rehabilitation studies. Within this work, we showed the high sensitivity of the electric field distribution to the lesion conductivity value and location by running tDCS simulations in data from 16 chronic stroke patients. This work facilitates lesion conductivity value estimation, which will increase the accuracy of brain stimulation simulations, ultimately allowing optimisation of electrode configuration and, therefore, more focal stimulations of the target volumes while guaranteeing the fulfilment of safety margins.

References

1. Mackay, J. & Mensah, G. A. *The atlas of heart disease and stroke*. (World Health Organization, 2004).
2. Kwakkel, G., Veerbeek, J. M., van Wegen, E. E. H. & Wolf, S. L. Constraint-induced movement therapy after stroke. *The Lancet Neurology* vol. 14 224–234 Preprint at [https://doi.org/10.1016/S1474-4422\(14\)70160-7](https://doi.org/10.1016/S1474-4422(14)70160-7) (2015).
3. Lefebvre, S. & Liew, S. L. Anatomical parameters of tDCS to modulate the motor system after stroke: A review. *Frontiers in Neurology* vol. 8 29 Preprint at <https://doi.org/10.3389/fneur.2017.00029> (2017).
4. Datta, A., Truong, D., Minhas, P., Parra, L. C. & Bikson, M. Inter-individual variation during transcranial direct current stimulation and normalisation of dose using MRI-derived computational models. *Front Psychiatry* **3**, 91 (2012).
5. van der Vliet, R., Ribbers, G. M., Vandermeeren, Y., Frens, M. A. & Selles, R. W. BDNF Val66Met but not transcranial direct current stimulation affects motor learning after stroke. *Brain Stimul* **10**, 882–892 (2017).
6. Huang, Y., Thomas, C., Datta, A. & Parra, L. C. Optimised tDCS for Targeting Multiple Brain Regions: An Integrated Implementation. In *2018 40th Annual International Conference of the IEEE Engineering in Medicine and Biology Society (EMBC)* 3545–3548 (IEEE, 2018). Doi:10.1109/EMBC.2018.8513034.
7. Bullard, D. E. & Makachinas, T. T. Measurement of tissue impedance in conjunction with computed tomography-guided stereotaxic biopsies. *J Neurol Neurosurg Psychiatry* **50**, 43–51 (1987).
8. Vatta, F., Bruno, P. & Inchingolo, P. EEG source localisation sensitivity due to brain lesions asking errors. *Annual Reports of the Research Reactor Institute, Kyoto University* vol. 1 913–916 Preprint at <https://doi.org/10.1109/iembs.2001.1019093> (2001).
9. Vatta, F., Bruno, P. & Inchingolo, P. Improving lesion conductivity estimate by means of EEG source localisation sensitivity to model parameter. *Journal of Clinical Neurophysiology* **19**, 1–15 (2002).
10. Chhatbar, P. Y. *et al.* Safety and tolerability of transcranial direct current stimulation to stroke patients – A phase I current escalation study. *Brain Stimul* **10**, 553–559 (2017).
11. Huang, Y., Datta, A., Bikson, M. & Parra, L. C. Realistic volumetric-approach to simulate transcranial electric stimulation – ROAST – a fully automated open-source pipeline. *J Neural Eng* **16**, 056006 (2019).
12. Schrader, S. *et al.* DUNEuro—A software toolbox for forward asking in bioelectromagnetism. *PLoS One* **16**, e0252431 (2021).
13. Thielscher, A., Antunes, A. & Saturnino, G. B. Field asking for transcranial magnetic stimulation: A useful tool to understand the physiological effects of TMS? *Proceedings of the Annual International Conference of the IEEE Engineering in Medicine and Biology Society, EMBS* vols 2015–Novem 222–225 Preprint at <https://doi.org/10.1109/EMBC.2015.7318340> (2015).
14. Ito, K. L., Kim, H. & Liew, S. L. A comparison of automated lesion segmentation approaches for chronic stroke T1-weighted MRI data. *Human Brain Mapping* vol. 40 4669–4685 Preprint at <https://doi.org/10.1002/hbm.24729> (2019).
15. Pustina, D. *et al.* Automated segmentation of chronic stroke lesions using LINDA: Lesion identification with neighborhood data analysis. *Hum Brain Mapp* **37**, 1405–1421 (2016).
16. Filatova, O. G. *et al.* Comparison of multi-tensor diffusion models’ performance for white matter integrity estimation in chronic stroke. *Front Neurosci* **12**, 247 (2018).
17. Piastra, M. C. *et al.* Donders Repository. *ASH: an Automatic pipeline to generate realistic and individualised chronic Stroke volume conduction Head models* https://data.donders.ru.nl/collections/di/dcmn/DSC_4020000.14_955?0 (2021) doi:10.34973/5752-rf24.

18. Penny, W., Friston, K., Ashburner, J., Kiebel, S. & Nichols, T. Statistical Parametric Mapping: The Analysis of Functional Brain Images. *Statistical Parametric Mapping: The Analysis of Functional Brain Images* Preprint at <https://doi.org/10.1016/B978-0-12-372560-8.X5000-1> (2007).
19. Gaser, C., Dahnke, R., Kurth, K., Luders, E. & Alzheimer's Disease Neuroimaging Initiative. A computational Anatomy Toolbox for the Analysis of Structural MRI Data. *Neuroimage* **2016**, 336–48 (2020).
20. Minjoli, S. *et al.* The impact of large structural brain changes in chronic stroke patients on the electric field caused by transcranial brain stimulation. *Neuroimage Clin* **15**, 106–117 (2017).
21. Brunoni, A. R. *et al.* Clinical research with transcranial direct current stimulation (tDCS): Challenges and future directions. *Brain Stimulation* vol. 5 175–195 Preprint at <https://doi.org/10.1016/j.brs.2011.03.002> (2012).
22. Datta, A., Baker, J. M., Bikson, M. & Fridriksson, J. Individualised model predicts brain current flow during transcranial direct-current stimulation treatment in responsive stroke patient. *Brain Stimul* **4**, 169–174 (2011).
23. Oostendorp, T. F., Delbeke, J. & Stegeman, D. F. The conductivity of the human skull: Results of in vivo and in vitro measurements. *IEEE Trans Biomed Eng* **47**, 1487–1492 (2000).
24. Antal, A. *et al.* Low intensity transcranial electric stimulation: Safety, ethical, legal regulatory and application guidelines. *Clinical Neurophysiology* vol. 128 1774–1809 Preprint at <https://doi.org/10.1016/j.clinph.2017.06.001> (2017).
25. Evans, C. *et al.* Dose-controlled tDCS reduces electric field intensity variability at a cortical target site. *Brain Stimul* **13**, 125–136 (2020).
26. Gomez Palacio Schjetnan, A., Faraji, J., Metz, G. A., Tatsuno, M. & Luczak, A. Transcranial direct current stimulation in stroke rehabilitation: A review of recent advancements. *Stroke Res Treat* **2013**, 170256 (2013).

Chapter 5

A method to experimentally estimate the conductivity of chronic stroke lesions: a tool to individualize transcranial electric stimulation

Joris van der Cruijssen, Maria Carla Piastra, Ruud W. Selles, Thom F. Oostendorp

Front. Hum. Neurosci. 15: 738200. Doi: 10.3389/fnhum.2021.738200

Abstract

The inconsistent response to transcranial electric stimulation in the stroke population is attributed to, amongst other factors, unknown effects of stroke lesion conductivity on stimulation strength at the targeted brain areas. Volume conduction models are promising tools to determine optimal stimulation settings. However, stroke lesion conductivity is often not considered in these models as a source of inter-subject variability.

The goal of this study is to propose a method that combines MRI, EEG, and transcranial stimulation to estimate the conductivity of cortical stroke lesions experimentally. In this simulation study, lesion conductivity was estimated from scalp potentials during transcranial electric stimulation in 12 chronic stroke patients. To do so, first, we determined the stimulation configuration where scalp potentials are maximally affected by the lesion. Then, we calculated scalp potentials in a model with a fixed lesion conductivity and a model with a randomly assigned conductivity. To estimate the lesion conductivity, we minimized the error between the two models by varying the conductivity in the second model. Finally, to reflect realistic experimental conditions, we test the effect of rotation of the measurement electrode orientation and the effect of the number of electrodes used.

We found that the algorithm converged to the correct lesion conductivity value when noise on the electrode positions was absent for all lesions. Conductivity estimation error was below 5% with realistic electrode coregistration errors of 0.1° for lesions larger than 50 ml. Higher lesion conductivities and lesion volumes were associated with smaller estimation errors.

In conclusion, this method can experimentally estimate stroke lesion conductivity, improving the accuracy of volume conductor models of stroke patients and potentially leading to more effective transcranial electric stimulation configurations for this population.

Introduction

Non-invasive electric brain stimulation techniques, such as transcranial direct current, alternating current, and random noise stimulation (tDCS, tACS, and tRNS), have been proposed to increase the effectiveness of stroke rehabilitation by passing a small current through the cortical regions related to impaired physiological systems.¹ Although favourable results of non-invasive brain stimulation on stroke survivors have been reported,² systematic reviews indicate that the effectiveness of brain stimulation is not consistent in, amongst others, motor recovery³ and aphasia.⁴

A possible cause for the lack of consistent effects is that the electrode configurations may not lead to stimulation reaching the targeted region as intended.^{5,6} This effect is even more accentuated in stroke subjects due to the influence of brain lesions on the electric field distribution.^{7,8} Simulation of brain stimulation using MRI-based volume conduction models is a means to quantify and optimize stimulation strength at targeted brain regions and has been applied in both healthy subjects⁹ and many patient populations, including stroke subjects.^{9,10}

A challenge of MRI-based volume conduction models in stroke patients is that 1) there is a large intersubject variability in lesion location and size,^{7,9} and 2) the electric conductivity of the lesion is likely a commonly overlooked source of variability. Currently, most models with stroke lesions assume that the lesion consists only of cerebrospinal fluid (CSF),^{7,9,10} primarily based on 1-week post-stroke histology experiments in rodents.^{11,12} However, by visual inspection of MRI of chronic stroke patients, the composition of stroke lesions does not always appear as solely CSF (for examples from our patient sample, see Figure 5.1). Furthermore, a recent review showed that non-invasive measurements of lesion conductivity were highly variable, ranging from 0.1 S/m to 1.77 S/m.¹³ Since simulation studies showed that the lesion conductivity could strongly affect the electric field generated by tDCS,^{8,14} knowing the lesion conductivity is vital in order to apply tDCS as intended.

Several methods have been proposed to estimate individualized head tissue conductivity (see McCann et al. (2019)¹³ for an overview). Amongst others, combined transcranial stimulation and scalp potentials have been used to estimate head tissue conductivity *in vivo*.¹⁵⁻¹⁷ A transcranial current is applied in these methods, and the induced scalp potentials are recorded using electroencephalography (EEG) electrodes. At the same time, a volume conductor model of the head is used to compute the scalp potentials assuming specific tissue conductivity. With the volume conductor model, the conductivity of one or more tissues can be estimated by varying the assumed tissue conductivity and minimizing the difference between the recorded and simulated potentials.

A combined transcranial stimulation-EEG-modelling approach has not yet been used for estimating stroke lesion conductivity. The goal of this simulation study is to demonstrate that simultaneous transcranial stimulation and EEG is suitable to estimate chronic stroke lesion conductivity in realistic experimental conditions.

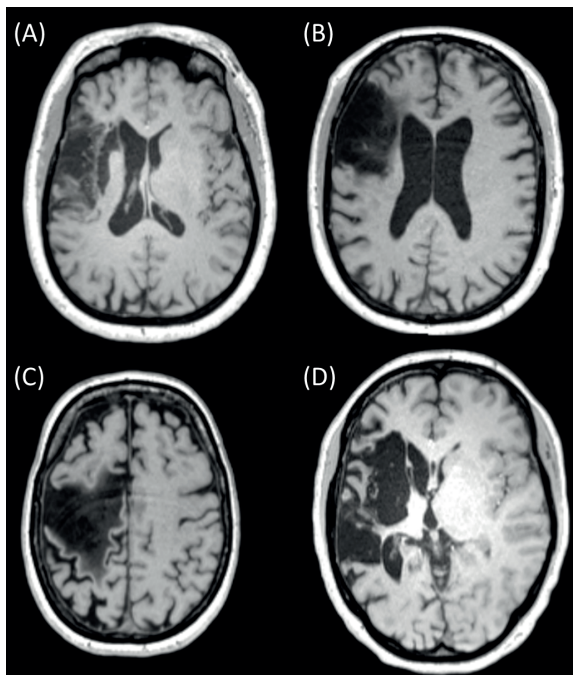


Figure 5.1. MRI slices of 4 different chronic stroke subjects showing lesions of various sizes and mixed composition (A (subject 042), B (subject 034) and C (subject 051)) and with primarily CSF (D (subject 055)). Ethical approval was acquired to record and publish the MRI slices with consent from the participants (see NL58437.091.17).

Methods

Data acquisition

T1-weighted MRI recordings were acquired from 12 chronic stroke subjects (all > 1 year post-stroke, see Table 5.1). All MRIs were recorded using a 3T MAGNETOM Prisma or 3T MAGNETOM PrismaFit scanner. The anonymized MRI scans are available online through the Donders Data Sharing Collection.¹⁸ All MRI data were acquired under the approval of the Ethics Committee ‘CMO regio Arnhem-Nijmegen’ (NL58437.091.17)¹⁸ with the written informed consent of all patients.

Table 5.1 Stroke lesion volume and optimal stimulation pairs to estimate the lesion conductivity for each subject.

Subject	Lesion volume [ml]	Lesion depth [mm]	Anode	Cathode
034	37.3	38.5	I2	FTT9h
035	11.9	35.0	TPP10h	Fp1
041	0.2	24.9	P9	FT10
042	13.1	40.5	T7	FTT10h
046	58.9	40.8	P10	F7
048	11.2	38.5	P10	TP7
050	0.1	38.2	P9	F8
051	48.9	37.7	P9	Fp2
053	0.3	25.2	I1	FT10
054	53.3	39.4	FTT10h	FTT9h
055	53.5	36.6	FT9	F8
056	85.2	35.8	TPP10h	TTP7h

Volume conductor model

A four-compartment boundary element model was created from the MRI scan of 12 chronic stroke subjects using the FieldTrip toolbox.¹⁹ The models consisted of scalp, skull, CSF, and brain compartments; all modelled with 3200 mesh elements. The lesion of each stroke patient was segmented using the LINDA algorithm.²⁰ The lesion volumes ranged from 0.1 ml to 85 ml. In order to assess the effects of lesion depth on the conductivity estimation, we calculated the depth of each lesion as the distance from the lesion centroid to the nearest scalp compartment node. For each patient, we created a model without and with the lesion.

MR images of subjects in our sample indicated that the lesion contained mainly CSF (1.71 S/m¹³) (Fig. 5.1 (D)), whereas other patients had clear signs of the presence of brain tissue (0.37 S/m) in the lesion (Fig 5.1. (A)-(C)). Given this variation and the range described in the literature (0.1 S/m to 1.77 S/m¹³), we modelled the lesion consecutively with three conductivities: 0.74 S/m, 1.23 S/m, and 1.71 S/m. The conductivities assigned to the scalp, skull, CSF, and brain were, respectively, 0.414 S/m, 0.016 S/m, 1.71 S/m, and 0.37 S/m.

The transcranial stimulation was simulated as described by Oostendorp et al.¹⁵: the stimulation electrodes were modelled as current monopoles and located 3 mm inside the scalp compartment. The scalp and skull surface meshes were refined near the stimulation electrodes to account for the large gradient of the electric potentials in that region, resulting in – for each patient – approximately 4,000 elements for the scalp and skull compartments. We used

the boundary element method to compute the electric potential at the surface of the tissue compartments,^{15,21–27} as the result of a 0.1 mA stimulation current.

Stimulation configurations

To estimate the lesion conductivity from recorded potentials, the recorded potentials needed to be affected substantially by the presence of a lesion. Therefore, we identified the optimal stimulation electrode pair for each lesion model as the pair with the highest root-mean-square difference (RMSD) in scalp potentials between the same head model with and without a lesion. We performed this step for all patients separately to control for any between-subject differences in the lesion location and size, which cannot be achieved with fixed electrode montages. We considered from the 128 EEG electrodes in the international 10/5 system²⁸ the subset of electrodes on the outer edge (Fp1/Fp2, F7/F8, FT9/FT10, FTT9h/FTT10h, T7/T8, TTP7h/TTP8h, TP7/TP8, TPP9h/TPP10h, P9/P10, I1/I2) as potential stimulation electrodes. For each possible pair of these stimulation electrodes, the resulting scalp potentials were calculated at the remaining 126 electrodes not used for stimulation. These scalp potentials were then used to identify the optimal electrode pair based on the RMSD between the model with the lesion and the model without the lesion.

Construction of recorded potentials

We simulated scalp potentials for the optimal stimulation pair and extracted data from either 8, 16, 32, 64, and 128 electrodes to investigate the quality of the conductivity estimation with an increasing number of electrodes. For the subset of 8 electrodes, we used the 8 electrodes closest to the Cz electrode (i.e., Cz, FCz, CPz, C1, C2, FFC1h, Fz, AFF1). We included an additional electrode at the nasion as the reference electrode for the EEG recordings.

To reflect realistic experimental scenarios, we simulated electrode position errors by imposing a rotation of 0 to 5 degrees (corresponding to mean displacements of 0 to 9 mm, respectively) of the electrode positions around the coronal and sagittal head axes.

Conductivity estimation

The computed electrode potentials for the optimal stimulation pair were regarded as the measured potentials in an experimental setting, and we will refer to it as the “recorded” potential ψ .

The lesion conductivity was then estimated by the non-linear parameter estimation procedure described in Oostendorp et al.¹⁵ In this procedure, first, 10 random initial estimates $\hat{\sigma}_0$ for the lesion conductivity are chosen in an interval between 0.033 and 2 S/m, and the simulated electrode potentials $\varphi(\hat{\sigma}_0)$ for every conductivity value are computed. Based on the difference between the “recorded” potentials ψ and the simulated model potentials $\varphi(\hat{\sigma}_0)$, an improved estimate of the lesion conductivity $\hat{\sigma}_1$ is determined. This process is re-iterated

until convergence is reached, defined as less than 0.1% change in the value of $\hat{\sigma}_{k-1}$ and $\hat{\sigma}_k$ at iteration k . We repeated this procedure for each combination of electrode numbers and position errors on the electrodes. Finally, we used the absolute error between the estimated conductivity $\hat{\sigma}_k$ and the actual conductivity used for the ‘recorded’ potentials as a measure for the quality of the conductivity estimation.

Results

Figure 5.2 shows the differences in scalp potentials between the models with and without the lesion for subject 035 (small lesion) and subject 055 (large lesion) for the optimal stimulation pair (for an overview of all subjects, see Table 5.1). For most subjects, the anodes of the optimal electrode pairs were primarily located around the left temporal area of the head and the cathodes around the right temporal area (see Supplementary Figure 5.1). However, subjects 034, 035, 051, and 053 had an electrode pair that consisted of frontal (Fp1/Fp2) or occipital (I1/I2) electrodes combined with a temporal electrode. The electric potential difference between the models with and without the lesion showed similar patterns for both subjects: positive potential differences in the vicinity of the anode and negative differences near the cathode. However, the effect of the larger lesion (subject 055, 53.5 ml) on the scalp potentials was about 4 times larger than for the smaller lesion (subject 035, 11.9 ml).

We found that the conductivity of all lesions was estimated correctly in the absence of electrode rotation (Fig. 5.3). For the lesions with the lowest conductivity (0.74 S/m), rotation in the coronal direction resulted in mean absolute errors of 0.12 ± 0.18 (mean \pm sd) S/m for 0.1° and 0.24 ± 0.18 for 0.5° rotation. In the sagittal direction, absolute errors of 0.12 ± 0.15 S/m and 0.43 ± 0.28 S/m were found for 0.1° and 0.5° rotation, respectively. Figure 5.3 also shows that the estimation errors were highly dependent on lesion size. However, lesion size alone could not fully explain the estimation errors. Lesions larger than 60 ml could be estimated with relative errors near 5%. Interestingly, the 48.9 ml and 58.9 ml lesions had lower estimation errors than the 53.2 ml and 85.2 ml lesions. These differences also did not seem to be related to lesion depth, as the smaller lesions were located deeper inside the brain (40.8 and 37.7 mm compared to 35.8 to 39.4 mm).

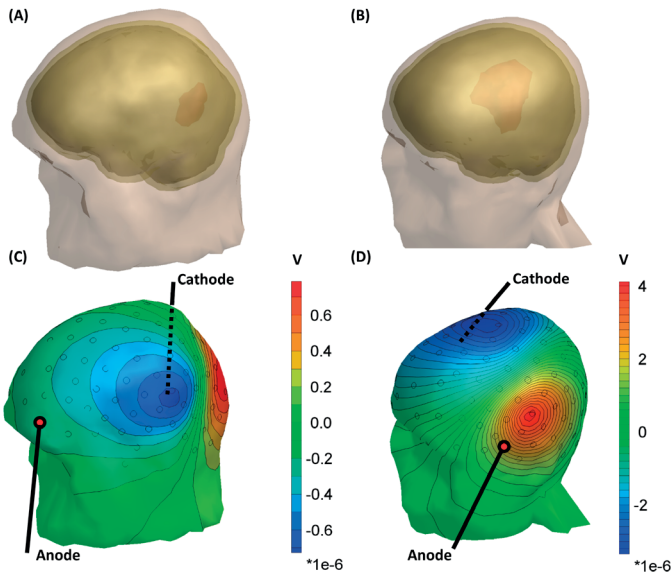


Figure 5.2. Head models of subject 035 (panel (A)) and subject 055 (panel (B)), showing the lesion volume in red. Panel (C) and (D) show the distribution of the difference in scalp potentials between the models with and without the lesion and isopotential lines for the optimal stimulation pair. Black circles represent the 128 measurement electrodes. Note that the magnitude of the color bar varies between the two subjects.

For both coronal and sagittal electrode rotation, the estimation error increased with increasing rotation angles, regardless of the lesion size. However, the estimation error did not appear to be consistently related to the number of electrodes used for the conductivity estimation. For instance, for 0.72 S/m lesions and 0.1° coronal rotation, the 11.2 ml lesion (subject 048) was estimated with an error of 0.01 S/m using 16 electrodes. However, the absolute error ranged from 0.06 to 0.17 S/m for the other electrode subsets. Furthermore, for 0.1° coronal rotation, the 37 ml lesion was estimated with an absolute error of at least 0.06 S/m. However, when rotated 0.1° in the sagittal direction, the 37 ml lesion was estimated with absolute errors below 0.05 S/m. For rotation up to 0.5° in the coronal direction, the conductivity of lesions larger than 48 ml was estimated with errors below 0.05 S/m for 64 and 128 electrode subsets. In contrast, an opposite pattern was observed for rotation in the sagittal direction: increasing the rotation to 0.5° resulted in estimation errors ranging up as high as the lesion conductivity itself, indicating high sensitivity for coronal rotation.

The effect of modelled lesion conductivity was also tested for all models and electrode rotations. The robustness to 0.5° rotation improved for higher lesion conductivity, with similar mean absolute errors but relative errors reducing from 0.32 ± 0.24 for 0.74 S/m lesions to

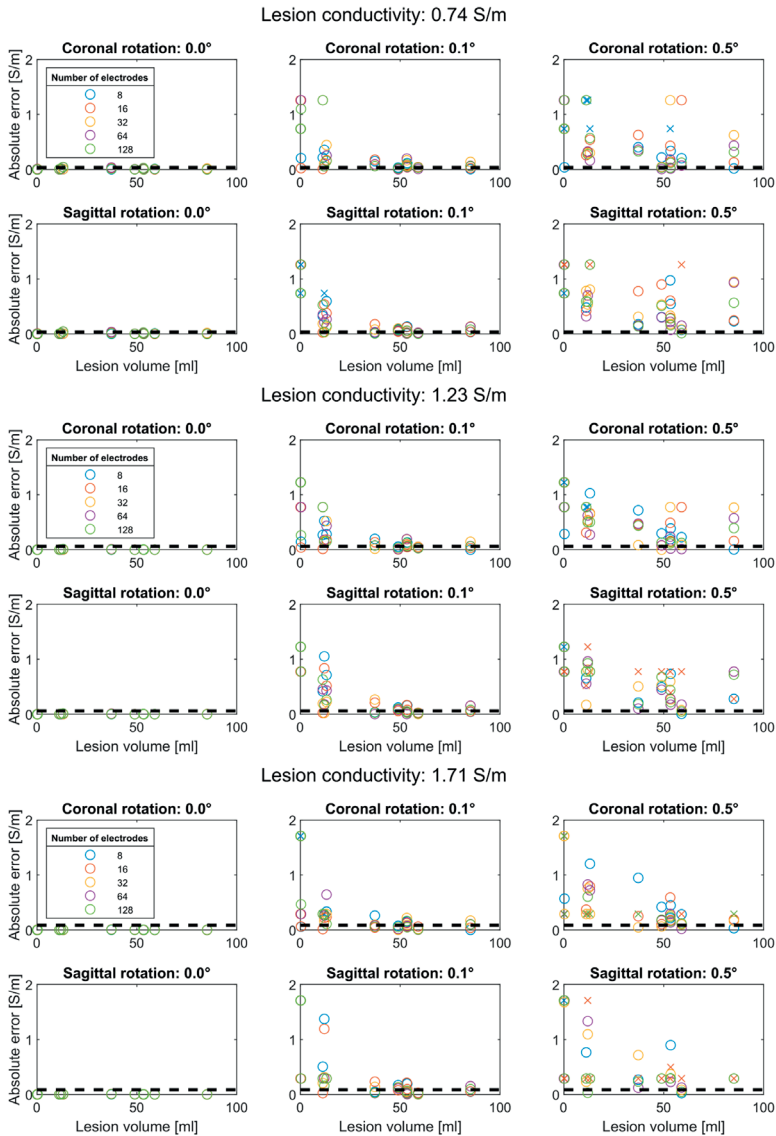


Figure 5.3. Conductivity estimation accuracy for coronal rotation (first row) and sagittal rotation (second row) for a lesion conductivity of 0.74 S/m, 1.23 S/m, and 1.71 S/m. Each colour represents a different subset of electrodes. The dashed black lines indicate a 5% relative error to the modelled conductivity. Conductivity estimations that did not converge are marked with an 'x'. Each panel shows that the absolute conductivity estimation error (y-axis) reduces with increasing lesion volume (x-axis) for rotations up to 0.5°. Without electrode rotation (left column), the conductivity is correctly estimated regardless of lesion size. At the lowest lesion conductivity (0.74 S/m), the estimation procedure is more sensitive to coronal and sagittal electrode rotation, as reflected by larger absolute errors, compared to higher lesion conductivity (1.23 S/m and 1.71 S/m).

0.21 ± 0.17 for 1.72 S/m lesions. For rotations above 1° in either coronal or sagittal direction, the optimization algorithm never converged to the correct lesion conductivity for any combination of electrode subset, lesion volume or lesion conductivity.

Discussion

We propose a method that combines MRI, EEG, and transcranial stimulation to estimate the conductivity of cortical stroke lesions experimentally. We simulated this method in head models of 12 chronic stroke patients with lesion volumes within the ranges reported in the literature²⁹ and evaluated the effect of the number of EEG recording electrodes and errors in EEG electrode placement. We found that the optimization algorithm converged to the correct lesion conductivity value when noise on the electrode positions was absent. In the case of electrode rotations, estimation error depended on lesion size. However, the conductivity of lesions larger than 50 ml could be estimated with low relative errors when coronal and sagittal rotations remained at 0.1° .

The method we propose requires only a single post-stroke MRI to estimate the lesion conductivity. In the first step of our method, we identified the optimal stimulation pair to estimate the lesion conductivity by evaluating the RMSD between a model with and without the lesion. We found optimal electrode pairs that were localized mainly around the left and right temporal areas. Likely, this is a consequence of the used patient sample, which consisted of stroke patients with lesions in approximately the same regions. Therefore, the optimal stimulation electrode pair is expected to be more variable for lesions at different locations.

The accuracy of the conductivity estimation method depends on several factors. For instance, the accuracy depended on lesion volume; larger lesions more strongly affect scalp potentials than smaller lesions. However, we observed some inconsistency in this pattern, which could not be explained by our measure of the lesion's depth. Nonetheless, more superficial lesions are expected to have a more profound effect on scalp potentials than lesions located deeper inside the brain. However, the measure we used for lesion depth – the distance between the lesion's centroid and the nearest scalp node – might not have been able to take this effect into account when calculated independently of the lesion's size.

Another explanation for the observed differences in estimation accuracy could be that the effects of small lesions were not sufficiently captured by the subsets of electrodes we used. For instance, Fig. 5.2 (C-D) shows that the lesion introduces only local electric potential differences at the scalp. At the same time, the subsets of 16 to 128 electrodes we used were

distributed uniformly over the scalp. Likewise, the subset of 8 electrodes around Cz could be suboptimal if it does not record the largest potential differences due to the lesion. Therefore, selecting a subset of electrodes including only the most affected electrodes – which would vary per subject – could improve our proposed method for small lesions.

An additional factor influencing the accuracy of our results is the lesion conductivity we assumed in the models. We modelled the lesion with three different conductivity values, in between two times the modelled brain conductivity and CSF conductivity. Like lesion volume, higher lesion conductivity increases the effect the lesion has on the scalp potentials. This is confirmed by the lower absolute errors we found for increased conductivity. Furthermore, the method proved more robust to electrode rotations for lesions with higher conductivity.

Although the conductivity of larger lesions (> 50 ml) could successfully be estimated, we found that the conductivity estimation procedure is sensitive to incorrect electrode positions. Especially, rotation in the sagittal direction was detrimental to the conductivity estimation accuracy, which may be explained by the orientation of the isopotential lines near the electrodes that record the strongest effect of the presence of the lesion (Fig. 5.2 I-(D)). For coronal rotation, the electrodes rotate more tangent to the isopotential lines, resulting in lower relative differences between the recorded and modelled scalp potentials. This hypothesis is in line with the relatively high robustness of the sagittal rotation of the 37.2 ml lesion of subject 034, for whom an optimal stimulation pair consisting of I2 and FTT9h was found.

For electrode rotations above 1° , the optimization algorithm did not correctly estimate the lesion conductivity. In this situation, scalp potential differences due to electrode position errors surpass those introduced by the lesion. As a consequence, the optimization algorithm can only minimize these errors with unrealistic lesion conductivities, resulting in high relative errors. However, it should be noted that systematic rotations represent a worst-case scenario: in experimental conditions, electrode placement errors may be distributed randomly. Nonetheless, the estimation method results suggest that mean recording electrode position errors should remain below 0.1° (1 mm mean displacement) to keep estimation errors below 5%. These accuracies can only be realized with 3D scanning techniques.³⁰ When applying this method in practice, the patients should ideally wear an MRI-compatible EEG cap during the MRI acquisition to minimize the co-registration error and maximize the conductivity estimation accuracy.

Future work comprises the estimation of the range of lesion conductivities in stroke patients. Furthermore, the effect of more realistic volume conductor models with a more realistic description of the brain, i.e., a separate grey matter and white matter volume, remains to be explored.

Limitations

We did not add random noise reflecting background EEG activity to the scalp potentials. The effect of random noise can be compensated for by either averaging over a prolonged stimulation time or increasing the stimulation intensity. At this point, we simulated stimulation at an intensity of 0.1 mA, which ensures the method can be applied with low discomfort to the patient. Also, we did not fully control for the depth of the lesions. The conductivity of lesions distant from the scalp, i.e., subcortical lesions, will be more challenging to estimate and potentially explain the inconsistency in the relation between lesion size and the conductivity estimation error we observed. However, considering lesion size and depth as independent measures may be an oversimplification that did not explain the inconsistency between lesion size and the observed conductivity estimation error.

We used a four-compartment model without a separate representation of grey and white matter. This simplification was made to reduce the computational load that the segmentation of the complex structure of the brain would introduce. As an alternative, the finite element method would be a more suitable approach to model the human head more efficiently and realistically. The modelled conductivities for the scalp, skull CSF and brain were based on literature¹³ and assumed to be known. However, skull conductivity varies significantly between individuals,¹³ and an inaccurate assumption would translate to low accuracy of the lesion conductivity estimation. One potential solution is to estimate the skull conductivity based on the scalp potentials in electrodes whose potentials are affected minimally by the lesion.

Conclusion

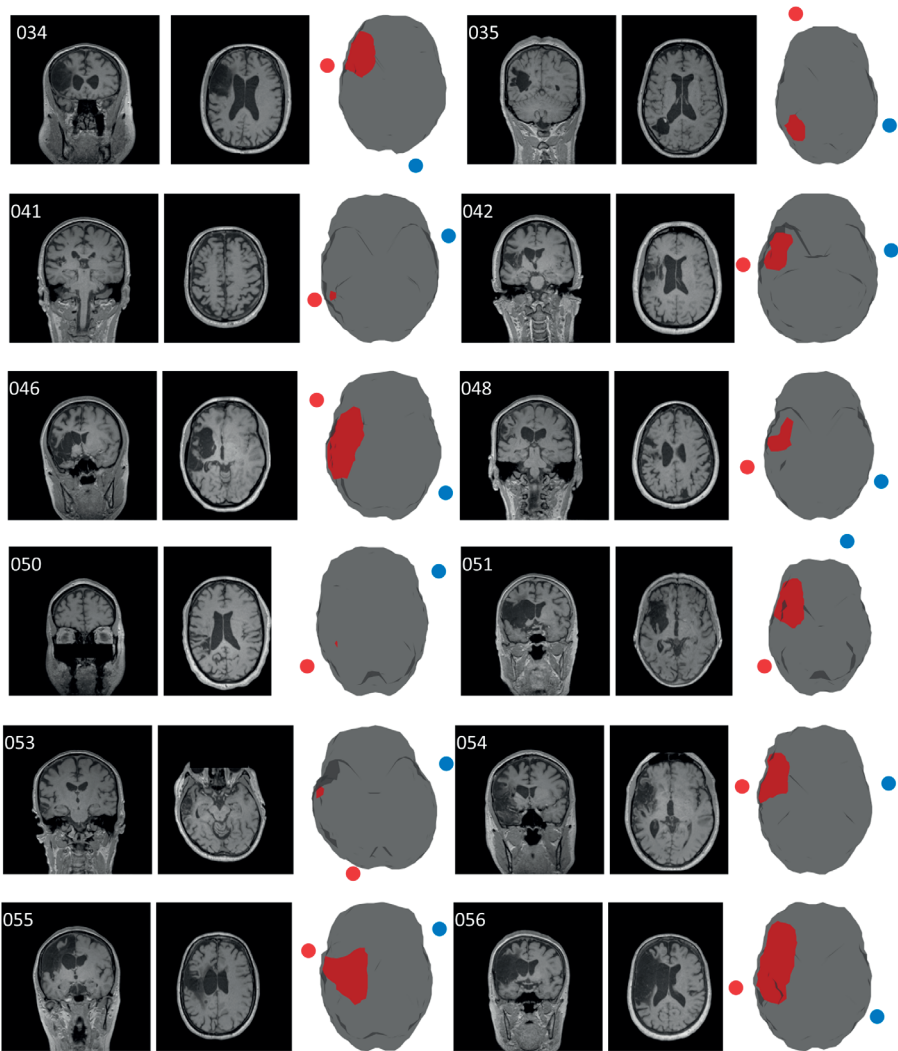
In conclusion, estimating the lesion conductivity can easily be incorporated into experimental procedures that combine tDCS, EEG and MRI for individualized head models. The achievable estimation accuracy depends on the balance between lesion volume, lesion depth, lesion conductivity and the measurement electrodes' co-registration error. The accuracy of MRI-based volume conductor models can be improved by including an individualized estimate of the stroke lesion conductivity with our proposed method. As a result, this can lead to the improved application of transcranial electric stimulation in stroke patients.

References

1. Schlaug, G., Renga, V. & Nair, D. Transcranial direct current stimulation in stroke recovery. *Archives of Neurology* vol. 65 1571–1576 Preprint at <https://doi.org/10.1001/archneur.65.12.1571> (2008).
2. Kim, D. Y. *et al.* Effect of transcranial direct current stimulation on motor recovery in patients with subacute stroke. *Am J Phys Med Rehabil* **89**, 879–886 (2010).
3. Lefebvre, S. & Liew, S. L. Anatomical parameters of tDCS to modulate the motor system after stroke: A review. *Frontiers in Neurology* vol. 8 1 Preprint at <https://doi.org/10.3389/fneur.2017.00029> (2017).
4. Elsner, B., Kugler, J., Pohl, M. & Mehrholz, J. Transcranial direct current stimulation (tDCS) for improving aphasia in adults with aphasia after stroke. *Cochrane Database of Systematic Reviews* vol. 2019 Preprint at <https://doi.org/10.1002/14651858.CD009760.pub4> (2019).
5. Vöröslakos, M. *et al.* Direct effects of transcranial electric stimulation on brain circuits in rats and humans. *Nat Commun* **9**, 1–17 (2018).
6. Laakso, I., Mikkonen, M., Koyama, S., Hirata, A. & Tanaka, S. Can electric fields explain inter-individual variability in transcranial direct current stimulation of the motor cortex? *Sci Rep* **9**, 1–10 (2019).
7. Minjoli, S. *et al.* The impact of large structural brain changes in chronic stroke patients on the electric field caused by transcranial brain stimulation. *Neuroimage Clin* **15**, 106–117 (2017).
8. Piastra, M. C. *et al.* ASH: an automatic pipeline to generate realistic and individualized chronic stroke volume conduction head models. *J Neural Eng* (2021) doi:10.1088/1741-2552/abf00b.
9. Wagner, T. *et al.* Transcranial direct current stimulation: A computer-based human model study. *Neuroimage* **35**, 1113–1124 (2007).
10. Datta, A., Baker, J. M., Bikson, M. & Fridriksson, J. Individualized model predicts brain current flow during transcranial direct-current stimulation treatment in responsive stroke patient. *Brain Stimul* **4**, 169–174 (2011).
11. Soltanian-Zadeh, H. *et al.* MRI tissue characterization of experimental cerebral ischemia in rat. *Journal of Magnetic Resonance Imaging* **17**, 398–409 (2003).
12. Jacobs, M. A. *et al.* A model for multiparametric MRI tissue characterization in experimental cerebral ischemia with histological validation in rat: Part 1. *Stroke* **32**, 943–949 (2001).
13. McCann, H., Pisano, G. & Beltrachini, L. Variation in Reported Human Head Tissue Electrical Conductivity Values. *Brain Topogr* **32**, 825–858 (2019).
14. Johnstone, A., Zich, C., Evans, C., Lee, J. & Ward, N. The impact of brain lesions on tDCS-induced electric field magnitude 2.3. *bioRxiv* 2021.03.19.436124 (2021) doi:10.1101/2021.03.19.436124.
15. Oostendorp, T. F., Delbeke, J. & Stegeman, D. F. The conductivity of the human skull: Results of in vivo and in vitro measurements. *IEEE Trans Biomed Eng* **47**, 1487–1492 (2000).
16. Gutiérrez, D., Nehorai, A. & Muravchik, C. H. Estimating brain conductivities and dipole source signals with EEG arrays. *IEEE Trans Biomed Eng* **51**, 2113–2122 (2004).
17. Dannhauer, M., Lanfer, B., Wolters, C. H. & Knösche, T. R. Modeling of the human skull in EEG source analysis. *Hum Brain Mapp* **32**, 1383–1399 (2011).
18. Piastra, M. C. *et al.* Donders Repository. ASH: an Automatic pipeline to generate realistic and individualized chronic Stroke volume conduction Head models https://data.donders.ru.nl/collections/di/dcmn/DSC_4020000.14_955?0 (2021) doi:10.34973/5752-rf24.
19. Oostenveld, R., Fries, P., Maris, E. & Schoffelen, J. M. FieldTrip: Open source software for advanced analysis of MEG, EEG, and invasive electrophysiological data. *Comput Intell Neurosci* **2011**, 1–9 (2011).
20. Pustina, D. *et al.* Automated segmentation of chronic stroke lesions using LINDA: Lesion identification with neighborhood data analysis. *Hum Brain Mapp* **37**, 1405–1421 (2016).

21. Barnard, A. C. L., Duck, I. M., Lynn, M. S. & Timlake, W. P. The Application of Electromagnetic Theory to Electrocardiology: II. Numerical Solution of the Integral Equations. *Biophys J* **7**, 463–491 (1967).
22. Akalin-Acar, Z. & Gençer, N. G. An advanced boundary element method (BEM) implementation for the forward problem of electromagnetic source imaging. *Phys Med Biol* **49**, 5011–5028 (2004).
23. Fuchs, M., Kastner, J., Wagner, M., Hawes, S. & Ebersole, J. S. *A standardized boundary element method volume conductor model. Clinical Neurophysiology* vol. 113 (2002).
24. Oostenveld, R. & Oostendorp, T. F. Validating the boundary element method for forward and inverse EEG computations in the presence of a hole in the skull. *Hum Brain Mapp* **17**, 179–192 (2002).
25. Kybic, J., Clerc, M., Faugeras, O., Keriven, R. & Papadopoulos, T. Generalized head models for MEG/EEG: Boundary element method beyond nested volumes. *Phys Med Biol* **51**, 1333–1346 (2006).
26. Stenroos, M. & Sarvas, J. Bioelectromagnetic forward problem: Isolated source approach revisited. *Phys Med Biol* **57**, 3517–3535 (2012).
27. Makarov, S. *et al.* Boundary Element Fast Multipole Method for Enhanced Modeling of Neurophysiological Recordings. *IEEE Trans Biomed Eng* 1–1 (2020) doi:10.1109/tbme.2020.2999271.
28. Oostenveld, R. & Praamstra, P. The five percent electrode system for high-resolution EEG and ERP measurements. *Clinical Neurophysiology* **112**, 713–719 (2001).
29. Chen, C. L., Tang, F. T., Chen, H. C., Chung, C. Y. & Wong, M. K. Brain lesion size and location: Effects on motor recovery and functional outcome in stroke patients. *Arch Phys Med Rehabil* **81**, 447–452 (2000).
30. Dalal, S. S., Rampp, S., Willomitzer, F. & Ettl, S. Consequences of EEG electrode position error on ultimate beamformer source reconstruction performance. *Front Neurosci* **8**, (2014).

Supplementary material



Supplementary Figure 5.1. Two MRI slices across the lesion and the brain (grey) and lesion (red) models for each subject, top view. The markers in the model plots indicate the anode (red) and cathode (blue) of the optimal stimulation pair.

Chapter 6

Addressing the inconsistent electric fields of tDCS by using patient-tailored configurations in chronic stroke: implications for treatment

Joris van der Crujsen, Renée F. Dooren, Alfred C. Schouten, Thom F. Oostendorp, Maarten A. Frens, Gerard M. Ribbers, Frans C.T. van der Helm, Gert Kwakkel, Ruud W. Selles, on behalf of the 4D EEG consortium

Neuroimage Clin. 36 2022. Doi: [10.1016/j.nicl.2022.103178](https://doi.org/10.1016/j.nicl.2022.103178)

Abstract

Transcranial direct current stimulation (tDCS) is a promising tool to improve and speed up motor rehabilitation after stroke, but inconsistent clinical effects refrain tDCS from clinical implementation. Therefore, this study aimed to assess the need for individualised tDCS configurations in stroke, considering interindividual variability in brain anatomy and motor function representation.

We simulated tDCS in individualised MRI-based finite element head models of 21 chronic stroke subjects and 10 healthy age-matched controls. An anatomy-based stimulation target, i.e. the motor hand knob, was identified with MRI, whereas a motor function-based stimulation target was identified with EEG. We simulated conventional anodal tDCS electrode configurations for every subject and optimised electrode configurations to maximise stimulation strength within the anatomical and functional target. The normal component of the electric field was extracted and compared between subjects with stroke and healthy, age-matched controls, for both targets, during conventional and optimised tDCS.

Electrical field strength was significantly lower, more variable and more frequently in opposite polarity for subjects with stroke compared to healthy age-matched subjects, both for the anatomical and functional target with conventional, i.e., non-individualised, electrode configurations. Optimised, i.e., individualised, electrode configurations increased the electrical field strength in the anatomical and functional target for subjects with stroke but did not reach the same levels as in healthy subjects.

Considering individual brain structure and motor function is crucial for applying tDCS in subjects with stroke. Lack of individualised tDCS configurations in subjects with stroke results in lower electric fields in stimulation targets, which may partially explain the inconsistent clinical effects of tDCS in stroke trials.

Introduction

Transcranial direct current stimulation (tDCS) is a promising tool to speed up and improve motor rehabilitation after stroke^{1,2} but inconsistent effects refrain tDCS from clinical implementation.³⁻⁸ The rationale behind tDCS in post-stroke motor rehabilitation is to drive an electric current through regions involved in a specific motor task, such as the primary motor cortex (M1) or premotor cortex.^{1,2} TDCS is suggested to increase synaptic plasticity and boost motor learning.⁹ However, several meta-analyses show inconsistent effects of tDCS on motor recovery after stroke, with a wide range of effect sizes between studies.³⁻⁸

Inconsistent tDCS effects in stroke randomised controlled trials (RCTs) may be explained by structural variability due to stroke lesions, resulting in alterations in local conductivity. Variability in conductivity can lead to differences in the electric current pathways in the brain between healthy subjects and subjects with stroke and within subjects with stroke, depending on the lesion's location, size, and conductivity.¹⁰⁻¹³

Another possible factor contributing to inconsistent tDCS effects in subjects with stroke is that the stroke lesion causes functional reorganisation¹⁴⁻¹⁶ which may change the brain areas that tDCS should target. Functional reorganisation of motor areas following stroke may involve the ipsilesional dorsal premotor cortex¹⁷⁻²⁰ and the contralesional primary motor cortex^{16,21}; areas not targeted with conventional tDCS electrode configurations.

Currently, it is unknown to what extent conventional tDCS protocols in subjects with stroke are robust to structural and functional interindividual variability or whether the tDCS electrode configurations need to be individualised. However, previous simulation studies showed that conventional tDCS resulted in highly variable electric fields within the motor hand knob in patients with chronic stroke.^{10,11} Clinical studies have used conventional electrode positions to stimulate the ipsilesional M1 and/or simultaneously suppressing the contralesional M1 or by stimulating the ipsilesional premotor cortex and found improved motor skill acquisition and gains in clinical outcome measures of variable effect sizes.^{8,22-25} None of these studies addressed the structural *and* functional variability within subjects with stroke. Thus, it remains unclear if the combined effect of structural and functional interindividual variability could explain the variable tDCS effects sizes in stroke subjects.

The goal of our study was to assess the need for individualising tDCS configurations in subjects with stroke by: 1) evaluating the electric field strength of conventional tDCS electrode configurations in subjects with stroke and healthy age-matched controls, taking into account individual brain structure and functional organisation, and 2) identifying optimal individual tDCS electrode configurations based on individual brain structure and functional

organisation, and 3) evaluating the electric field strength of these optimised configurations in the anatomical and functional targets. To do so, we first simulated the electric fields generated by conventional anodal tDCS protocols in a target based on structural imaging (anatomical target) and in a target based on functional neuroimaging (functional target) recorded during a motor task. Second, we identified the optimal individual tDCS electrode configuration corresponding to the maximal achievable electric field strength in both targets and subsequently, compared the field strength obtained with these configurations in each stroke patient and healthy age-matched subjects.

Methods

The data in this study were collected by the 4D EEG consortium.²⁶ A full description of the participants and the experimental design for collecting the EEG and MRI data was described in the study of Vlaar et al. (2017)²⁶ and will be summarised below. The Medical Ethics Reviewing Committee of the VU University Medical Centre (Amsterdam, the Netherlands) approved the study (NL47079.029.14). All experimental procedures complied with the Declaration of Helsinki.

Recruitment and clinical assessments

This study includes 21 chronic stroke patients (i.e., at least 6 months post-stroke at the time of inclusion, with initial hemiparesis). The full recruitment procedure is described by Vlaar et al. (2017).²⁶ Upper extremity motor function was assessed for the stroke patients at the time of inclusion using the Fugl-Meyer Assessment of the upper extremity (FM-UE)²⁷ and sensory function with the Erasmus modified Nottingham Sensory Assessment (EmNSA).²⁸ As a control group, 10 healthy, age-matched subjects were recruited.

Head models

To create individualised head models for tDCS simulation and EEG source localisation, we used structural T1w MRIs of each participant. All T1w MRIs were acquired at the VU University Medical Center, Amsterdam, using a Discovery MR750 3 T scanner (GE, Waukesha, WI, USA) with a 3D fast spoiled gradient-recalled-echo sequence consisting of 172 sagittal slices (256 x 256), using the following acquisition parameters: TR = 8.208 ms, TE = 3.22 ms, inversion time = 450 ms, flip angle = 12°, voxel size 1 x 0.94 x 0.94 mm.²⁶ Locations of the nasion and the preauricular points were visually identified from the MRI to align the EEG cap.

SimNIBS 3.2 was used to create finite element volume conductor models of the head for the simulation of non-invasive brain stimulation.²⁹ The head models generated by SimNIBS were created using *headreco*³⁰ and *CAT12*, and consisted of six different tissue types: eyes, skin, skull,

cerebrospinal fluid (CSF), grey matter and white matter. Tetrahedral meshes were created with default settings, resulting in an average of 3.93 million (range: [3.46 to 4.62 million]) tetrahedral elements. Computational time was 2:45 hours for *headreco* and 20 minutes for calculating the leadfield (using the *Pardiso* solver) required for optimisation on a mobile computer (Windows 11, AMD Ryzen 9 5900HX, 32 GB RAM).

We incorporated the stroke lesions in the model by applying the LINDA algorithm³¹ on the T1w MRI to define a lesion mask. Then, we relabelled any CSF/grey matter/white matter elements of the SimNIBS model that overlapped with the lesion mask to 'lesion', resulting in a 7-tissue head model.¹¹ Conductivity values of all tissues were set at: eyes: 0.500 S/m; skin: 0.465 S/m; skull 0.010 S/m; CSF: 1.654 S/m; grey matter: 0.275 S/m; white matter: 0.126 S/m) and set the lesion conductivity equal to CSF conductivity (1.654 S/m).

Stimulation targets

To quantify the stimulation strength of all simulated tDCS configurations, we evaluated the normal component of the simulated electric field in the middle layer of the grey matter. This normal component was calculated for different tDCS configurations in stimulation targets based on either brain anatomy or functional motor organisation.

Anatomical target

To identify the individual anatomical tDCS targets, we visually identified the motor hand knob (from now on referred to as the anatomical target) on the T1w MRI for all subjects. The hand knob has an interindividual consistent folding pattern, with a small variety of typical hand knob structures.³² As such, it can be determined from the T1w MRI.³² We extracted the coordinates of the anterior side of the hand knob as the anatomical target. The anterior side was preferred above the posterior side due to its more prominent role in movement initiation.³³

Functional target

To identify the individual functional motor tDCS targets, we analysed EEG recorded with 62 Ag/AgCl electrodes (TMSi, the Netherlands) while participants performed a robotic wrist-manipulator task. The EEG cap was arranged according to the international 10/10 system³⁴ and recorded by a biosignal amplifier (Refa128, TMSi). All data were recorded at 2048 Hz, with only an anti-aliasing filter. A snap-on electrode at the left mastoid served as the ground electrode. The impedance of all EEG electrodes was below 20 kOhm before the experiment started. In addition, all electrode positions, the nasion, and both preauricular points were digitised for co-registration with the MRI.

To evoke cortical activity, the robotic wrist-manipulator continuously perturbed the impaired wrist of the stroke patients and the dominant right hand of the healthy controls during

a passive and an active task. In the passive task, participants relaxed their wrist, following the motion of the manipulator to stimulate the somatosensory system. During the active task, participants maintained a wrist flexion torque of 20% of the maximum voluntary contraction to elicit motor activity. The maximum voluntary contraction was determined per subject for the perturbed arm.

Participants performed 20 trials of 12.5 seconds for each task. Every trial consisted of 10 repetitions of 1.25 seconds of the same perturbation. One stroke patient was not able to perform the active motor task. After cleaning the data, an average of 136 (range: 84 to 184) and 124 (range: 0 to 206) repetitions remained for the stroke patients' passive and active tasks, respectively. An average of 133 (range: 99 to 182) and 144 (range: 96 to 177) repetitions remained for the passive and active tasks for the healthy subjects, respectively.

We pre-processed all recorded EEG data offline using MATLAB (The MathWorks, Inc., USA), EEGLAB v14 toolbox³⁵ and the Fieldtrip toolbox.³⁶ As a first step, the EEG channel locations were aligned with the head model. Next, the EEG data were zero-phase band-pass filtered (0.5 to 40 Hz, FIR filter, order: 1691 and 87, respectively), cleaned from bad channels, and then re-referenced to the common average. On average, we removed 3.1 channels from the data. Next, the passive and active trials were divided into 1.25-second epochs and noisy epochs were visually identified and discarded from the data.

In the next step, we removed eye blinks and muscular artefacts using extended Infomax independent component analysis (ICA^{37,38}) on the combined passive and active EEG epochs. Artefact components were visually identified and removed based on their power spectra and topographic activation. Finally, we used the *dipfit* function from the Fieldtrip toolbox to perform source localisation by fitting equivalent dipoles to the remaining independent components in the individualised head models. The source space of the equivalent dipoles was restricted to nodes inside the brain.

In the last step of selecting the functional motor target, we extracted the coordinates of the fitted dipoles based on: 1) the residual variance of the dipole had to be below 10%³⁹ and 2) differences in the alpha (8 to 12 Hz) and beta (14 to 30 Hz) power between passive and active trials, reflecting active motor engagement.⁴⁰ The middle grey matter node closest to the selected equivalent dipole location was used as the functional target. We converted the functional target's coordinates to MNI (Montreal Neurological Institute) space coordinates and extracted the Brodmann area (BA) closest to the functional target to validate the source localisation.

Simulation of tDCS

We also used SimNIBS 3.2 to extract the normal component of the electric field during conventional anodal tDCS in the anatomical and functional targets and to find optimal tDCS electrode configuration per subject. Additionally, we used SimNIBS to optimise electrode configurations to maximise the normal component of the electric field, separately inside the anatomical and functional target. The normal component of the electric field was used as the outcome measure due to the hypothesised working mechanism of tDCS, which is polarity dependent.^{41–43} We modelled all stimulation electrodes as rubber, circular disks (diameter: 10 mm; thickness: 3 mm; conductivity: 29.4 S/m). The simulated injected current was fixed at 2 mA.

Conventional anodal tDCS electrode configurations

To assess the electric field strength in the anatomical and functional target with conventional anodal tDCS, we modelled an anode over the affected motor cortex at the C3 or C4 electrode location for the stroke subjects and always at C3 for the healthy subjects. The cathode was placed at the contralesional supra orbita (Fp1 or Fp2) for stroke subjects and at Fp2 for healthy subjects.

Optimised tDCS electrode configurations

To find the maximum normal component of the electric field in each subject's anatomical and functional target, we used SimNIBS to find the optimal electrode positions, without considering electric field focality. The full optimisation procedure is described by Saturnino et al. (2019).⁴⁴ Constraining focality would require additional assumptions on the allowable electric field strength in the brain areas outside the target. The stimulation electrodes were limited to 80 electrodes of the 10/10 system.

Statistical analysis

We compared the stimulation strength in the anatomical and functional targets by extracting the mean normal component of the simulated electric field within a 25 mm radius sphere centred around the grey matter node closest to the anatomical target and functional target coordinate, following Pimentel et al. (2013) and Mosayebi-Samani et al. (2021).^{45,46} We extracted the electric field from the anatomical and functional targets for conventional anodal tDCS and all optimised tDCS configurations.

We applied a linear mixed-effects model to assess the effect of optimised electrode configurations relative to conventional anodal tDCS. In this model, we set fixed effects for *stroke* (yes or no), *stimulation type* (conventional or optimised tDCS configuration) and *stimulation target* (anatomical or functional) and all two-way interaction terms between *stroke*, *stimulation type* and *stimulation target*. A random intercept was set for each subject per stimulation target to

consider individual differences in stimulation strength. We performed posthoc tests to assess differences in electric field strength between stroke patients and healthy subjects for conventional anodal tDCS and optimised tDCS configurations for the anatomical and functional targets. The significance threshold was Bonferroni-corrected for multiple testing accordingly and set at 0.005.

Results

Participants

We analysed data of twenty-one chronic hemiparetic stroke subjects (time post-stroke: 47 ± 35 months (mean \pm standard deviation); age: 48 to 77 years (range); 6 females) and a mean FM-UE score of 44 (range: 8 to 66) and an average total EmNSA score of 33 (range: 9 to 40). Table 6.1 describes the demographics and functional assessments of all stroke subjects. Ten healthy age-matched subjects (51 to 75 years) underwent the same experimental protocol and served as a control group.

Stimulation target locations

We visually identified the anatomical target in the T1w MRI for 19/21 stroke subjects and all healthy subjects. No anatomical target could be identified in two stroke subjects because the lesion included the motor hand knob.

Due to excessive EMG artefacts, no functional target was identified from the EEG data in one stroke subject and two healthy subjects. In healthy subjects, the functional target was always located in the contralateral hemisphere. In the stroke subjects, the functional targets were localised in different cortical areas of the ipsilesional and contralesional hemisphere (Figure 6.1/Table 6.2): the premotor cortex/supplementary motor cortex (BA6), primary motor cortex (BA4), Wernicke's area (BA22), intermediate frontal cortex (BA8), pars opercularis (BA44), primary somatosensory cortex (BA1), somatosensory association cortex (BA5), and the supramarginal gyrus (BA40). For 11/20 stroke patients, the functional target was located in the ipsilesional hemisphere and for 9 patients in the contralesional hemisphere.

Electric field strength in stimulation targets

Figure 6.2 shows the simulated normal component of the electric field in the anatomical and functional targets for conventional anodal tDCS and optimised tDCS, grouped by stroke and healthy subjects (see Figure 6.1 for two exemplar stroke patients). In stroke patients, stimulation strength was highly variable for conventional anodal tDCS targeting the anatomical target, ranging from 0.035 V/m to 0.090 V/m. In the functional target of stroke patients, stimulation strength was distributed around 0.016 V/m, with stimulation intensities ranging from -0.013

Table 6.1. Patient demographics and clinical assessment scores

ID	Age (years)	Sex	Affected side	Time post-stroke (months)	FM-UE	EmNSA
1	64	M	L	82	13	40
2	62	M	R	49	39	40
3	77	M	L	7	62	34
4	66	F	R	212	9	9
5	76	F	L	35	63	37
6	54	M	L	21	8	9
7	67	M	R	26	54	39
8	55	M	L	75	58	40
9	59	M	L	70	9	34
10	68	F	R	67	66	40
11	49	F	L	40	59	40
12	57	M	L	9	66	40
13	48	M	L	80	10	33
14	65	M	L	22	64	36
15	50	F	R	52	59	35
16	50	M	R	33	48	40
17	56	M	L	8	56	38
18	48	M	R	88	66	40
19	61	F	R	10	60	39
20	72	M	L	15	26	20
21	68	M	L	142	20	15

Sex (F: female, M: male); Affected side (L: left, R: right); FM-UE: Fugl-Meyer Assessment of upper extremity; EmNSA: Total score Erasmus MC Modifications to the Nottingham Sensory Assessment.

V/m to 0.064 V/m. For 2 out of 20 stroke subjects, conventional anodal tDCS resulted unintentionally in negative stimulation of the functional target. Negative stimulation did not occur in the anatomical target for healthy subjects. However, negative stimulation occurred in the functional target (-0.001 V/m) in 1 of the 8 healthy subjects where we identified a functional target.

In the anatomical target, posthoc tests on the linear mixed-effects model (see Table 6.3 for the estimated model coefficients) revealed a significantly lower mean stimulation strength ($F_{1,107} = 12.18$, $p < 0.001$) in stroke patients compared to healthy subjects. Optimisation of the electrode configurations for the anatomical target marginally increased the stimulation strength for stroke patients ($F_{1,107} = 5.42$, $p < 0.022$) but not for healthy subjects ($F_{1,107} = 0.27$, ns). After optimisation, the normal component of the electric field always had the correct, positive polarity. Furthermore, although optimisation of the electrode configura-

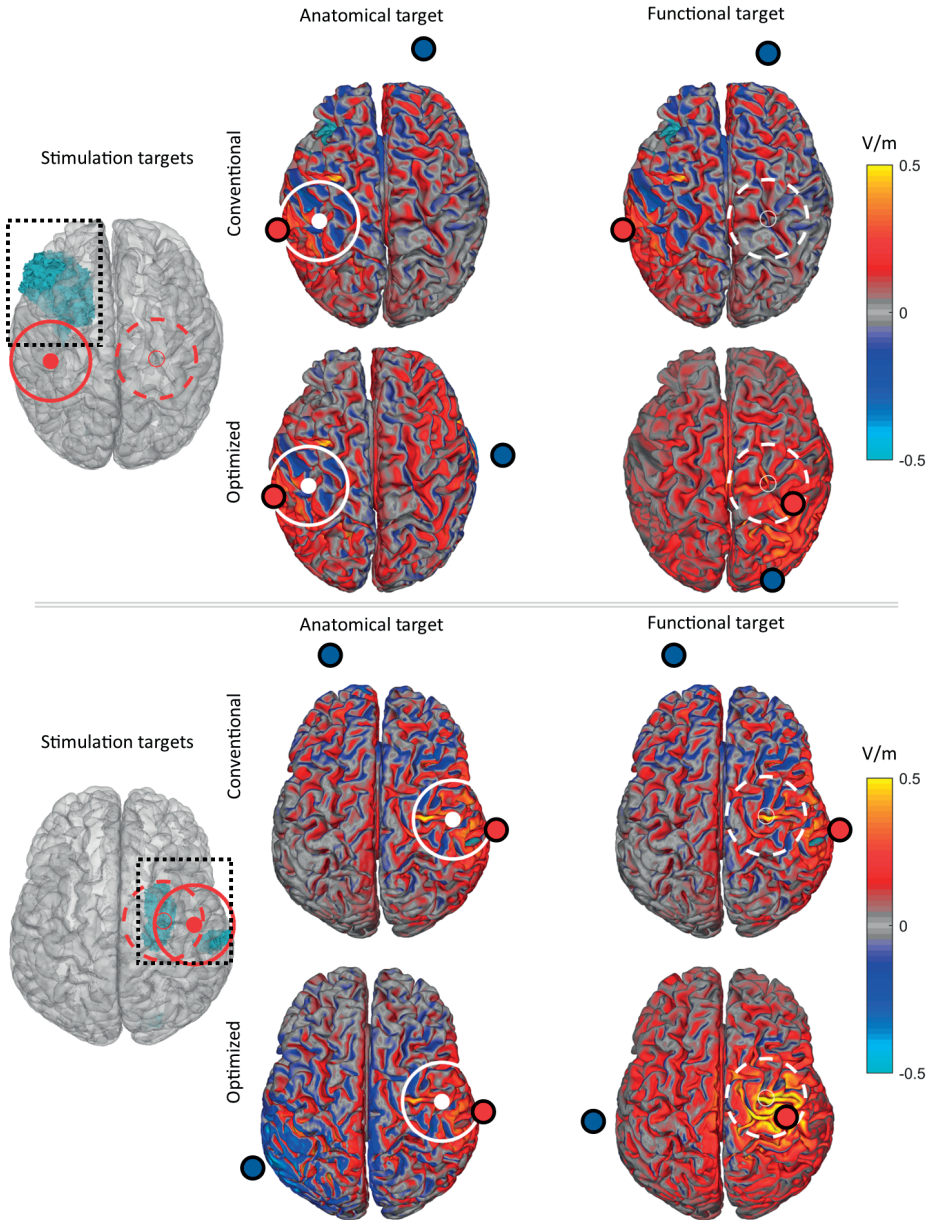


Figure 6.1. Brain model (left column) showing the stroke lesion in blue (boxed) and the consequent anatomical target (red circle), and the functional target (red dashed circle) of two stroke subjects. For the electric field during conventional tDCS electrode configuration, we show the normal component in the anatomical motor target (middle column) and the functional motor target (right column). For the electric field during optimised tDCS electrode configuration, we show the normal component of the electric field in the functional motor target and the anatomical motor target row 2 and 4); The white circles in each panel mark the intended stimulation target.

Table 6.2. Electric field normal within the anatomical and functional target during conventional stimulation and optimised tDCS.

Lesion ¹	Func. Target ²	BA ³	Anatomical target				Functional target			
			Conventional		Optimised		Conventional		Optimised	
			C3/C4-Fp2/ Fp1	E [V/m]	A	C	C3/C4-Fp2/ Fp1	E [V/m]	A	C
R	R	4	0.062	0.064	C4	F9	0.030	0.051	CP2	T10
L	-	-	0.045	0.052	C1	T10	-	-	-	-
R	R	6	0.035	0.046	C4	P1	0.025	0.038	FC6	PO3
L	R	6	-	-	-	-	0.012	0.043	FC2	T8
R	L	6	0.055	0.061	C4	T9	0.013	0.045	C1	T9
R	R	6	0.041	0.060	C2	P9	0.038	0.056	C2	F10
L	R	6	0.071	0.076	C3	T8	0.005	0.052	C2	I2
R	R	6	0.057	0.066	C4	CP3	0.061	0.109	C2	TP9
R	R	22	0.068	0.074	C2	F10	0.026	0.044	CP6	T7
L	L	6	0.060	0.065	C3	TP8	0.013	0.044	Cz	P9
R	R	4	0.071	0.076	C4	TP7	0.064	0.069	C4	P9
R	R	8	0.077	0.083	C4	T7	0.061	0.095	FC4	I1
R	L	44	-	-	-	-	-0.013	0.062	FC3	C6
R	L	1	0.047	0.053	C4	TP7	0.006	0.048	C1	FT10
L	R	5	0.090	0.095	C3	T10	0.015	0.055	CP2	FT10
L	L	6	0.056	0.057	C3	F6	0.022	0.068	C1	P9
R	L	8	0.045	0.052	C2	FT9	0.002	0.060	FCz	T10
L	L	1	0.071	0.085	C1	FT10	0.017	0.035	C1	FT9
L	R	1	0.073	0.087	C1	PO10	-0.001	0.070	CP4	T7
R	L	1	0.049	0.052	C4	T9	0.010	0.060	C1	FT9
R	R	6	0.042	0.054	C2	T9	0.026	0.054	C2	T10
Healthy subjects										
-	L	8	0.069	0.074	C3	T10	-0.001	0.051	FCz	FT9
-	-	-	0.057	0.066	C1	T10	-	-	-	-
-	L	6	0.071	0.077	C3	P10	0.046	0.066	C1	I1
-	-	-	0.089	0.095	C3	P10	-	-	-	-
-	L	1	0.064	0.072	C3	FT9	0.060	0.074	CP3	T10
-	L	6	0.082	0.096	C1	P10	0.053	0.084	C1	PO9
-	L	6	0.093	0.100	C3	PO10	0.024	0.084	FC1	T9
-	L	6	0.093	0.094	C1	T10	0.083	0.087	C3	T10
-	L	40	0.057	0.061	CP1	FT9	0.062	0.067	CP3	FT10
-	L	4	0.086	0.089	C3	FT10	0.060	0.064	C3	T10

¹ Impaired hemisphere (L: left; R: right; -: healthy subject); ² Hemisphere containing the functional target; ³ Nearest Brodmann Area to the functional target; E: normal component of the electric field within the stimulated target; A: anode; C: cathode.

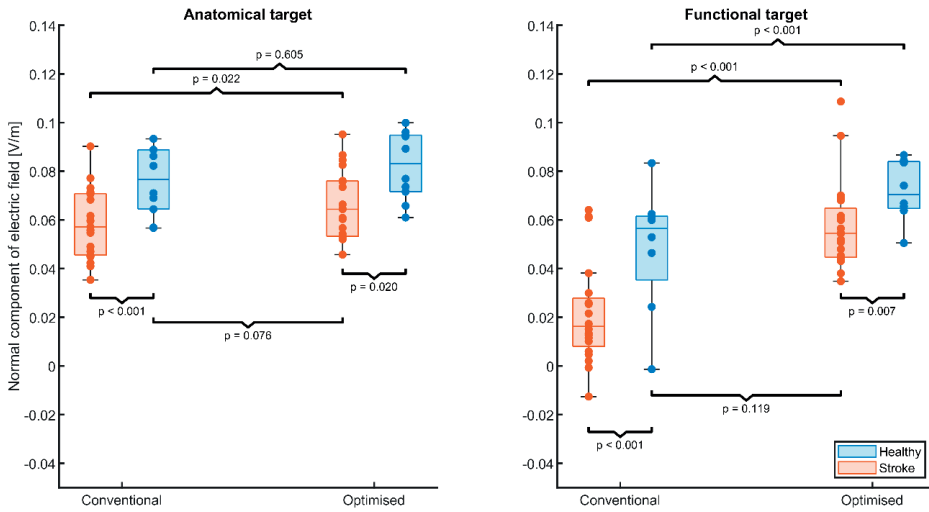


Figure 6.2. Stimulation strength in the anatomical target (left panel) and functional target (right panel) for stroke subjects (red) and healthy subjects (blue). Each box shows the median stimulation strength with the interquartile range; minimum and maximum data points (whiskers) and the outliers (data points beyond the maximum/minimum ± 1.5 times the interquartile range). Each panel shows the simulated normal component of the electric field within each target during conventional anodal tDCS and after optimisation of the electrode configuration to maximise the electric field. Optimisation based on individual characteristics increases the electric field in patients to similar levels as conventional anodal tDCS in healthy age-matched controls.

tions raised the electric field in the anatomical target of all stroke patients (mean \pm sd: 0.062 ± 0.019 V/m), it remained lower than the electric fields acquired after optimisation in healthy subjects (mean \pm sd: 0.082 ± 0.014 V/m; $F_{1,107} = 5.61$, $p = 0.020$). However, the optimised electrode positions in stroke patients resulted in similar electric field strengths as non-optimised, conventional electrode positions (i.e., C3-Fp2) in healthy subjects ($F_{1,107} = 3.21$, $p = 0.076$).

In the functional target, post hoc tests on the linear mixed-effects model revealed that the electric field strength from conventional anodal tDCS was lower for stroke patients and healthy subjects ($F_{1,107} = 14.59$, $p < 0.001$). Optimisation of the electrode configurations for the functional target increased the electric field strength for stroke patients ($F_{1,107} = 77.30$, $p < 0.001$) and for healthy subjects ($F_{1,107} = 27.46$, $p < 0.001$). After optimisation, the electric field strength within the functional target remained lower for the stroke patients (mean \pm sd: 0.058 ± 0.018 V/m) compared to healthy subjects (mean \pm sd: 0.013 ± 0.072 V/m; $F_{1,107} = 7.52$, $p = 0.007$). However, optimised electrode positions in stroke patients resulted in similar electric field strengths as non-individualised electrode positions in healthy subjects ($F_{1,107} = 2.47$, $p = 0.119$).

Table 6.3. Summary of the estimates linear mixed-effect model that describes the mean normal component of the electric field in the anatomical and functional target for stroke patients and healthy subjects, shown in Figure 6.2. This model served as the input for the post-hoc tests to determine whether the electric fields differed between stroke patients and healthy subjects for the different combinations of stimulation configurations and targets.

Variable	Estimate [-]	SE	t(DF)	p	CI95
Intercept	0.022	0.004	6.12 (107)	< 0.001	[0.015, 0.029]
Anatomical target	0.035	0.004	8.69 (107)	< 0.001	[0.027, 0.043]
Optimised	0.034	0.004	8.79 (107)	< 0.001	[0.027, 0.042]
Healthy	0.024	0.006	3.82 (107)	< 0.001	[0.011, 0.036]
Anatomical Target: Optimised	-0.025	0.005	-4.97 (107)	< 0.001	[-0.035, -0.015]
Anatomical Target: Healthy	-0.003	0.006	-0.52 (107)	0.601	[-0.014, 0.008]
Optimised: Healthy	-0.007	0.005	-1.24 (107)	0.219	[-0.018, 0.004]

Optimal electrode configurations

The optimal electrode positions for both stimulation targets (anatomical and functional) and patient groups (healthy and stroke) are shown in Table 6.2 (for the resulting electric field of all optimal electrode configuration, see Supplementary Material). The variability in anode location was greatest within the functional target, with 12 unique locations for stroke subjects and 5 for healthy subjects. For stroke subjects within the anatomical target, the optimal anode was found at the C1/C2 electrode 7 times and 12 times for the conventional C3/C4 electrode. The C3 electrode was the optimal anode location 6/10 cases for healthy subjects. For the optimal cathode locations, no clear pattern was found.

Discussion

This study investigated the variability in the electric field strengths generated in anatomical and functional targets by conventional tDCS configurations in stroke subjects and healthy age-matched controls. In addition, the study investigated the electrode configurations optimally stimulating these targets and the electric fields associated with these configurations. Our results show that the anatomical and functional target stimulation strength is lower for stroke patients than for healthy subjects when using conventional anodal tDCS. Optimising the electrode configurations resulted in more different electrode locations in subjects with stroke than in healthy subjects, increasing the electric field strengths in stroke patients, although not to the same level as in healthy subjects, likely due to the stroke lesions. In healthy subjects, optimisation of the electrode positions did not significantly increase electric field strengths in the anatomical target. Finally, optimised electrode configurations in the functional target resulted in higher and more consistent stimulation levels in stroke patients and healthy age-matched subjects, preventing

negative stimulation. However, electric field strengths in stroke patients remained lower than those in healthy subjects. The above findings suggest that interindividual variability in electrical field strengths may have contributed to the lack of beneficial effects of tDCS found in clinical trials targeting the most-affected upper limb post-stroke.

An important implication of our study is the need to individualise tDCS configurations in subjects with stroke, following from the difference in stimulation strength during conventional anodal tDCS between stroke patients and healthy subjects. The anatomical target (motor hand knob) is a frequently used stimulation target in both healthy subjects and stroke patients. In healthy subjects, the simulated electric fields match previous modelling studies targeting the motor hand knob⁴¹ but stroke patients had lower electric field strengths overall. Meta-analyses and reviews show that most clinical tDCS studies apply heterogenic stimulation paradigms, with C3 and C4 as anode locations as the only common factor between studies.^{47,48} Our results argue that individualised electrode positions in stroke patients reduce the difference in electric field strength compared to healthy subjects while keeping the stimulation current equal. While electric field strength in stimulation targets is only one factor that affects tDCS effects,⁴⁹ these findings indicate that individualising electrode positions reduces one factor of variability, simplifying the comparison of reported tDCS effects in stroke patients and healthy subjects.

One factor commonly attributed to interindividual variability in stimulation strength is the local thickness of the CSF layer.^{46,50,51} Since the thickness of the CSF layer is age-dependent,^{51,52} and we compared the stroke patients with age-matched healthy controls, this might not be a key factor in our analysis. Additionally, optimised electrode positions resulted in lower electric field strengths for stroke patients as healthy subjects. Therefore, the achievable electric field strength for conventional anodal tDCS seems to be limited by lesion characteristics. Previous tDCS simulation studies have demonstrated that lesions can significantly alter local electric fields in the vicinity of a stimulation target, depending on the lesion size, conductivity, and location relative to the stimulation target.^{10–13,53}

Considering the functional reorganisation following stroke, the need to individualise the tDCS configurations becomes even more evident. Functional targets were found predominantly in or near parts of the sensorimotor network previously associated with functional reorganisation following stroke.^{14,54} As expected, conventional anodal tDCS – designed to target the ipsilesional motor hand knob – resulted in more variable stimulation strength and sometimes reversed polarity for the functional targets compared to the anatomical target. In particular, this was found in functional targets localised in the contralesional hemisphere. Optimisation of electrode positions resolved both the variable magnitude and the polarity in both the anatomical and the functional targets in stroke patients and increased the electric

field strength, but not to the same level as optimised electrode positions in healthy subjects. Solving unintended negative stimulation seems an important finding, as negative stimulation of the functional target has potentially detrimental effects on neuroplasticity and motor learning.⁵⁵⁻⁵⁷ While some patients may benefit from inhibiting the contralesional M1, others may benefit from stimulation of contralesional or ipsilesional motor regions.^{51,52} However, the most suitable stimulation locations and polarities should be determined per individual patient from functional neuroimaging to avoid promoting maladaptive reorganisation of the motor system.⁵⁸

The findings of our study follow from several strengths that should be noted. First, our study combined structural and functional neuroimaging in a relatively large sample of 21 stroke subjects and performed a direct comparison with age-matched healthy subjects. Furthermore, we used 62-channel EEG to derive functional motor targets for tDCS, allowing us to investigate functional reorganisation following stroke. Source localisation and tDCS simulation were both performed in the same accurate, individualised finite element models.

Our study also has limitations. First, our source localisation method did not result in functional targets for all subjects. As a source localisation method, we fitted equivalent dipoles to independent components resulting from ICA. For some subjects, no motor task-related components were found due to excessive noise in the EEG recording. Furthermore, EEG source localisation has a lower spatial resolution than alternative methods such as functional MRI or TMS-based identification of the stimulation target.⁵⁹ Therefore, it might be that the actual source of brain activity and modelled equivalent dipole did not completely match. The modelling inaccuracy is reflected by the MNI-transformed dipole locations, which were sometimes localised outside the sensorimotor network (i.e., BA8, 22, 44). However, visual inspection of these functional targets showed that these sources were close to sensorimotor regions. A previous modelling study showed that optimised electric field strengths are relatively robust to small variations of the target location.¹³ Thus, we consider the source localisation method a minor limitation for interpreting our results.

Our study included 21 patients with chronic stroke and 10 healthy age-matched but not gender-matched controls, which poses an additional limitation because structural MRI studies describe age-related and gender-related differences in the brain structure in the elderly.⁶⁰ Furthermore, while the number of stroke patients is relatively high compared to similar modelling studies, the absolute number remains low. It is, therefore, unknown how our results generalise to larger samples. Patients with other lesion characteristics or different functional organisation of the motor system likely require different stimulation configurations, emphasising the need to individualise electrode locations to reduce intersubject variability in the electric field strength in the targeted brain region. An additional limitation follows

from the small electrodes used in our simulations. The electrode size is of interest in tDCS research because smaller electrodes allow 1) more focal stimulation with higher electric fields than achievable with large sponge electrodes⁶¹ and 2) simultaneous recording of EEG during tDCS, an anticipated future combination with tES⁶² However, more focal stimulation increases interindividual variability in electric field strength.⁶¹ It is thus unknown if our results apply to larger electrodes. Nonetheless, our results show less interindividual variability in the healthy control group than in the subjects with stroke, supporting our findings and modelling choice.

In our analysis, we focussed on the normal component of the electric field in each stimulation target due to the putative polarity-dependent effects of tDCS.^{41,43,55} However, MEP magnitudes in TMS studies were recently positively associated with particularly the magnitude and the tangent component of the electric field within the M1.⁶³ At this moment, it is unclear how such relationships fit within the polarity-dependent effects of tDCS. Exploring such relationships further requires combining simulation and optimisation of tDCS with experimental paradigms, which was beyond the scope of the current study.

Finally, our individualised head models assumed known conductivities for all tissue types in the model. Literature shows that skull conductivity is highly variable⁶⁴ and negatively correlates with electric field strengths.⁶⁵ Furthermore, we assumed CSF conductivity for the lesion, which might not represent all subjects in our sample, although commonly used.^{10,53} An individualised estimate of the skull and lesion conductivity are important next steps to improve the accuracy and validity of tDCS simulations.^{11,66}

In conclusion, our study shows that considering individual brain structure and functional motor targets is vital to applying tDCS in patients with chronic stroke and, to a lesser extent, also in healthy subjects. Without simulating tDCS in individualised head models, the electric field strength is lower and more variable in stroke patients, as may be the tDCS effects on clinical outcome measures at patient and group level. In future clinical studies, the effects of individualised tDCS targeting the motor hand knob and regions involved in functional reorganisation remain to be tested.

References

1. Hamoudi, M. *et al.* Transcranial Direct Current Stimulation Enhances Motor Skill Learning but Not Generalization in Chronic Stroke: <https://doi.org/10.1177/1545968318769164> **32**, 295–308 (2018).
2. Schlaug, G., Renga, V. & Nair, D. Transcranial Direct Current Stimulation in Stroke Recovery. *Arch Neurol* **65**, 1571–1576 (2008).
3. Chhatbar, P. Y. *et al.* Transcranial Direct Current Stimulation Post-Stroke Upper Extremity Motor Recovery Studies Exhibit a Dose–Response Relationship. *Brain Stimul* **9**, 16 (2016).
4. Santos Ferreira, I. *et al.* Searching for the optimal tDCS target for motor rehabilitation. *Journal of NeuroEngineering and Rehabilitation* vol. 16 90 Preprint at <https://doi.org/10.1186/s12984-019-0561-5> (2019).
5. Hashemirad, F., Zoghi, M., Fitzgerald, P. B. & Jaberzadeh, S. The effect of anodal transcranial direct current stimulation on motor sequence learning in healthy individuals: A systematic review and meta-analysis. *Brain Cogn* **102**, 1–12 (2016).
6. Bornheim, S. *et al.* Evaluating the effects of tDCS in stroke patients using functional outcomes: a systematic review. <https://doi.org/10.1080/09638288.2020.1759703> (2020) doi:10.1080/09638288.2020.1759703.
7. Lefebvre, S. & Liew, S. L. Anatomical parameters of tDCS to modulate the motor system after stroke: A review. *Frontiers in Neurology* vol. 8 1 Preprint at <https://doi.org/10.3389/fneur.2017.00029> (2017).
8. Elsner, B., Kwakkel, G., Kugler, J. & Mehrholz, J. Transcranial direct current stimulation (tDCS) for improving capacity in activities and arm function after stroke: A network meta-analysis of randomised controlled trials. *J Neuroeng Rehabil* **14**, 1–12 (2017).
9. Stagg, C. J. & Nitsche, M. A. Physiological basis of transcranial direct current stimulation. *Neuroscientist* **17**, 37–53 (2011).
10. Minjoli, S. *et al.* The impact of large structural brain changes in chronic stroke patients on the electric field caused by transcranial brain stimulation. *Neuroimage Clin* **15**, 106–117 (2017).
11. Piastra, M. C. *et al.* ASH: an automatic pipeline to generate realistic and individualized chronic stroke volume conduction head models. *J Neural Eng* (2021) doi:10.1088/1741-2552/abf00b.
12. Johnstone, A., Zich, C., Evans, C., Lee, J. & Ward, N. The impact of brain lesions on tDCS-induced electric field magnitude 2 3. *bioRxiv* 2021.03.19.436124 (2021) doi:10.1101/2021.03.19.436124.
13. Dmochowski, J. P. *et al.* Targeted transcranial direct current stimulation for rehabilitation after stroke. *Neuroimage* **75**, 12–19 (2013).
14. Jones, T. A. & Adkins, D. L. Motor System Reorganization After Stroke: Stimulating and Training Toward Perfection. *Physiology* **30**, 358 (2015).
15. Ward, N. S. Mechanisms underlying recovery of motor function after stroke. *Postgrad Med J* **81**, 510–514 (2005).
16. Volz, L. J. *et al.* Motor cortex excitability and connectivity in chronic stroke: a multimodal model of functional reorganization. *Brain Struct Funct* **220**, 1093–1107 (2015).
17. Fridman, E. A. *et al.* Reorganization of the human ipsilesional premotor cortex after stroke. *Brain* **127**, 747–58 (2004).
18. O’Shea, J., Johansen-Berg, H., Trief, D., Göbel, S. & Rushworth, M. F. S. Functionally Specific Reorganization in Human Premotor Cortex. *Neuron* **54**, 479–490 (2007).
19. Werhahn, K. J., Conforto, A. B., Kadom, N., Hallett, M. & Cohen, L. G. Contribution of the ipsilateral motor cortex to recovery after chronic stroke. *Ann Neurol* **54**, 464–72 (2003).
20. Ward, N. Assessment of cortical reorganisation for hand function after stroke. *J Physiol* **589**, 5625–5632 (2011).

21. Murase, N., Duque, J., Mazzocchio, R. & Cohen, L. G. Influence of interhemispheric interactions on motor function in chronic stroke. *Ann Neurol* **55**, 400–9 (2004).
22. Andrade, S. M. *et al.* Constraint-Induced Movement Therapy Combined with Transcranial Direct Current Stimulation over Premotor Cortex Improves Motor Function in Severe Stroke: A Pilot Randomized Controlled Trial. *Rehabil Res Pract* **2017**, (2017).
23. Bolognini, N. *et al.* Neurophysiological and Behavioral Effects of tDCS Combined With Constraint-Induced Movement Therapy in Poststroke Patients: <http://dx.doi.org/10.1177/1545968311411056> **25**, 819–829 (2011).
24. Lindenberg, R., Renga, V., Zhu, L. L., Nair, D. & Schlaug, G. Bi-hemispheric brain stimulation facilitates motor recovery in chronic stroke patients. *Neurology* **75**, 2176–2184 (2010).
25. Lefebvre, S. *et al.* Dual-tDCS Enhances Online Motor Skill Learning and Long-Term Retention in Chronic Stroke Patients. *Front Hum Neurosci* **0**, 343 (2013).
26. Vlaar, M. P. *et al.* Quantification of task-dependent cortical activation evoked by robotic continuous wrist joint manipulation in chronic hemiparetic stroke. *J Neuroeng Rehabil* **14**, (2017).
27. Fugl-Meyer, A. R., Jääskö, L., Leyman, I., Olsson, S. & Steglind, S. The post-stroke hemiplegic patient. 1. A method for evaluation of physical performance. *Scand J Rehabil Med* **7**, 13–31 (1975).
28. Stolk-Hornsveld, F., Crow, J. L., Hendriks, E. P., van der Baan, R. & Harmeling-van der Wel, B. C. The Erasmus MC modifications to the (revised) Nottingham Sensory Assessment: a reliable somatosensory assessment measure for patients with intracranial disorders. *Clin Rehabil* **20**, 160–172 (2006).
29. Thielscher, A., Antunes, A. & Saturnino, G. B. Field asking for transcranial magnetic stimulation: A useful tool to understand the physiological effects of TMS? In *Proceedings of the Annual International Conference of the IEEE Engineering in Medicine and Biology Society, EMBS* vols 2015–Novem 222–225 (2015).
30. Nielsen, J. D. *et al.* Automatic skull segmentation from MR images for realistic volume conductor models of the head: Assessment of the state-of-the-art. *Neuroimage* **174**, 587–598 (2018).
31. Pustina, D. *et al.* Automated segmentation of chronic stroke lesions using LINDA: Lesion identification with neighborhood data analysis. *Hum Brain Mapp* **37**, 1405–1421 (2016).
32. Caulo, M. *et al.* New morphologic variants of the hand motor cortex as seen with MR imaging in a large study population. *AJNR Am J Neuroradiol* **28**, 1480–1485 (2007).
33. Terumitsu, M., Ikeda, K., Kwee, I. L. & Nakada, T. Participation of primary motor cortex area 4a in complex sensory processing: 3.0-T fMRI study. *Neuroreport* **20**, 679–683 (2009).
34. Oostenveld, R. & Praamstra, P. The five percent electrode system for high-resolution EEG and ERP measurements. *Clinical Neurophysiology* **112**, 713–719 (2001).
35. Delorme, A. & Makeig, S. EEGLAB: an open source toolbox for analysis of single-trial EEG dynamics including independent component analysis. *J Neurosci Methods* **134**, 9–21 (2004).
36. Oostenveld, R., Fries, P., Maris, E. & Schoffelen, J.-M. FieldTrip: Open source software for advanced analysis of MEG, EEG, and invasive electrophysiological data. *Comput Intell Neurosci* **2011**, 156869 (2011).
37. Makeig, S., Bell, A. J., Jung, T.-P. & Sejnowski, T. J. Independent component analysis of electroencephalographic data. *Adv Neural Inf Process Syst* **8**, (1996).
38. Bell, A. J. & Sejnowski, T. J. An Information-Maximization Approach to Blind Separation and Blind Deconvolution. *Neural Comput* **7**, 1129–1159 (1995).
39. Delorme, A., Palmer, J., Onton, J., Oostenveld, R. & Makeig, S. Independent EEG sources are dipolar. *PLoS One* **7**, (2012).

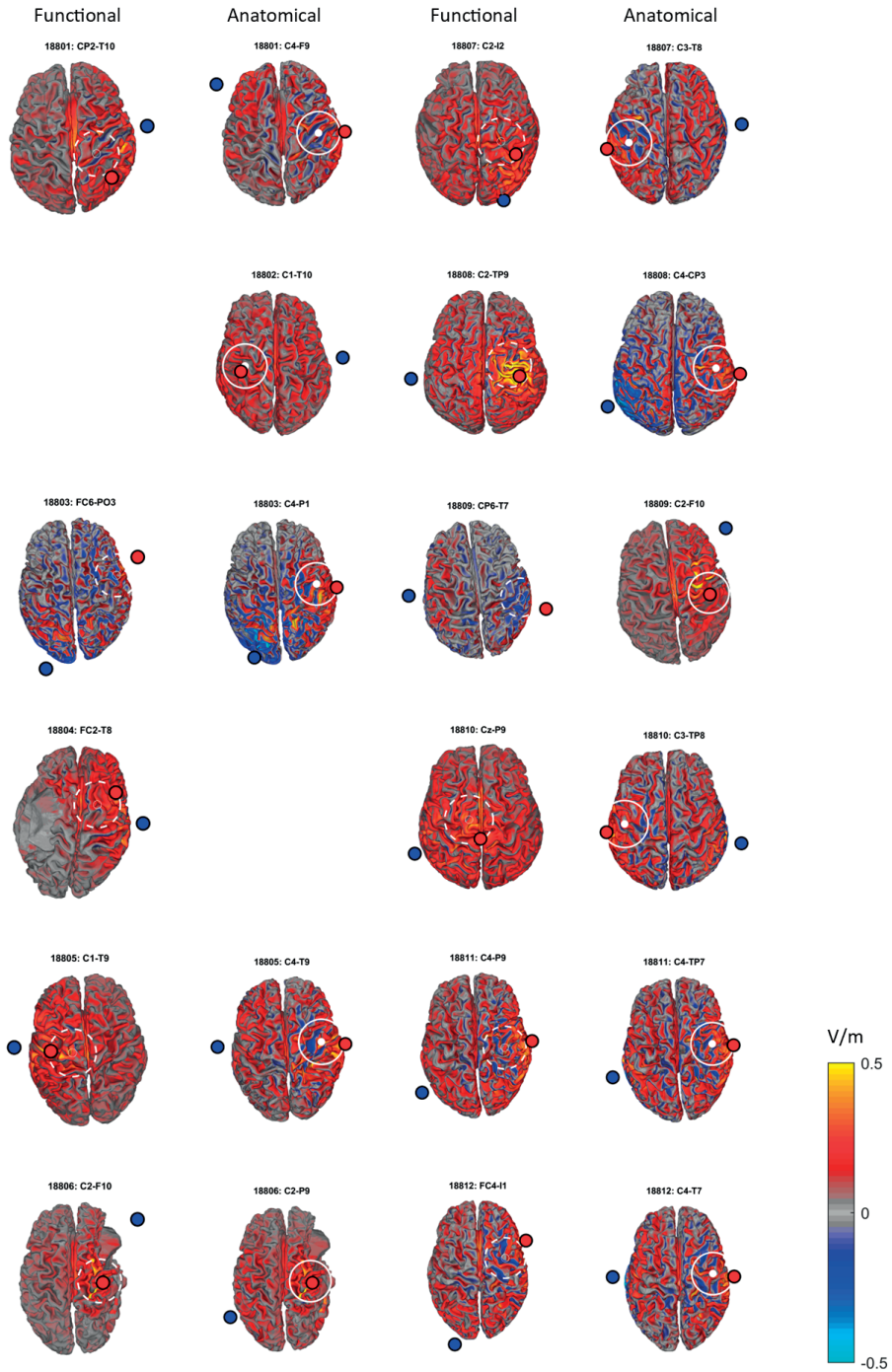
40. Pfurtscheller, G., Stancák, A. & Neuper, Ch. Event-related synchronization (ERS) in the alpha band — an electrophysiological correlate of cortical idling: A review. *International Journal of Psychophysiology* **24**, 39–46 (1996).
41. Rawji, V. *et al.* tDCS changes in motor excitability are specific to orientation of current flow. *Brain Stimul* **11**, 289–298 (2018).
42. Radman, T., Ramos, R. L., Brumberg, J. C. & Bikson, M. Role of cortical cell type and morphology in subthreshold and suprathreshold uniform electric field stimulation in vitro. *Brain Stimulation: Basic, Translational, and Clinical Research in Neuromodulation* **2**, 215–228.e3 (2009).
43. Jacobson, L., Koslowsky, M. & Lavidor, M. TDCS polarity effects in motor and cognitive domains: A meta-analytical review. *Experimental Brain Research* vol. 216 1–10 Preprint at <https://doi.org/10.1007/s00221-011-2891-9> (2012).
44. Saturnino, G. B., Siebner, H. R., Thielscher, A. & Madsen, K. H. Accessibility of cortical regions to focal TES: Dependence on spatial position, safety, and practical constraints. *Neuroimage* **203**, 116183 (2019).
45. Pimentel, M. A. F., Vilela, P., Sousa, I. & Figueiredo, P. Localization of the hand motor area by arterial spin asking and blood oxygen level-dependent functional magnetic resonance imaging. *Hum Brain Mapp* **34**, 96–108 (2013).
46. Mosayebi-Samani, M. *et al.* The impact of individual electrical fields and anatomical factors on the neurophysiological outcomes of tDCS: A TMS-MEP and MRI study. *Brain Stimul* **14**, 316–326 (2021).
47. Orrù, G., Conversano, C., Hitchcott, P. K. & Gemignani, A. Motor stroke recovery after tDCS: A systematic review. *Rev Neurosci* **31**, 201–218 (2020).
48. Bornheim, S. *et al.* Evaluating the effects of tDCS in stroke patients using functional outcomes: a systematic review. *Disability and Rehabilitation* vol. 44 13–23 Preprint at <https://doi.org/10.1080/09638288.2020.1759703> (2022).
49. López-Alonso, V., Cheeran, B., Río-Rodríguez, D. & Fernández-Del-Olmo, M. Inter-individual variability in response to non-invasive brain stimulation paradigms. *Brain Stimul* **7**, 372–380 (2014).
50. Laakso, I., Tanaka, S., Koyama, S., De Santis, V. & Hirata, A. Inter-subject variability in electric fields of motor cortical tDCS. *Brain Stimul* **8**, 906–913 (2015).
51. Antonenko, D. *et al.* Inter-individual and age-dependent variability in simulated electric fields induced by conventional transcranial electrical stimulation. *Neuroimage* **224**, 117413 (2021).
52. Wanifuchi, H., Shimizu, T. & Maruyama, T. Age-related changes in the proportion of intracranial cerebrospinal fluid space measured using volumetric computerized tomography scanning. *J Neurosurg* **97**, 607–610 (2002).
53. Datta, A., Baker, J. M., Bikson, M. & Fridriksson, J. Individualized model predicts brain current flow during transcranial direct-current stimulation treatment in responsive stroke patient. *Brain Stimul* **4**, 169–174 (2011).
54. Ward, N. S. Functional reorganization of the cerebral motor system after stroke. *Curr Opin Neurol* **17**, 725–730 (2004).
55. Stagg, C. J. *et al.* Polarity and timing-dependent effects of transcranial direct current stimulation in explicit motor learning. *Neuropsychologia* **49**, 800–804 (2011).
56. Tazoe, T., Endoh, T., Kitamura, T. & Ogata, T. Polarity Specific Effects of Transcranial Direct Current Stimulation on Interhemispheric Inhibition. *PLoS One* **9**, e114244 (2014).
57. Horvath, J. C., Vogrin, S. J., Carter, O., Cook, M. J. & Forte, J. D. Effects of a common transcranial direct current stimulation (tDCS) protocol on motor evoked potentials found to be highly variable within individuals over 9 testing sessions. *Exp Brain Res* **234**, 2629–42 (2016).

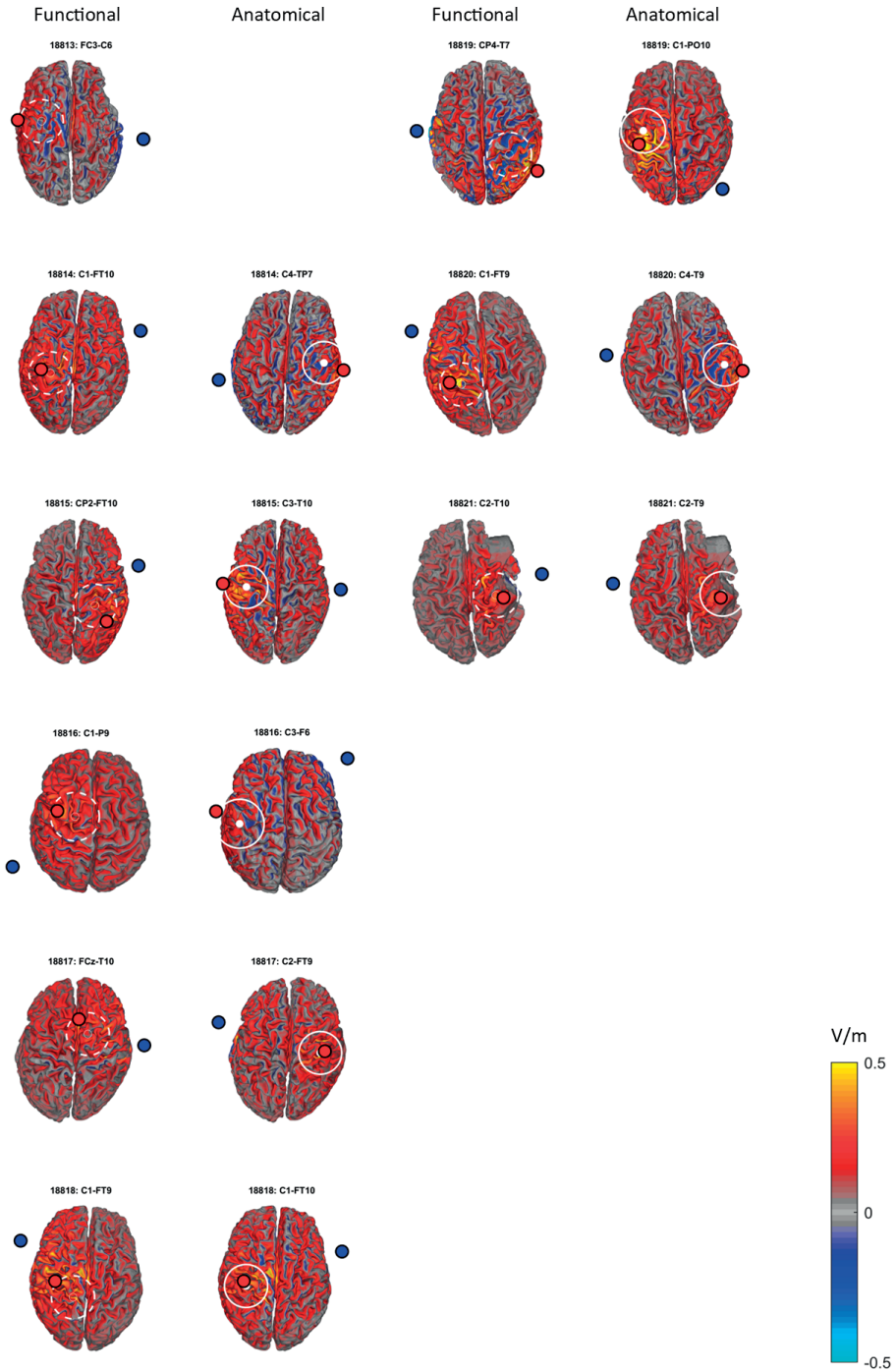
58. Cunningham, D. A. *et al.* Stimulation targeting higher motor areas in stroke rehabilitation: A proof-of-concept, randomized, double-blinded placebo-controlled study of effectiveness and underlying mechanisms. *Restor Neurol Neurosci* **33**, 911–926 (2015).
59. Numssen, O. *et al.* Efficient high-resolution TMS mapping of the human motor cortex by nonlinear regression. *Neuroimage* **245**, (2021).
60. Greenberg, D. L. *et al.* Aging, gender, and the elderly adult brain: an examination of analytical strategies. *Neurobiol Aging* **29**, 290 (2008).
61. Mikkonen, M., Laakso, I., Tanaka, S. & Hirata, A. Cost of focality in TDCS: Interindividual variability in electric fields. *Brain Stimul* **13**, 117–124 (2020).
62. Thut, G. *et al.* Guiding transcranial brain stimulation by EEG/MEG to interact with ongoing brain activity and associated functions: A position paper. *Clinical Neurophysiology* **128**, 843–857 (2017).
63. Weise, K., Numssen, O., Thielscher, A., Hartwigsen, G. & Knösche, T. R. A novel approach to localize cortical TMS effects. *Neuroimage* **209**, 116486 (2020).
64. McCann, H., Pisano, G. & Beltrachini, L. Variation in Reported Human Head Tissue Electrical Conductivity Values. *Brain Topogr* **32**, 825–858 (2019).
65. McCann, H. & Beltrachini, L. Does participant's age impact on tDCS induced fields? Insights from computational simulations. *Biomed Phys Eng Express* **7**, (2021).
66. van der Cruijssen, J., Piastra, M. C., Selles, R. W. & Oostendorp, T. F A Method to Experimentally Estimate the Conductivity of Chronic Stroke Lesions: A Tool to Individualize Transcranial Electric Stimulation. *Front Hum Neurosci* **15**, 599 (2021).

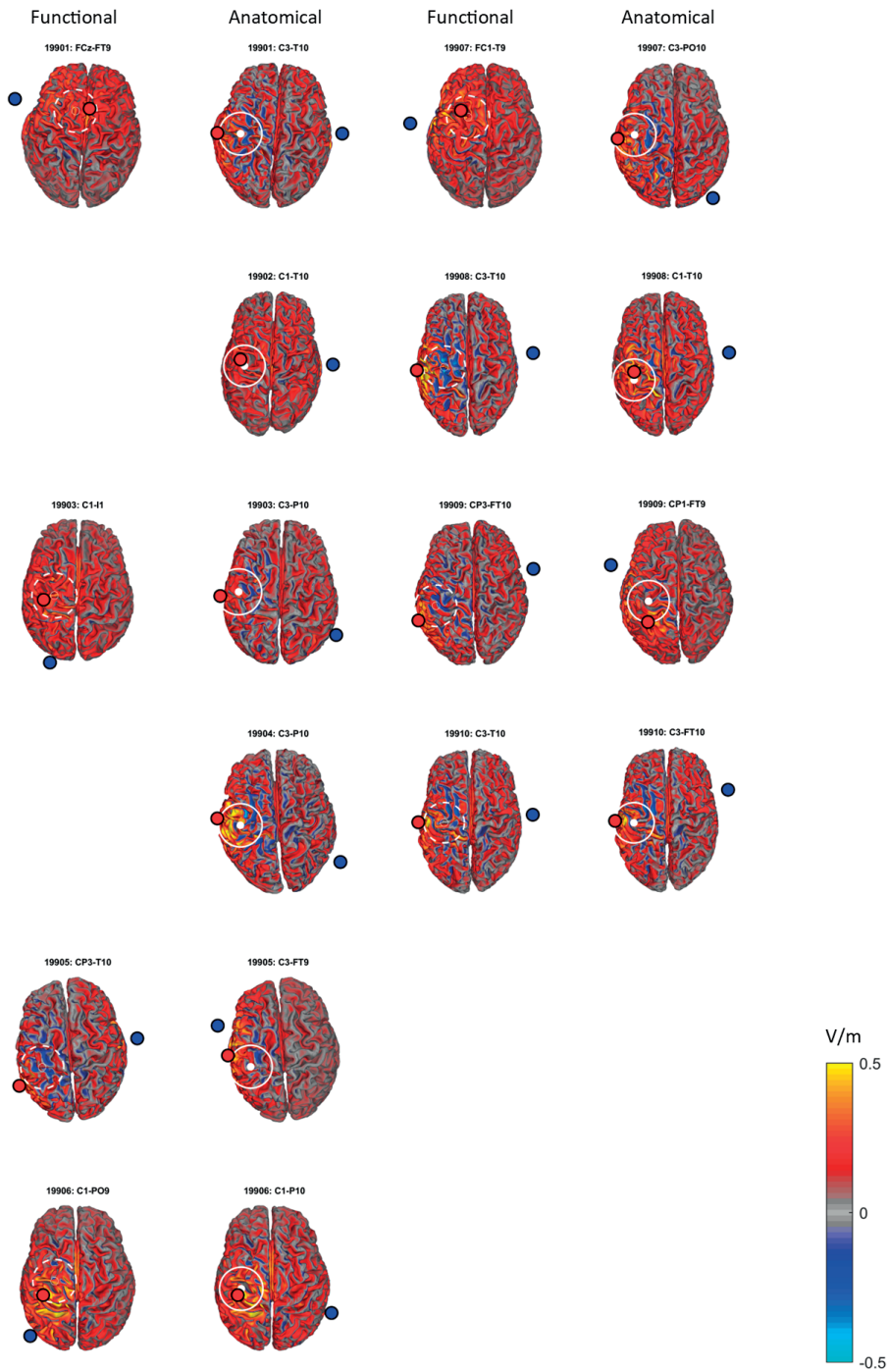
Supplementary material

The following pages show the optimal electrode positions for patients with chronic stroke and healthy controls. In each panel, anodes are plotted in red, cathodes in blue, stimulation regions of interest are marked with white circles. The normal component of the electric field is plotted on the middle layer of the grey matter of each subject. Page 2-3: subjects with chronic stroke; Page 4: healthy controls.

For subjects 18802, 19902, and 19904, no functional target could be identified. For subjects 18804 and 18813, no anatomical target could be identified.







Chapter 7

General Discussion

The research described in this thesis aims to improve the effectiveness of transcranial direct current stimulation (tDCS) in stroke patients. The following five objectives were defined: 1) explore objective neurophysiological measures of explicit motor learning; 2) verify whether targeting tDCS to the motor network improves corticospinal excitability more than conventionally targeting only the contralateral M1; 3a) simplify the creation of MRI-based head models of stroke patients to simulate tDCS; 3b) determining the individualized estimation of the stroke lesion's conductivity, and 4) compare the variability in electric fields strength due to interindividual differences in brain anatomy and motor function, between healthy individuals and patients with stroke. The following sections discuss each of these goals and how they contribute to increasing the effectiveness of tDCS for motor rehabilitation in patients with stroke.

Electrophysiology of explicit motor learning

Motor rehabilitation of stroke patients may be improved by modulating their brain activity using tDCS. The three most popular frameworks to explain motor behaviour after stroke in terms of neurophysiological patterns are the interhemispheric inhibition model, the vicariation model and the bimodal balance recovery model. tDCS interventions should be designed differently according to which of these three models is considered. A prospect of tDCS research is the real-time modulation of the brain regions involved in learning a specific motor task, based on the cortical activity of those brain regions during that specific motor task. Therefore, the goal of Chapter 2 was to determine the brain regions and dynamics involved in learning an explicit motor learning task.

In the research described in Chapter 2, healthy subjects performed both a complex and a simple motor learning task. In both tasks, participants controlled a force transducer to move a cursor to predefined targets at time points indicated by auditory metronome cues. Based on the differences in EEG power between the complex and the simple task, EEG activity related to learning the movement was separated from activity related to moving itself. The clusters of brain activity corresponding to these two types of activity were categorized into a cognitive component, comprising the cingulate cortical regions, and a motor component, comprising the contralateral and ipsilateral primary motor cortices. The brain dynamics related to these areas were primarily manifested in the theta band (5 – 8 Hz) in the cingulate cortical areas and the contralateral primary motor cortex (M1). In addition, beta (14 – 30 Hz) power suppression was more prominent in the ipsilateral M1, but that was not correlated to higher learning rates.

Theta power from the cingulate cortical region reflects a cognitive component of motor learning and can be used to monitor motor learning. Right after the auditory cues indicat-

ing when individual targets in the task had to be reached, theta bursts from the cingulate clusters were observed. These likely represent the processing of visual feedback related to performance in the motor task. Previous research has associated theta power with cognitive aspects of (motor) learning, such as error processing.^{1,2} In order to increase performance, participants must be able to learn from the errors they make, implying that detecting errors is a prerequisite of learning. The relationship between error amplitude and theta power differs between subjects, depending on individual learning dynamics.³ By changing the scale of how feedback on performance is presented, theta power/error sensitivity and motor learning can be increased.⁴ These relationships between movement error and theta power imply that cingulate cortex theta power may reflect whether participants are aware of suboptimal motor performance.

Bilateral beta desynchronization in the contralateral and ipsilateral M1 during task execution may be an electrophysiologic measure to monitor motor learning. Although no linear relationship between motor learning rates and the amount of bilateral M1 desynchronization was found, bilateral activation may be informative for motor learning. Bilateral M1 activity during unimanual tasks has previously been related to task difficulty in healthy subjects and patients with stroke, depending on task complexity.⁵⁻⁸ In line with this dependence on task difficulty, ipsilateral M1 beta desynchronization likely supports complex motor behaviour. As such, the amount of ipsilateral M1 involvement can be monitored during learning, and when a task becomes easier to perform, it is expected to reduce over time.

In cross-sectional studies with stroke patients, contralesional activity during unimanual motor tasks of the paretic upper limb is often associated with worse behavioural outcome measures than purely ipsilesional activity patterns.^{9,10} Inspired by TMS studies that demonstrate increased interhemispheric inhibition at rest from the nonparetic hemisphere to the lesioned hemisphere,^{11,12} some tDCS interventions attempt to suppress the contralesional M1 in order to enhance motor learning. However, several other studies show that interhemispheric inhibition from the ipsilateral to the contralateral hemisphere is reduced prior to movement onset in healthy elderly subjects¹³ and patients with stroke.¹⁴ Therefore, the relationship between interhemispheric inhibition and the functional role between the ipsilateral M1 and contralateral M1 does not seem fully understood. A better understanding of the contralesional hemisphere's supportive or restrictive role is needed to determine the optimal tDCS parameters in individual patients with stroke. It is crucial to consider these two potential roles of the contralesional M1, as suppressing the ipsilateral hemisphere reduces learning rates in healthy individuals and could thus have detrimental effects on motor rehabilitation in patients with stroke.¹⁵

In summary, cingulate theta power and bilateral M1 beta power could serve as electrophysiologic measures to monitor explicit motor learning; theta power to monitor how participants process feedback on performance and beta power to monitor the effort required to perform the motor task. For patients with stroke specifically, elucidating the role of the contralesional beta band in motor learning is important to determine if tDCS should be used to enhance or inhibit such activity.

TDCS and corticospinal excitability

The previous section discussed the EEG dynamics of the contralateral and ipsilateral M1 in explicit motor learning in healthy subjects. Currently, most non-invasive brain stimulation studies in healthy subjects ignore the ipsilateral M1 (i.e., conventional anodal tDCS targets the contralateral M1 only) or, following the interhemispheric inhibition framework, even intentionally inhibit the ipsilateral M1 (bilateral/dual tDCS with a cathode on the ipsilateral M1). In 2017, Fischer et al. (2017) simultaneously stimulated both primary motor cortices [motor network tDCS¹⁶] in healthy individuals and reported a twofold increase in corticospinal excitability compared to conventional anodal tDCS. As such, motor network tDCS is an exciting approach for motor rehabilitation that matches demanding motor tasks involving both primary motor cortices. However, replication rates of tDCS studies are generally low,^{17,18} and motor network tDCS, so far, has only been applied once. Therefore, the goal of Chapter 3 was to investigate if motor network tDCS indeed increases corticospinal excitability more than conventional tDCS.

In **Chapter 3** of this thesis, the effects of motor network tDCS, conventional anodal tDCS and sham tDCS on corticospinal excitability over time in healthy individuals were compared. Based on the data reported by Fischer et al. (2017), our experimental design had an *a priori* statistical power of 99% to detect differences between motor network tDCS and sham tDCS, and a power of 86% to detect differences in conventional anodal tDCS and sham tDCS, respectively. However, only one in 21 subjects had increased corticospinal excitability following motor network tDCS and conventional tDCS relative to sham stimulation. No average group effect of motor network tDCS or conventional tDCS relative to sham stimulation was found.

The data described in Chapter 3, therefore, provide no evidence that either motor network tDCS or conventional tDCS increases corticospinal excitability. The inability to replicate the tDCS effects is not unique to Chapter 3, but is a significant issue withholding tDCS from fulfilling its suggested therapeutic potential. Even for corticospinal excitability, once reported as the only outcome measure modulated consistently by tDCS,¹⁸ modulation does not always follow stimulation.^{3,19,20} However, the variability in tDCS stimulation parameters

complicates the direct comparison between studies. Reviews show that tDCS studies use different electrode sizes, stimulation durations, and injection currents that may explain these differences in stimulation effects on corticospinal excitability.¹⁸

Results from different stimulation parameters have led to the proposition that tDCS responses scale non-linearly with stimulation current. A common factor of these stimulation parameters is their relation to the amount of electric charge that passes through the targeted cortical region for the duration of the stimulation session. For instance, Jamil et al. (2017), stimulating for 15 minutes with 35 cm² electrodes, acquired the most substantial tDCS effects after stimulation at 1 mA and not at 1.5 or 2.0 mA.²¹ However, a different study showed opposite effects after 20 minutes of cathodal tDCS at 2.0 mA and 1.0 mA.²² Reversed tDCS effects have also been described as related to stimulation duration for anodal tDCS at 1.0 mA²³ and 2.0 mA.²⁴

The hypothesized non-linear dose/response relationship may explain the absence of a consistent response for conventional tDCS and motor network tDCS due to their differences in electric field strength at the M1. However, the exact electric field for each stimulation configuration depends on the size of the stimulation electrodes,²⁵ and the conductivity and distribution of the different tissue types comprising the head of individual subjects.²⁶ The relationship between stimulation dose and stimulation effects can be explored by modelling the electric fields generated by specific tDCS configurations in individualized MRI-based head models. Since no MRI data were available to model tDCS in Chapter 3, it cannot be concluded (nor ruled out) that a non-linear dose/response relationship resulted in the reported findings.

In summary, the study presented in Chapter 3 provides no evidence that motor network tDCS or conventional anodal tDCS enhance corticospinal excitability. Literature suggests that these effects could be absent due to interindividual differences in electric field strength at the stimulation target between motor network tDCS and conventional anodal tDCS. However, since the response to motor network tDCS and conventional anodal tDCS was equal to sham stimulation, Chapter 3 also challenges the potential effects of tDCS on corticospinal excitability. Simulation of tDCS may help determine the fundamental relationship between tDCS parameters and neurophysiologic/behavioural responses.

Simulation of tDCS in stroke patients

The previous section suggested that modelling electric fields can help to understand the relationship between tDCS effects and the electric field strength at the targeted brain regions. In

patients with stroke, tDCS has been simulated in small sample sizes only^{27–29} because identifying and modelling stroke lesions is currently subjective and labour-intensive. However, the studies of Minjoli et al. (2017) and Wagner et al. (2007) show that lesions affect the electric fields generated by tDCS. Consequently, including lesions in head models is vital to simulate tDCS accurately. Therefore, the goal of the study described in Chapter 4 was to develop a pipeline to incorporate stroke lesions in models for the simulation of tDCS.

The study presented in Chapter 4 described an automatic pipeline to create finite element head models of patients with stroke by combining already existing open-source toolboxes (SimNIBS (for simulation of tDCS in head models of healthy individuals³⁰) and LINDA (for lesion segmentation³¹) to model the lesion as a distinct type of tissue. The lesion was implemented by relabelling cerebrospinal fluid, grey and white matter elements overlapping with the lesion to ‘lesion’, which allowed varying the conductivity of the lesion independently of the other tissue types. The pipeline was applied to MRI recordings of 16 patients with chronic stroke. In these patients, it was shown that stroke lesions with conductivities different than the brain alter the magnitude of the local electric field during conventional anodal tDCS, depending on the lesion size and proximity to the stimulation target.

The automatic pipeline allows the creation of head models of patients with stroke from structural T1 MRI without requiring additional input from the researcher. This pipeline simplifies modelling tDCS in patients with stroke because all tDCS simulation functions of SimNIBS are preserved. The effects stroke lesions exerted on the local electric field within stimulation targets were dependent on the lesion volume and proximity to the stimulation target, as was reported in other studies.^{27,32} In addition, Chapter 4 supported that the stroke lesion’s conductivity needs consideration, as more current is shunted away from the target as the lesion conductivity increases. However, the change in the electric field strength within the target can be positive (increasing the electric field) or negative (reducing the electric field),³² depending on the stimulation electrode positions and a combination of lesion volume, location, and conductivity.

The previous results demonstrate that including the conductivity of the lesion is important to accurately model the lesion’s effects on the electric field around stimulation targets. Previous studies that simulated tDCS in head models of patients with stroke assumed stroke lesions as volumes of CSE,^{27–29} but MRI of patients with stroke suggests that this assumption might not hold for all subjects. An estimation of the lesion conductivity could thus potentially further increase the accuracy of head models of patients with stroke used to simulate tDCS. Therefore, the objective of Chapter 5 was to develop a method to estimate the conductivity of stroke lesions.

The study of Chapter 5 investigated whether the conductivity of stroke lesions can be estimated from scalp EEG recordings during tDCS. MRI-based boundary element models were created from MRI recordings of patients with stroke. In these models, stroke lesions (segmented using LINDA³¹) were inserted as sub-compartments of the brain compartment. Through simulation, transcranial current was applied to the model, and the corresponding electric potentials were recorded by (simulated) EEG electrodes. Scalp potentials were extracted from a model with a fixed lesion conductivity (i.e., the patient in practice) and a model with variable lesion conductivity. An estimate of the lesion conductivity was derived by minimizing the error between the two models. Lesion conductivity estimation is possible with relative errors below 5% for specific lesion properties (a combination of lesion volume, location, and conductivity) purely from tDCS-generated electric potentials picked up with scalp EEG. However, the method's accuracy is sensitive to EEG electrode position registration errors and is unsuitable for lesions that are small or located deeper inside the brain and for lesions that have a conductivity closer to the conductivity of the brain.

Chapter 5 showed that combined tDCS and EEG recordings could be used to estimate the conductivity of stroke lesions. In particular, the conductivity of lesions that most strongly affect the electric field generated by tDCS can be estimated with the lowest relative error. The variation in conductivity of stroke lesions on tDCS-induced electric fields has not been addressed experimentally. However, the changes in electric field strength for different lesion conductivities – up to 30%³²) or 11 to -63% (Chapter 4) – fall within the same range as the studies that reported a non-linear tDCS dose/response relationship by varying stimulation current between 1 and 2 mA.^{21,22} Consequently, differences in lesion characteristics may interfere with reliably determining the response to tDCS in patients with stroke, and simulation can be a helpful tool to prevent this.

In summary, in Chapters 4 to 5 tools were described to determine the electrode positions to stimulate a predefined stimulation target by 1) simplifying the generation of finite element head models of patients with stroke and 2) developing a method to estimate the conductivity of stroke lesions.

Simulation of tDCS in patients with stroke

The effects of lesions on the local electric field during conventional anodal tDCS have not yet been investigated in a large sample of patients with stroke. TDCS simulations have often been applied to find optimal tDCS configurations^{16,33,34} and to understand the relationships between electric fields and electrophysiologic responses^{35,36} but only in healthy individuals. Therefore, the objective of Chapter 6 was to compare the electric fields generated by conventional anodal

tDCS patients with stroke to those of healthy, age-matched controls and to assess the need for individualized tDCS configurations in patients with stroke.

In Chapter 6, the pipeline generated in Chapter 4 is used to simulate conventional anodal tDCS in an anatomy-based and EEG-based stimulation target. The normal component of the electric field was extracted from these regions for conventional anodal tDCS and compared to the same targets in healthy individuals. In addition, the electrode positions maximally stimulating the anatomical and functional target were found by optimization. The normal component of the electric fields within stimulation targets was significantly lower in patients with stroke than in healthy age-matched controls. In addition, it was shown that choosing different stimulation electrode locations from the standard ones increases the electric field strength to similar levels as in healthy controls, solving the reduced stimulation levels in patients with stroke.

In Chapter 6 is shown that a one-size-fits-all approach of conventional anodal tDCS is unsuitable for patients with stroke. This conclusion holds for the anatomy-based target (the motor hand knob derived from the T1-weighted MRI) and the EEG-based target. Optimizing the electrode positions to maximize the stimulation of the anatomical and functional target brings the normal component of the electric field within those stimulation targets to similar levels as found in healthy, age-matched controls. It is, as yet, unclear if reducing the variability in electric field strength within stimulation targets will solve the inconsistent behavioural responses of tDCS.

The main question that Chapter 6 does not solve is whether the results can help to retrospectively interpret the mixed results of previous tDCS studies in patients with stroke. In the absence of experimental data, this can only be speculated, as the results of Chapter 6 do not generalize to other patients with stroke because of the inherent variability in how lesions affect the brain between patients.³⁷ Interestingly, a meta-analysis showed that only conventional cathodal tDCS, i.e., targeting the contralesional M1, had a consistent effect on upper limb activities in the daily life of patients with stroke.³⁸ The effectiveness of conventional cathodal tDCS matches the observations of Chapter 6, as stroke lesions affect the contralesional hemisphere less than the ipsilesional hemisphere. Therefore, the electric fields within the contralesional M1 may be more like those of healthy subjects, as is the behavioural response. However, as noted before, tDCS responses are also variable in healthy individuals with less structural and functional variability. Individualizing the electrode positions solves the variability in electric field strength within stimulation targets but not the variable outcomes of tDCS if all other factors affecting tDCS outcome remain unsolved.

In summary, Chapter 6 shows the importance of designing individualized tDCS configurations for patients with stroke, as the variability in electric field strength within stimulation targets is larger compared to healthy controls in conventional anodal tDCS. Optimization of the electrode positions reduces this variability, such that the electric field strength in the stimulation targets of patients with stroke rises similar levels as in healthy individuals.

Methodological considerations

There are several methodological considerations to the content of this thesis. First, in **Chapter 2** the neural correlates of explicit motor learning were investigated. During explicit motor learning, participants know how to improve the outcome measure of interest, whereas implicit learning keeps participants unaware of how to increase performance.³⁹ Consequently, both types of learning have different cognitive loads. For motor rehabilitation in patients with stroke, cognitive function may be impaired and vary between patients; thus, it depends on the individual whether patients learn a task best implicitly or explicitly. Therefore, the findings described in Chapter 2, particularly those concerning feedback processing, may not generalize to implicit motor learning tasks. For motor cortex activation, however, neuroimaging studies show bilateral M1 activation in healthy subjects and patients with neurological disorders for both explicit and implicit learning.^{40,41}

Another limitation of the study presented in Chapter 2 follows from the study design. Participants performed only a single motor learning session. Consequently, it was impossible to investigate how bilateral beta desynchronization was reduced with increased skill acquisition in the motor learning task. Multiple sessions of the motor learning task would be required to explore whether the bilateral beta desynchronization could be related to motor skill acquisition. In Chapter 2, a homogeneous study sample of young, healthy people instead of elderly or patients with stroke participated. Previous research in healthy young, healthy elderly, and patients with stroke showed differences in baseline beta power, movement-related beta desynchronization, and post-movement beta rebound.⁴² However, besides these differences, well-recovered patients with stroke showed similar patterns of bilateral beta dynamics during motor learning as those described in Chapter 2.^{5,6}

In the study described in Chapter 3, healthy participants received three different types of tDCS to the motor cortex to attempt to replicate previously reported results of motor network tDCS.¹⁶ Conventional anodal tDCS, motor network tDCS, and sham tDCS had similar effects on corticospinal excitability. There are several potential causes for the lack of consistent effects.⁴³ Due to the relatively small sample size of 21 participants, it was impossible to perform sub-analyses. In addition, no structural MRI of the participants was

available to simulate the electric fields generated by the different tDCS configurations to analyse the existence of a dose-response relationship. Another limitation follows from the TMS protocol used to measure tDCS affects corticospinal excitability. Although commonly used, TMS MEPs are highly variable, and repetitive TMS pulses may affect corticospinal excitability,⁴⁴ thus intervening with potential tDCS effects. However, if a series of TMS pulses with random inter-stimulus intervals already interferes with tDCS effects, then that questions both the suitability of MEPs as an outcome measure to quantify tDCS effects and the potential added value of tDCS.

A common limitation of the results of Chapters 4 to 6 comes from the assumptions underlying the volume conductor models used for simulation. All models rely on assumptions on the electric conductivity of the different types of tissue comprising the model. In particular, the conductivity of the skull varies significantly between subjects.⁴⁵ Not accounting for this variability may lead to inaccurate source localization of EEG data and less accurate electric field strengths from tDCS simulation. Given the age-related differences in skull conductivity^{46,47} and the age differences between samples of healthy subjects and patients with stroke, there could be an interaction effect of age with electric field strength at the stimulation targets that requires consideration in future studies.

In addition to the previous limitation, Chapters 4 to 6 would have benefitted from experimental validation of the simulations. Due to the lack of experimental data, lesion conductivity estimation remains to be validated with the described combination of EEG and tDCS. In addition, Chapter 6 showed optimized tDCS electrodes resulted in similar electric fields in patients with stroke as in healthy subjects. However, it remains to be tested whether reducing the variability in electric field strength at the stimulation targets reduces the variability in behavioural and electrophysiologic response to tDCS.

Implications

The study described in Chapter 2 of this thesis revealed bilateral beta desynchronization during motor learning, potentially reflecting a relation with the perceived difficulty of the motor learning task. From observing these bilateral activation patterns during a motor task in patients with stroke remains unclear what the most suitable stimulation configuration would be to improve the learning rate. In the context of tDCS, stroke, and interhemispheric inhibition, at first sight, it seems to make sense to inhibit the contralesional M1 in the presence of bilateral M1 activity. However, as observed in Chapter 2, these dynamics could also reflect patterns observed in 'healthy' individuals performing a difficult task. Therefore, new intervention studies should

consider the cortical dynamics associated with a specific motor task of interest to determine the electrode positions and current polarity to modulate the motor system.

Motor network tDCS targets the motor regions involved in motor learning and, therefore, seems by design suitable to modulate learning rates in complex motor tasks. However, the absence of any group effect on corticospinal excitability of motor network tDCS and conventional anodal tDCS provides no fundament to take these configurations towards modulation of motor learning in healthy individuals or patients with stroke. In patients with stroke, stroke lesions complicate the application of tDCS by structural changes within the brain and functional changes of the motor system, indicating that the clinical implementation of tDCS in a patient group is even less straightforward than in healthy subjects.

This thesis addressed several sources of interindividual variability in patients with stroke to improve tDCS in these patients. The variability requires the individual assessment of motor learning dynamics and brain structure to develop patient-tailored tDCS configurations to modulate the motor system and promote learning/rehabilitation. In addition, individual skull and stroke lesion conductivity estimates help improve the accuracy of tDCS simulation and explore the existence of a stimulation dose/response relationship.

Future research

The results of this thesis increased the distance to the point on the horizon of clinically implementing tDCS in patients with stroke. Although this thesis addressed stroke lesions as important sources of variability in patients with stroke, the variability in tDCS already present in healthy subjects remains an open topic. Additional steps have to be made in 1) understanding the electrophysiology of motor learning in healthy subjects and patients with stroke, 2) quantifying the effects of tDCS on physiology and behavioural measures, and 3) understanding the relationship between electric field strength and stimulation effect. Several follow-up studies may address these three topics.

Concerning electrophysiology and motor learning, it would be interesting to determine the relationship between the bilateral beta desynchronization during movement, the level of difficulty for a specific motor learning task and the corresponding learning rates. A recent motor learning study showed that healthy elderly had higher retention rates after a motor task with lower difficulty than a more difficult task.⁸ The higher-difficulty task was also associated with a more bilateral EEG pattern, as reported in Chapter 2 of this thesis. Controllable environments, such as virtual reality and rehabilitation robotics, could be suitable to investigate the effect between learning rates, task difficulty, and primary motor cortex beta

lateralization and to optimize objective feedback on performance. In addition, EEG could help to investigate the relationship between the left and right primary motor cortices to determine how to apply non-invasive brain stimulation to facilitate motor learning and motor rehabilitation.

An additional topic for future research concerns quantifying the response to tDCS with alternatives to TMS-based measures, such as EEG. EEG is suitable for this purpose due to its high time resolution and unobtrusive nature. Early tDCS studies could not simultaneously record EEG due to the presence of large stimulation electrodes with surface areas up to 35 cm². However, cap-based stimulation systems allow this combination to explore EEG-based measures of corticospinal excitability. Therefore, the high-density EEG data additionally collected in Chapter 3 provides a unique opportunity to develop an EEG-based measure of corticospinal excitability that could easily be monitored over time to explore the effects of different tDCS configurations without potentially intervening with those effects.

Finally, Chapters 4 to 6 presented work that relied primarily on simulations of tDCS and the resulting electric fields at the scalp and within cortical stimulation targets. Based on these results, stroke lesions need to be included in the design of tDCS configurations to stimulate the motor system as intended. By individualizing electrode configurations, electric field strengths in patients with stroke can reach similar levels as those in healthy subjects, but experiments are needed to see if this also leads to less variability in outcome measures of interest. With the results and implications of Chapter 2 in mind, a better fundamental understanding of motor learning dynamics in patients with stroke is a more reasonable initial goal to allow a more hypothesis-driven approach when applying tDCS.

Besides a better understanding of motor learning dynamics, a better understanding of the working mechanism of tDCS is also required to uncover if tDCS truly has clinical potential. Low replicability rates in tDCS research due to generally low sample sizes, potential publication bias and lack of pre-registered studies make it difficult to distinguish true positive/negative from false positive/negative findings.¹⁷ The literature suggests that basic stimulation parameters such as stimulation current and duration draw only a thin line between positive, negative, or null effects. However, given the low replication rates, it is impossible to identify which studies describe genuine tDCS effects and thus can provide reliable directions for follow-up research. Before the application of tDCS can be considered in stroke rehabilitation, solving these inconsistencies is crucial. In particular, if tDCS has the clinical potential once awarded, incompletely controlling these basic tDCS parameters could lead to maladaptive functional reorganization in patients with stroke. However, as two decades of tDCS research have not been able to capture the effects of basic parameters in tDCS research fully, it seems

not realistic in the foreseeable future that tDCS can be reliably applied to improve motor rehabilitation in patients with stroke.

References

1. Holroyd, C. B. & Coles, M. G. H. The neural basis of human error processing: Reinforcement learning, dopamine, and the error-related negativity. *Psychol Rev* **109**, 679–709 (2002).
2. Luu, P., Tucker, D. M. & Makeig, S. Frontal midline theta and the error-related negativity: Neurophysiological mechanisms of action regulation. *Clinical Neurophysiology* **115**, 1821–1835 (2004).
3. Jonker, Z. D. *et al.* No effect of anodal tDCS on motor cortical excitability and no evidence for responders in a large double-blind placebo-controlled trial. *Brain Stimul* **14**, 100–109 (2021).
4. Watanabe, T., Mima, T., Shibata, S. & Kirimoto, H. Midfrontal theta as moderator between beta oscillations and precision control. *Neuroimage* **235**, 118022 (2021).
5. Espenhahn, S. *et al.* Sensorimotor cortex beta oscillations reflect motor skill learning ability after stroke. *Brain Commun* **2**, (2020).
6. Espenhahn, S. *et al.* Cortical beta oscillations are associated with motor performance following visuo-motor learning. *Neuroimage* **195**, 340–353 (2019).
7. Bueteftisch, C. M., Revill, K. P., Shuster, L., Hines, B. & Parsons, M. Motor demand-dependent activation of ipsilateral motor cortex. *J Neurophysiol* **112**, 999–1009 (2014).
8. Bootsma, J. M. *et al.* Neural Correlates of Motor Skill Learning Are Dependent on Both Age and Task Difficulty. *Front Aging Neurosci* **13**, 115 (2021).
9. Rehme, A. K., Fink, G. R., von Cramon, D. Y. & Grefkes, C. The role of the contralesional motor cortex for motor recovery in the early days after stroke assessed with longitudinal fMRI. *Cerebral Cortex* **21**, 756–768 (2011).
10. Bestmann, S. *et al.* The role of contralesional dorsal premotor cortex after stroke as studied with concurrent TMS-fMRI. *Journal of Neuroscience* **30**, 11926–11937 (2010).
11. Murase, N., Duque, J., Mazzocchio, R. & Cohen, L. G. Influence of interhemispheric interactions on motor function in chronic stroke. *Ann Neurol* **55**, 400–409 (2004).
12. Boddington, L. J. & Reynolds, J. N. J. Targeting interhemispheric inhibition with neuromodulation to enhance stroke rehabilitation. *Brain Stimul* **10**, 214–222 (2017).
13. Wischniewski, M. *et al.* Demand on skillfulness modulates interhemispheric inhibition of motor cortices. *J Neurophysiol* **115**, 2803–2813 (2016).
14. Xu, J. *et al.* Rethinking interhemispheric imbalance as a target for stroke neurorehabilitation. *Ann Neurol* **85**, 502–513 (2019).
15. Zimmerman, M., Heise, K.-F., Gerloff, C., Cohen, L. G. & Hummel, F. C. Disrupting the Ipsilateral Motor Cortex Interferes with Training of a Complex Motor Task in Older Adults. *Cerebral Cortex* **24**, 1030–1036 (2014).
16. Fischer, D. B. *et al.* Multifocal tDCS targeting the resting state motor network increases cortical excitability beyond traditional tDCS targeting unilateral motor cortex. *Neuroimage* **157**, 34–44 (2017).
17. Minarik, T. *et al.* The importance of sample size for reproducibility of tDCS effects. *Front Hum Neurosci* **10**, 1–5 (2016).
18. Horvath, J. C., Forte, J. D. & Carter, O. Evidence that transcranial direct current stimulation (tDCS) generates little-to-no reliable neurophysiologic effect beyond MEP amplitude modulation in healthy human subjects: A systematic review. *Neuropsychologia* **66**, 213–236 (2015).
19. Horvath, J. C., Vogrin, S. J., Carter, O., Cook, M. J. & Forte, J. D. Effects of a common transcranial direct current stimulation (tDCS) protocol on motor evoked potentials found to be highly variable within individuals over 9 testing sessions. *Exp Brain Res* **234**, 2629–42 (2016).
20. Wiethoff, S., Hamada, M. & Rothwell, J. C. Variability in response to transcranial direct current stimulation of the motor cortex. *Brain Stimul* **7**, 468–475 (2014).

21. Jamil, A. *et al.* Systematic evaluation of the impact of stimulation intensity on neuroplastic after-effects induced by transcranial direct current stimulation. *J Physiol* **595**, 1273–1288 (2017).
22. Batsikadze, G., Moliadze, V., Paulus, W., Kuo, M. F. & Nitsche, M. A. Partially non-linear stimulation intensity-dependent effects of direct current stimulation on motor cortex excitability in humans. *J Physiol* **591**, 1987 (2013).
23. Monte-Silva, K. *et al.* Induction of late LTP-like plasticity in the human motor cortex by repeated non-invasive brain stimulation. *Brain Stimul* **6**, 424–432 (2013).
24. Hassanzahraee, M., Nitsche, M. A., Zoghi, M. & Jaberzadeh, S. Determination of anodal tDCS duration threshold for reversal of corticospinal excitability: An investigation for induction of counter-regulatory mechanisms. *Brain Stimul* **13**, 832–839 (2020).
25. Mikkonen, M., Laakso, I., Tanaka, S. & Hirata, A. Cost of focality in TDCS: Interindividual variability in electric fields. *Brain Stimul* **13**, 117–124 (2020).
26. Laakso, I., Tanaka, S., Koyama, S., De Santis, V. & Hirata, A. Inter-subject variability in electric fields of motor cortical tDCS. *Brain Stimul* **8**, 906–913 (2015).
27. Minjoli, S. *et al.* The impact of large structural brain changes in chronic stroke patients on the electric field caused by transcranial brain stimulation. *Neuroimage Clin* **15**, 106–117 (2017).
28. Wagner, T. *et al.* Transcranial direct current stimulation: A computer-based human model study. *Neuroimage* **35**, 1113–1124 (2007).
29. Datta, A., Baker, J. M., Bikson, M. & Fridriksson, J. Individualized model predicts brain current flow during transcranial direct-current stimulation treatment in responsive stroke patient. *Brain Stimul* **4**, 169–174 (2011).
30. Thielscher, A., Antunes, A. & Saturnino, G. B. Field modeling for transcranial magnetic stimulation: A useful tool to understand the physiological effects of TMS? in *Proceedings of the Annual International Conference of the IEEE Engineering in Medicine and Biology Society, EMBS* vols 2015–Novem 222–225 (2015).
31. Pustina, D. *et al.* Automated segmentation of chronic stroke lesions using LINDA: Lesion identification with neighborhood data analysis. *Hum Brain Mapp* **37**, 1405–1421 (2016).
32. Johnstone, A., Zich, C., Evans, C., Lee, J. & Ward, N. The impact of brain lesions on tDCS-induced electric field magnitude 2 3. *bioRxiv* 2021.03.19.436124 (2021) doi:10.1101/2021.03.19.436124.
33. Rampersad, S. M. *et al.* Simulating transcranial direct current stimulation with a detailed anisotropic human head model. *IEEE Transactions on Neural Systems and Rehabilitation Engineering* **22**, 441–452 (2014).
34. Dmochowski, J. P. *et al.* Targeted transcranial direct current stimulation for rehabilitation after stroke. *Neuroimage* **75**, 12–19 (2013).
35. Ahn, S. & Fröhlich, F. Pinging the brain with transcranial magnetic stimulation reveals cortical reactivity in time and space. *Brain Stimul* **14**, 304–315 (2021).
36. Laakso, I., Mikkonen, M., Koyama, S., Hirata, A. & Tanaka, S. Can electric fields explain inter-individual variability in transcranial direct current stimulation of the motor cortex? *Sci Rep* **9**, 1–10 (2019).
37. Ward, N. S., Brown, M. M., Thompson, A. J. & Frackowiak, R. S. J. Neural correlates of outcome after stroke: A cross-sectional fMRI study. *Brain* **126**, 1430–1448 (2003).
38. Elsner, B., Kwakkel, G., Kugler, J. & Mehrholz, J. Transcranial direct current stimulation (tDCS) for improving capacity in activities and arm function after stroke: a network meta-analysis of randomised controlled trials. *J Neuroeng Rehabil* **14**, (2017).
39. Stadler, M. A. Distinguishing implicit and explicit learning. *Psychon Bull Rev* **4**, 56–62 (1997).

40. Chettouf, S., Rueda-Delgado, L. M., de Vries, R., Ritter, P. & Daffertshofer, A. Are unimanual movements bilateral? *Neuroscience and Biobehavioral Reviews* vol. 113 39–50 Preprint at <https://doi.org/10.1016/j.neubiorev.2020.03.002> (2020).
41. Revill, K. P. *et al.* Evaluating the Abnormality of Bilateral Motor Cortex Activity in Subacute Stroke Patients Executing a Unimanual Motor Task With Increasing Demand on Precision. *Front Neurol* **13**, (2022).
42. Rossiter, H. E., Davis, E. M., Clark, E. v., Boudrias, M. H. & Ward, N. S. Beta oscillations reflect changes in motor cortex inhibition in healthy ageing. *Neuroimage* **91**, 360–365 (2014).
43. López-Alonso, V., Cheeran, B., Río-Rodríguez, D. & Fernández-Del-Olmo, M. Inter-individual variability in response to non-invasive brain stimulation paradigms. *Brain Stimul* **7**, 372–380 (2014).
44. Pellicciari, M. C., Miniussi, C., Ferrari, C., Koch, G. & Bortoletto, M. Ongoing cumulative effects of single TMS pulses on corticospinal excitability: An intra- and inter-block investigation. *Clinical Neurophysiology* **127**, 621–628 (2016).
45. McCann, H. & Beltrachini, L. Does participant's age impact on tDCS induced fields? Insights from computational simulations. *Biomed Phys Eng Express* **7**, (2021).
46. Antonakakis, M. *et al.* Inter-Subject Variability of Skull Conductivity and Thickness in Calibrated Realistic Head Models. *Neuroimage* **223**, 117353 (2020).
47. Ciechanski, P., Carlson, H. L., Yu, S. S. & Kirton, A. Modeling Transcranial Direct-Current Stimulation-Induced Electric Fields in Children and Adults. *Front Hum Neurosci* **12**, 268 (2018).

Summary

Transcranial electric stimulation (tES) is a non-invasive neuromodulation technique that passes low currents through the brain via electrodes on the scalp. Dependent on the current polarity, tES can inhibit or enhance the activity of motor areas that are active during motor learning tasks. As such, transcranial electric stimulation could potentially play a role in the recovery of motor impairments after stroke by restoring the balance between hemispheres (interhemispheric inhibition) or by supporting the increased involvement of motor areas that were less involved pre-stroke (vicariation model) in a patient-specific way (bimodal balance recovery model). The studies described in this thesis aimed to evaluate and improve the application of tES, with a focus on tDCS, in patients after a stroke by 1) identifying and understanding electrophysiologic correlates of motor learning, 2) replicating a new type of tES that targets the entire resting-state motor network, 3) developing methods to include stroke lesions in volume conductor models, and 4) determining if conventional stimulation protocols are suitable to stimulate the motor regions of patients without individualization to brain anatomy and function.

In Chapter 1, a general introduction to stroke and the potential role of transcranial electric stimulation in the recovery of motor impairments following stroke. This thesis aims to understand the current challenges of the application of tDCS in patients with stroke using EEG and tDCS simulation in MRI-based head models of patients. Chapter 2 describes a study in which EEG-correlates of motor learning were identified in healthy subjects. Subjects performed simple and complex motor learning tasks requiring equal force but different precision. Higher theta power within the contralateral primary motor cortex and the cingulate regions was associated with higher learning rates, that is, a larger increase of absolute performance over time. This increase in theta power likely reflects the cognitive aspect of processing errors during motor learning. In addition, ipsilateral M1 beta suppression was larger in the complex task but not associated with higher learning rates. In the contralateral hemisphere, beta power did not differ between motor tasks. These findings suggest that monitoring contralateral M1 beta power may not be informative of motor learning rates, however, the learning-dependent progression of particularly the ipsilateral M1 beta suppression might be.

Chapter 3 evaluated the performance of a new transcranial direct current stimulation (tDCS) configuration that stimulates the entire resting-state motor network, using a total of 8 electrodes distributed over the motor cortex. As such, motor network stimulation takes a new direction compared to conventional protocols that stimulate only the contralateral hemisphere, while either ignoring or suppressing the ipsilateral M1. Subjects were randomized to motor network tDCS, conventional anodal tDCS, and sham tDCS sessions. Surprisingly, motor network tDCS and conventional tDCS both did not increase corticospinal excitability more than sham stimulation. Literature lists several sources of intersubject and intrasubject variability that may explain this lack of consistent stimulation effects. However, the results also contribute to an increasing body of literature that challenges the potential of tDCS to

consistently modulate corticospinal excitability and motor learning. In summary, the findings of Chapter 3 provide no basis for follow-up measurements of motor network tDCS in stroke patients.

In Chapter 4, a method to simulate the electric fields from tES in patients with stroke was developed. This pipeline allows the automated modelling of stroke lesions as a separate compartment in the brain by combining already existing toolboxes. The method was successfully applied in chronic stroke patients to study how the stroke lesion conductivity affects the magnitude of the electric field in the motor hand knob. The local electric field within the stimulation target was altered by the lesion, depending on the lesion conductivity, lesion size, and location relative to the region of interest. This study, therefore, showed that ignoring the lesion in the application of tDCS in patients with stroke may lead to suboptimal stimulation. In particular, the conventional assumption of the lesion as a volume of cerebrospinal fluid may lead to incorrect estimates of the effects of the lesion on the local electric field. Incorporating the stroke lesions in volume conductor models can help target tDCS in stroke patients.

Chapter 5 addresses the estimation of the electric conductivity of stroke lesions. The method uses (simulated) scalp potentials plus noise resulting from tDCS simulation in a model with a fixed lesion conductivity (i.e., the patient), and a model in which the lesion conductivity was variable. By minimizing the error between the two models, the conductivity of the lesion could be estimated. The relative estimation error of the method was assessed for varying electrode numbers, lesion conductivities, and lesion volumes. High lesion conductivity, large lesion volumes, and low lesion depth resulted in lower conductivity estimation errors. The method had relative estimation errors below 5% in the presence of minor EEG electrode coregistration errors but performed poorly for lesions smaller than 50 ml. These results suggest that the conductivity of the lesions that exert the largest effects on the local electric fields can be estimated with the highest confidence. Experimental data is required to validate the described method.

In Chapter 6 was investigated if a one-fits-all approach for the electrode configurations is suitable for applying tDCS in patients with stroke. MRI was used to identify an anatomy-based stimulation target in the motor cortex and EEG to identify a functional motor target. Stimulation electrodes maximally stimulating anatomical and functional targets were identified by optimization. Patients with stroke had more variable, significantly lower, and more frequently reversed electric field strengths within stimulation targets than healthy controls when using a one-fits-all conventional approach. Optimizing the electrode positions to maximize the electric field strength increased the stimulation strength of patients with stroke in both stimulation targets to the same level as conventional anodal tDCS in healthy controls. However, it remained significantly lower than optimized electrode positions in healthy con-

trols. These results imply that the conventional anodal tDCS leads to small and inconsistent electric field strength in patients with stroke and may contribute to the mixed findings in clinical tDCS trials. Experimental data should be collected to verify if reducing the electric field strength variability also reduces the stimulation response variability.

In Chapter 7, the main findings of each chapter of this thesis are discussed, followed by the implications and methodological considerations within the broader context of applying tDCS in patients with stroke, proposing several future research directions.

Samenvatting

Transcraniële elektrische stimulatie (tES) is een niet-invasieve neuromodulatietechniek waarbij lage stromen door de hersenen worden gestuurd via elektroden op de hoofdhuid. Afhankelijk van de stroompolariteit kan tES de activiteit van motorische gebieden die actief zijn tijdens motorische leertaken remmen of versterken. Daardoor zou transcraniële elektrische stimulatie mogelijk een rol kunnen spelen in het herstel van motorische stoornissen na een beroerte door het evenwicht tussen hemisferen te herstellen (interhemisferische inhibitie) of door verdere ondersteuning van de verhoogde betrokkenheid van motorische gebieden die voor de beroerte minder betrokken waren (vicariatmodel) op een patiënt-specifieke manier (bimodaal evenwichtsherstelmodel). Dit proefschrift is gericht op het evalueren en verbeteren van de toepassing van tES, met een focus op tDCS, bij patiënten na een beroerte door 1) het identificeren en begrijpen van elektrofyysiologische maten voor motorisch leren, 2) het repliceren van een nieuw type tES dat zich richt op het gehele *resting-state* motorisch netwerk, 3) het ontwikkelen van methoden om beroerte laesies op te nemen in volumegeleidingsmodellen, en 4) het bepalen of conventionele stimulatie protocollen geschikt zijn om de motorische gebieden van patiënten te stimuleren zonder individualisering naar de hersenanatomie en functie.

Hoofdstuk 1 gaf een algemene inleiding op beroerte en de potentiële rol van transcraniële elektrische stimulatie in het herstel van motorische stoornissen na een beroerte. Dit proefschrift beoogt de huidige uitdagingen van de toepassing van tDCS bij patiënten met een beroerte te begrijpen met behulp van EEG en tDCS simulatie in op MRI gebaseerde hoofdmodellen van patiënten. Hoofdstuk 2 beschrijft een studie waarin EEG-maten van motorisch leren werden geïdentificeerd bij gezonde proefpersonen. Proefpersonen voerden een eenvoudige en complexe motorische leertaak uit die dezelfde kracht maar verschillende precisie vereisten. Een hoger theta *power* in de contralaterale primaire motorische cortex en de cinguli gebieden was geassocieerd met een hogere leersnelheid: een grotere toename van de absolute prestatie in de tijd. Deze toename in theta *power* vertegenwoordigt waarschijnlijk het cognitieve aspect van het verwerken van fouten tijdens het motorisch leren. Bovendien was de ipsilaterale M1 bèta-suppressie groter in de complexe taak, maar niet geassocieerd met hogere leersnelheden. In de contralaterale hemisfeer verschilde bèta *power* niet tussen de leertaken. Deze bevindingen suggereren dat het monitoren van contralaterale M1 beta *power* mogelijk niet informatief is voor motorische leren, maar de verandering van vooral de ipsilaterale M1 beta suppressie gedurende het leren dat mogelijk wel is.

In Hoofdstuk 3 werden de effecten onderzocht van een nieuwe transcraniële gelijkstroom stimulatie (tDCS) configuratie die het gehele *resting-state* motorische netwerk stimuleert middels een totaal van 8 elektroden verdeeld over de motorische cortex. Motorische netwerk stimulatie neemt daarmee een nieuwe benadering in vergelijking met conventionele protocollen die alleen de contralaterale hemisfeer stimuleren en de ipsilaterale M1 ofwel negeren danwel onderdrukken. Proefpersonen ontvingen motorisch netwerk tDCS, conventionele

anodale tDCS, en *sham* tDCS sessies in willekeurige volgorde in 3 aparte experimentele sessies waar tenminste 48 uur tussen zat. Motorische netwerk tDCS en conventionele tDCS leidden verrassend genoeg niet tot een verhoging van corticospinale exciteerbaarheid ten opzichte van *sham* stimulatie. De literatuur noemt verschillende bronnen van variabiliteit binnen en tussen proefpersonen die dit gebrek aan consistente stimulatie effecten kunnen verklaren. Echter, de resultaten dragen ook bij aan een toenemende hoeveelheid literatuur die de potentie van tDCS om corticospinale exciteerbaarheid en motorisch leren te moduleren betwist. Samenvattend bieden de bevindingen van hoofdstuk 3 bieden geen basis voor vervolgmetingen van het motorisch netwerk tDCS bij patiënten met een beroerte.

In hoofdstuk 4 is een methode ontwikkeld om de elektrische velden van tES bij patiënten met een beroerte te simuleren. Deze methode combineert twee bestaande toolboxes om het automatisch modelleren van laesies na een beroerte in de hersenen mogelijk te maken. De methode werd toegepast bij patiënten met een chronische beroerte om de invloed van de geleidbaarheid van de laesie op het elektrische veld rondom het motorisch handgebied te bepalen. Het lokale elektrische veld binnen het stimulatiedoel werd veranderd door de laesie, afhankelijk van de elektrische geleidbaarheid van de laesie, de laesiegrootte en de locatie ten opzichte van het gebied van interesse. Deze studie toonde dan ook aan dat het negeren van de laesie in de toepassing van tDCS bij patiënten met een beroerte kan leiden tot suboptimale stimulatie. Indien de gebruikelijke aanname dat de laesie een volume van hersenvocht is niet klopt, kan dit leiden tot onjuiste schattingen van de effecten van de laesie op het lokale elektrische veld. Het opnemen van laesies ten gevolge van beroerte in volumegeleidingsmodellen kunnen helpen tDCS beter te richten in deze patiënten.

Hoofdstuk 5 behandelt de schatting van de elektrische geleidbaarheid van laesies van patiënten met een beroerte. De methode gebruikt (gesimuleerde) elektrische potentialen op de hoofdhuid, met ruis, als gevolg van tDCS-simulatie in een model met een vaste geleidbaarheid van de laesie (d.w.z. de patiënt), en een model waarin de geleidbaarheid van de laesie variabel was. Door het minimaliseren van de fout tussen de twee modellen, kon de geleidbaarheid van de laesie worden geschat. De relatieve schattingsfout van de methode werd beoordeeld voor verschillende aantallen elektroden, laesiegeleiding en laesievolumes. Hogere geleidbaarheid van de laesie, grotere laesievolumes en minder dieper gelegen laesies resulteerden in lagere fout van de geschatte geleidbaarheid. De methode had relatieve schattingsfouten onder 5% bij kleine fouten in de EEG-elektrode locatie registratie, maar presteerde slecht voor laesies kleiner dan 50 ml. Deze resultaten suggereren dat de geleidbaarheid van de laesies die de grootste effecten uitoefenen op de lokale elektrische velden in de hersenen met de hoogste betrouwbaarheid kunnen worden geschat. Experimentele gegevens zijn nodig om de beschreven methode te valideren.

Hoofdstuk 6 onderzocht of een one-fits-all benadering voor de stimulatie elektrode configuraties geschikt is voor het toepassen van tDCS bij patiënten met een beroerte. MRI werd gebruikt om een op anatomie gebaseerde stimulatiedoel in de motorische cortex te bepalen en EEG werd geanalyseerd om een motorisch doel op basis van functioneren te bepalen. De stimulatie-elektroden die beide doelen maximaal stimuleerden werden geïdentificeerd door optimalisatie. Patiënten met een beroerte hadden meer variabele, significant lagere en vaker omgekeerde elektrische veldsterktes binnen stimulatiedoelen dan gezonde controles bij gebruik van de conventionele, one-fits-all benadering van tDCS. Het optimaliseren van de elektrodeposities om de elektrische veldsterkte te maximaliseren verhoogde de elektrische velden van patiënten met een beroerte voor zowel de anatomische als de functionele doelen naar hetzelfde niveau als conventionele anodale tDCS in gezonde controles. Het bleef echter significant lager dan geoptimaliseerde elektrodeposities in gezonde controles. Deze resultaten impliceren dat de conventionele anodale tDCS leidt tot kleinere en inconsistente elektrische veldsterkte bij patiënten met een beroerte en kan de gemengde bevindingen in klinische tDCS experimenten mogelijk deels verklaren. Experimentele gegevens moeten worden verzameld om na te gaan of het verminderen van de elektrische veldsterkte variabiliteit ook leidt tot een vermindering van de variabiliteit op de stimulatie respons.

In hoofdstuk 7 worden de belangrijkste bevindingen van elk hoofdstuk van dit proefschrift besproken, gevolgd door de implicaties en methodologische overwegingen binnen de bredere context van de toepassing van tDCS bij patiënten met een beroerte, waarbij verschillende richtingen voor toekomstige onderzoek worden voorgesteld.

About the author

Curriculum Vitae

Joris van der Cruijssen was born on 8 March 1989 in Nijmegen and grew up in Vianen, Noord-Brabant. After completing high school in Cuijk (Merletcollege), he studied Built Environment for 6 months before moving to Delft to study Aeronautical Engineering at Hogeschool Inholland. After internships at the Biomechanics Laboratory of Erasmus MC and the Delft Institute for Prosthetics and Orthotics, Joris started with the pre-master Biomedical Engineering at the Delft University of Technology and thereafter the MSc Biomedical Engineering in 2014. He performed his master thesis project in the research group of prof. Vivian Weerdesteyn at the department of Rehabilitation of the Radboudumc, where, supervised by dr. Teodoro Solis-Escalante, he performed the first EEG measurements on the Radboud Falls Simulator. After graduating in 2016, Joris briefly worked as a research assistant within the department of Rehabilitation, followed by a short period in industry.

In 2017, Joris started his PhD project within the department of Rehabilitation of Erasmus University Medical Center in Rotterdam, with the goal to develop tools to monitor brain function during motor learning and volume conduction models to understand the effects of stroke lesions on current flow. During his PhD project, Joris conducted experimental studies in which he collected and analysed EEG, TMS and tDCS data and performed simulation studies to demonstrate the influence of stroke lesions on the electric fields generated by tDCS.

In 2021, Joris started as a postdoc in the lab of prof. Alfred Schouten and prof. Frans van der Helm to work on the 4D EEG project, focussing on longitudinal changes in somatosensory processing in people with stroke and EEG source localization. In March 2022, Joris returned to the Rehabilitation department of the Radboudumc to work in the research groups of prof. Vivian Weerdesteyn and dr. Jorik Nonnekes to investigate the relationships between EEG and gait and balance function in healthy individuals and people with neurological conditions such as Parkinson's disease and stroke.

List of publications

Publications included in this thesis

Van der Cruijssen, J., Manoochehri, M., Jonker, Z. D., Andrinopoulou, E. R., Frens, M. A., Ribbers, G. M., Schouten, A. C., & Selles, R. W. (2021). Theta but not beta power is positively associated with better explicit motor task learning. *NeuroImage*, *240*. <https://doi.org/10.1016/j.neuroimage.2021.118373>

Van der Cruijssen, J., Piastra, M. C., Selles, R. W., & Oostendorp, T. F. (2021). A Method to Experimentally Estimate the Conductivity of Chronic Stroke Lesions: A Tool to Individualize Transcranial Electric Stimulation. *Frontiers in Human Neuroscience*, *15*, 599. <https://doi.org/10.3389/fnhum.2021.738200>

Piastra, M. C., **Van der Cruijssen, J.**, Piai, V., Jeukens, F. E. M., Manoochehri, M., Schouten, A. C., Selles, R. W., & Oostendorp, T. (2021). *ASH: an Automatic pipeline to generate realistic and individualized chronic Stroke volume conduction Head models*. *Journal of Neural Engineering*. <https://doi.org/10.34973/5752-rf24>

Van der Cruijssen, J., Dooren, R. F., Schouten, A. C., Oostendorp, T. F., Frens, M. A., Ribbers, G. M., van der Helm, F. C. T., Kwakkel, G., & Selles, R. W. (2022). Addressing the inconsistent electric fields of tDCS by using patient-tailored configurations in chronic stroke: Implications for treatment. *NeuroImage: Clinical*, *36*, 103178. <https://doi.org/10.1016/j.nicl.2022.103178>

Van der Cruijssen, J., Jonker, Z. D., Andrinopoulou, E.-R., Wijngaarden, J. E., Tangkau, D. A., Tulen, J. H. M., Frens, M. A., Ribbers, G. M., & Selles, R. W. (2022). Transcranial Direct Current Stimulation Targeting the Entire Motor Network Does Not Increase Corticospinal Excitability. *Frontiers in Human Neuroscience*, *16*, 265. <https://doi.org/10.3389/fnhum.2022.842954>

Contributions to publications not included in this thesis

Jonker, Z. D., van der Vliet, R., Maquelin, G., **van der Cruijssen, J.**, Ribbers, G. M., Selles, R. W., Donchin, O., & Frens, M. A. (2021). Individual differences in error-related frontal midline theta activity during visuomotor adaptation. *NeuroImage*, *245*, 118699. <https://doi.org/10.1016/j.neuroimage.2021.118699>

Solis-Escalante, T., **van der Cruijssen, J.**, de Kam, D., van Kordelaar, J., Weerdesteyn, V., & Schouten, A. C. (2019). Cortical dynamics during preparation and execution of reactive balance responses with distinct postural demands. *NeuroImage*, *188*, 557–571. <https://doi.org/10.1016/j.neuroimage.2018.12.045>

Portfolio

Name PhD student:	Joris van der Cruijssen	PhD period:	2017-2023
Erasmus MC department:	Rehabilitation Medicine	Promotors:	Prof.dr. R.W. Selles Prof.dr. M.A. Frens
Research school:	Netherlands Institute for Health Sciences (NIHES)	Co-promotor:	Dr. T.F. Oostendorp

1. PhD training

General academic skills

- Research integrity	Erasmus MC, Rotterdam	2020	0.3
----------------------	-----------------------	------	-----

Courses

- Advanced Statistics (TW2550)	TU Delft, Delft	2018/2019	6
- Partial Differential Equations (TW2070)	TU Delft, Delft	2018/2019	6

Presentations

- Dutch Conference Rehabilitation Medicine - workshop	Maastricht	2017	0.5
- VVbN symposium - oral presentation	Utrecht	2018	0.5
- Werkgroep CVA - oral presentation	Utrecht	2018	0.5
- NeuroRehabilitation and Neural Repair - poster	Maastricht	2019	0.3
- Convergentiebijeenkomst - oral presentation	Rotterdam	2020	0.5
- Dutch Conference Rehabilitation Medicine - posters	Online	2020	0.3
- Dutch Biomedical Engineering conference - oral presentation	Online	2021	0.5
- Dutch Conference Rehabilitation Medicine - mini symposium	Online	2021	0.5
- TMSi Expert Talk Webinar	Online	2021	0.3
- Brain Stimulation Conference - mini symposium and poster	Lisbon	2023	0.8

Conferences

- Dutch Biomedical Engineering conference	Egmond aan Zee	2017	1
- Dutch Conference Rehabilitation Medicine	Maastricht	2017	0.3
- NeuroRehabilitation and Neural Repair	Maastricht	2017	0.7
- VVbN symposium	Utrecht	2018	0.3
- NeuroRehabilitation and Neural Repair	Maastricht	2019	0.7
- Dutch Conference Rehabilitation Medicine	Online	2020	0.7

- World Congress for NeuroRehabilitation	Online	2020	1.4
- Dutch Biomedical Engineering conference	Online	2021	0.7
- Dutch Conference Rehabilitation Medicine	Online	2021	0.7
- Brain Stimulation Conference	Lisbon	2023	1

Workshops

- Donders Brain Stimulation Toolkit	Nijmegen	2017	1.4
- PhD-day	Erasmus MC, Rotterdam	2017	0.2
- NeuroCIMT Summer School	TU Delft/Erasmus MC	2017	1.7
- NeuroCIMT Summer School	Chicago	2019	1.7
- NeuroCIMT Symposia	Various	2017/2021	2.7
- CareTech Symposium	Nunspeet	2022	0.7
- NeuroCIMT Workshops	Various	2018/2019	1.2

Other

- Scientific meetings	dept. of Rehabilitation Medicine	2017/2021	2
	dept. of Neuroscience	2017/2019	0.5

2. Teaching activities

Supervision of students

- Yvonne Greeuw	TU Delft	2017/2018	2.3
- Jessica Wijngaarden	TU Delft	2018/2019	0.9
- Floor Jeukens	TU Delft	2019	1.7
- Shirley van der Hoek	Erasmus MC	2019/2020	2.3
- Ditte Tangkau	Haagse Hogeschool	2019/2020	0.7
- Renée Dooren	TU Delft	2020/2021	2.3
- Alan Knaani	Universiteit Maastricht	2020/2021	2.3

